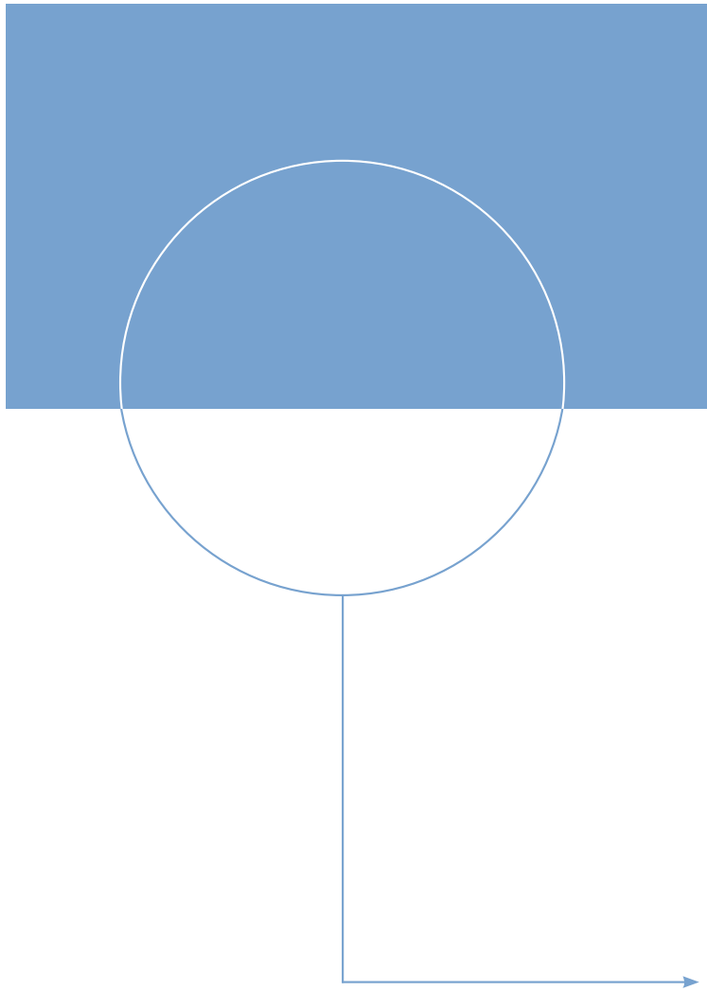

Master's thesis

2020

Andrea Therese Rognstad, Ingeranne Strøm Nakstad

Master's thesis

NTNU
Norwegian University of
Science and Technology
Faculty of Engineering
Department of Marine Technology

Andrea Therese Rognstad
Ingeranne Strøm Nakstad

Numerical Study for Single Blade Installation of an Offshore Wind Turbine

Comparing a Jack-up and a Semi-submersible Crane Vessel in Intermediate Water Depths

June 2020

NTNU
Norwegian University of
Science and Technology

NTNU
Norwegian University of
Science and Technology

NTNU
Norwegian University of
Science and Technology

Numerical Study for Single Blade Installation of an Offshore Wind Turbine

Comparing a Jack-up and a Semi-submersible Crane Vessel in Intermediate Water Depths

Andrea Therese Rognstad
Ingeranne Strøm Nakstad

Marine Technology
Submission date: June 2020
Supervisor: Zhen Gao

Norwegian University of Science and Technology
Department of Marine Technology

NTNU Trondheim
Norwegian University of Science and Technology
Department of Marine Technology

MSC THESIS IN MARINE TECHNOLOGY

SPRING 2020

FOR

Andrea Therese Rognstad & Ingeranne Strøm Nakstad

Numerical Study for Single Blade Installation of an Offshore Wind Turbine

- Comparing a Jack-up and a Semi-submersible Crane Vessel in Intermediate Water Depths

Background:

EU has set a target for offshore wind development to achieve 150 GW by 2030. This implies a significant amount of marine operation work related to transportation, installation as well as operation and maintenance of offshore wind turbine systems. On average, more than one thousand turbines need to be installed every year. Most of the offshore wind turbines today are based on bottom-fixed foundations, including monopile, tripod, jacket and GBS, which are typically installed piece by piece at the offshore site. The increase in turbine size will help to reduce the number of turbines and therefore offshore operations, but this trend, including the increase in water depth and distance to shore, will impose new challenges for onsite installations.

Currently, jack-up vessels are used to install wind turbine blades, nacelle and tower. Foundations might be installed using floating installation vessels. Jack-up vessel can provide a stable platform when installing blades with its onboard cranes. However, positioning the jack-up vessel by lowering the legs into the seabed and lifting up the vessel hull above the water line can only be done in very small sea states. When the water depth increases from 10-30m to 40-60m, the dynamic responses of the jack-up vessels in waves will also increase due to resonance. It is therefore interesting to consider floating installation vessels for wind turbine blade installation. However, the main challenge for a floating installation vessel is its large rigid-body motions in waves and induced blade root motions, which makes the connection of the blade root to the hub at the top of the tower more challenging.

In this master thesis that will be carried out by two master students, a comparative study based on numerical simulations will be carried out for offshore crane installation of a single wind turbine blade using a jack-up vessel and using a floating installation vessel (semi-submersible). The intermediate water depth of 60m will be considered. One student will focus on the numerical analysis using the jack-up vessel and the other on the floating vessel. The comparison should be made for typical response parameters for selected wave conditions, such as vessel motions, crane tip and blade motions, as well as lift wire and tugger line tension.

Assignment:

The following tasks should be addressed in the thesis work:

1. A literature review on installation methods for wind turbine blades and the corresponding installation vessels should be made.

2. A brief review on the theories related to aerodynamic loads on wind turbine blades, hydrodynamic loads on jack-up and semi-submersible floating vessels and coupled response analysis should be carried out.

3. Based on the numerical models from Dr. Yuna Zhao and with the given information of the jack-up and floating installation vessels, new models in Sima for 60m of water depth will be established, while considering the same blade model.

3. Comparison of the basic dynamic behaviour of the two models, in terms of the natural periods of rigid-body motions and vibrations will be made.

4. Perform regular wave analysis for a set of wave conditions and obtain the RAOs of different response parameters. Discuss the response features of the jack-up and semi-sub installation vessels.

5. A set of the sea states (turbulent wind and irregular wave conditions) are defined for the numerical analysis of the two installation systems. Comparison of the vessel, crane tip and blade motion responses as well as lift wire and tugger line tension in terms of spectra and statistics will be performed, to see the advantages and the disadvantages of the two concepts.

6. Conclude the work and write the thesis.

In the thesis the candidate shall present his/her personal contribution to the resolution of problem within the scope of the thesis work.

Theories and conclusions should be based on mathematical derivations and/or logic reasoning identifying the various steps in the deduction.

The candidate should utilize the existing possibilities for obtaining relevant literature.

The thesis should be organized in a rational manner to give a clear exposition of results, assessments, and conclusions. The text should be brief and to the point, with a clear language. Telegraphic language should be avoided.

The thesis shall contain the following elements: A text defining the scope, preface, list of contents, summary, main body of thesis, conclusions with recommendations for further work, list of symbols and acronyms, reference and (optional) appendices. All figures, tables and equations shall be numerated.

The supervisor may require that the candidate, in an early stage of the work, present a written plan for the completion of the work. The plan should include a budget for the use of computer and laboratory resources that will be charged to the department. Overruns shall be reported to the supervisor.

The original contribution of the candidate and material taken from other sources shall be clearly defined. Work from other sources shall be properly referenced using an acknowledged referencing system.

The thesis shall be submitted in Inspera:

- Signed by the candidate
- The text defining the scope included
- Other thesis work information, like computer codes, etc. should be organized in a separate folder.

Supervisor:
Prof. Zhen Gao

Deadline for master thesis: 10.6.2020

Abstract

The market for offshore wind are growing and the size of the wind turbines are increasing. The efficiency of a wind turbine is affected by the turbine size and a steady wind. A consequence will be more installations of offshore wind turbines longer from shore and at deeper water depths. Even though floating solutions will enter the market, the technology is not ready today and the market for bottom-fixed wind turbines will continue to grow. However, larger bottom-fixed wind turbines longer from shore will lead to engineering challenges and increased expenses.

A feasibility study of the mating phase of a single blade installation of a bottom-fixed offshore wind-turbine at 60 meters water depth has been conducted. The analysed installation systems are a jack-up crane vessel and a semi-submersible crane vessel (SSCV). The jack-up crane vessel are modelled with four flexible legs, a vessel hull, crane and a blade. The SSCV are installed with the same crane and lifting arrangement as the jack-up vessel. This analysis was conducted by numerical analysis in the simulation software SIMA, a software owned by MARINTEK. A fully coupled SIMO-RIFLEX-Aero simulation code developed by Y. Zhao was used and modifications were done to adjust the models from 30 meters to 60 meters water depth. SIMO models the non-linear motions of the complex multi-body systems in the time domain. RIFLEX uses finite element method to analyse slender structure and the aerodynamic forces was calculated with the Aero-code.

A regular wave analysis was performed in order to identify the natural periods of the installation systems. As the systems are complex, the natural periods were found for each part of the installation system separately. Further, an irregular wave analysis was performed with only wave loads and with wind and wave loads acting on the system. Different environmental conditions were simulated, and the wave direction, wind direction, spectral peak period and significant wave height varied. The response statistics were firstly analysed for each installation system separately, then compared between the to installation systems. The main response parameters analysed were the vessel response in six DOFs, the crane tip response in three DOFs and the blade response in six DOFs. Further, the bending mode of the jack-up legs was included in the regular wave analysis.

The jack-up vessel experience resonant motion for low periods, while the SSCV experience resonant motions for high periods. Even though the SSCV natural frequency are in general outside the frequency range of incident waves, it was found that the response motion for both vessels are in the same range. Further, it was found that the response motion are dominated by the wave loads compared to the wind loads. The response motion increased with the alignment of wind and wave loads towards beam sea. For both vessel, head sea is the preferable wave condition. It was found that the installation vessels are competitive, and the blade responses for both vessels are in the same range. The findings can potentially contribute to change the commercial installation procedure in the industry. It will be interesting to continue the feasibility study, in order to obtain the best solution.

Sammendrag

Markedet for havvind vokser samtidig som størrelsen på vindmøllene øker. Effektiviteten til en vindturbin påvirkes av turbinstørrelsen og stabile vindforhold. En følge av dette vil være flere installasjoner av vindmøller lenger fra land og på dypere vanndyp. Selv om flytende løsninger vil komme, er teknologien ikke klar i dag, og markedet for bunnfaste vindturbiner vil fortsette å vokse. Større bunnfaste vindturbiner lenger fra land vil føre til tekniske utfordringer og økte utgifter. Derfor er valg av installasjonsprosess en avveining mellom teknisk gjennomførbarhet og økonomisk bærekraft.

Et sammenligningstudie av bladinstallationen ved bruk av metoden "single blade installation" av en bunnfast offshore vindturbin på 60 meters vanndybde er utført i denne oppgaven. De analyserte installasjonssystemene er en oppjekkbar plattform og et halvt nedsenkbart kranfartøy (SSCV). Den oppjekkbare plattformen er modellert med fire fleksible ben, et skrog, en kran og et blad. SSCV er installert med samme kran og løfteinnretning som den oppjekkbare plattformen. Analysen ble utført ved numerisk analyse i simuleringsprogramvaren SIMA, en programvare som eies av MARINTEK. En fullstendig koblet SIMO-RIFLEX-Aero simuleringskode utviklet av Y. Zhao ble brukt som grunnlag, og modifikasjoner ble gjort for å justere modellene fra 30 meter til 60 meters vanndybde. SIMO modellerer de ikke-lineære bevegelsene til de komplekse subsystemene i tidsdomene. RIFLEX bruker elementmetoden for å analysere slanke strukturer og de aerodynamiske kreftene ble beregnet med Aero-koden.

En regulær bølgeanalyse ble gjort for å identifisere de naturlige periodene i installasjonssystemene. Siden systemene er komplekse, ble de naturlige periodene funnet for hver del av installasjonssystemet separat. Videre ble en uregelmessig bølgeanalyse utført med bare bølgelast og deretter med vind- og bølgelaster som virket på systemet. Ulike sammensetninger av ytre laster ble simulert, og bølgeretningen, vindretningen, spektral topperiode og signifikant bølgehøyde er variert. Responsen ble først analysert for hvert installasjonssystem separat, deretter sammenlignet mellom installasjonssystemene. Responsparametrene som ble analysert var fartøyets respons i seks frihetsgrader, enden av kranen i tre frihetsgrader og bladresponsen i seks frihetsgrader. Videre ble bøyemomentet for bena til den oppjekkbare plattformen også inkludert i den regulære bølgeanalysen.

Den oppjekkbare plattformen får resonans ved lave bølgeperioder, mens SSCV får resonans i høye bølgeperioder. Selv om SSCVens naturlige frekvens generelt ligger utenfor frekvensområdet for de innkommende bølgene, ble det funnet at responsbevegelsen for begge fartøyer er i samme område i frekvens området som ble testet. Videre ble det funnet at responsbevegelsen hovedsakelig er dominert av bølgelastene sammenlignet med vindlastene. Responsbevegelsen økte når både vind- og bølgelaster virket på tvers av skipet. For begge fartøyene er den foretrukne bølgetilstanden at bølgene kommer rett på baugen. Det ble funnet at installasjonsfartøyene er konkurransedyktige, og bladresponsene for begge fartøyene er i samme område. Funnene kan potensielt bidra til å endre den kommersielle prosedyren for installasjon i industrien. Det vil være nødvendig med flere analyser for å bekrefte om installasjonen er mulig og deretter hvilken metode som gir den beste løsningen.

Preface

This thesis is submitted to the Norwegian University of Science and Technology for a fulfilment of a master degree the spring of 2020. The thesis is a cooperation between the two students from the institute of Marin Technology, Ingeranne Strøm Nakstad and Andrea Therese Rognstad.

The thesis presents a comparative study of a jack-up vessel and semi-submersible crane vessel used to preform blade installation of offshore, bottom fixed wind turbines at a water depth of 60 meters. The main objective is to preform a numerical analysis of the coupled system and compare the motion response.

Nakstad has a specialisation in hydrodynamics while Rognstad a specialisation in marine structures. Respectively, the analysis of the semi-submersible and the jack-up vessel is divided between the students. The work have been preformed at the Department of Marine Technology, NTNU, Trondheim, with Professor Zhen Gao as main supervisor.

Trondheim, June 8th, 2020

Ingeranne Strøm Nakstad

Andrea Therese Rognstad

Acknowledgement

We would like to express our gratitude to our supervisor Zhen Gao, for our weekly meetings and additional mail-correspondence with good discussion and great guidance. These conversations have resulted in deeper insight and a better understanding necessary for us to complete this thesis work. As the semester suddenly changed due to COVID-19, we especially appreciate his engagement through digital tools, which gave us the possibility to complete the thesis, despite the situation.

The help we received from Yuna Zhao is also highly appreciated. She provided us with her SIMA models and additional guidance and advise in SIMA throughout the thesis work.

In addition, a great thank you to George Katsikogiannis is in order for providing us with the MATLAB-codes used for extracting the results in SIMA. He have also been a great support throughout the thesis work assisting with problems that occurred in SIMA.

Finally, a big thanks to our fellow students at the Department of Marine Technology for the good academical and social environment in our years at NTNU. Also, thank you to the students at C1.058, for great discussion, good laughs and many coffee breaks.

Symbols and Abbreviations

θ_{wd}	Wind incident angle
θ_{wv}	Wave incident angle
COG	Center of Gravity
DOF	Degree of Freedom
H_s	Significant wave height
O - XYZ	Global coordinate system
O_b - x_b,y_b,z_b	Blade related coordinate system
O_v - x_v,y_v,z_v	Vessel related coordinate system
RAO	Response Amplitude Operator
SSCV	Semi-Submersible crane Vessel
T_p	Spectral Peak Period
Surge	Translation in local x-direction
Sway	Translation in local y-direction
Heave	Translation in local z-direction
Roll	Rotation around local x-axis
Pitch	Rotation around local y-axis
Yaw	Rotation around local z-axis
Head Sea	Waves propagating in global y-direction
Beam Sea	Waves propagating in global x-direction
Quartering Sea	Waves propagating 45 degrees from global y-axis

Table of contents

List of Tables

List of Figures

Chapter 1

Introduction

1.1 Background and Motivation

Comprehensive climate changes have triggered a radical political change with regards to energy and climate politics. This has resulted in different measures and globally agreements. One of which is the ambitious Paris agreement, designed to combat the climate changes. The main aim of this agreement is to keep the global temperature rise below 2 degrees Celsius, and aiming for 1.5 degrees Celsius. The need for energy is constantly increasing, and an energy transition to renewable sources is crucial to achieve the goals of the Paris agreement. Wind energy is one of the biggest sources with high potential of renewable energy [25]. In order to utilize the maximum potential of the source, offshore wind technology has to be further explored and developed.

1.1.1 Offshore Wind - Market and Development

In 2019, Europe installed 15.4 GW of new wind energy, out of which 3.6 GW were offshore wind installations. This is 27% more than in 2018. In total, wind energy covered 15% of Europe's electricity demand in 2019[26]. As illustrated in Figure 1.1, wind energy together with solar PV, are the energy sources with the most rapid growth over the last decade.

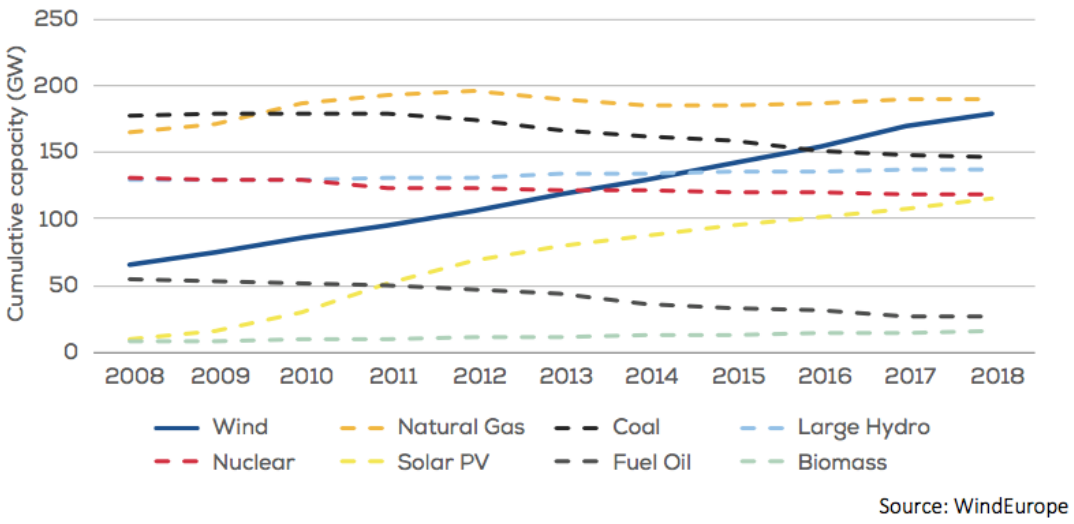

Figure 1.1: Cumulative capacity for different energy sources [7].

There are several reasons why it would be beneficial to install wind farms offshore instead of onshore. Firstly, a stronger and more steady wind exists offshore compared to onshore. Secondly,

for onshore wind farms is space a limiting factor, especially when the turbine sizes increases. This conflict makes the arguments for offshore wind stronger, where there is unlimited with space. Therefore an increasing trend in offshore wind farms is seen. Until recently, offshore wind farms are installed with a bottom fixed foundation support. Now the technology is developing and there are several undergoing projects exploring the possibility of floating foundation supports.[27]

How the market outlook for offshore wind turbines looks like is highly discussed with different opinions. According to the global wind report 2018, there will be a strong growth for wind turbines with bottom fixed support structures as well as floating solutions. Figure 1.2 presents the cumulative and yearly outlook comparison for both bottom fixed wind turbines and floating solutions. The GWEC predicts an increase in both cases. However, the bottom fixed structures will play the dominant role for offshore wind farms [8]. A limiting factor for the bottom fixed structures is the water depth, where floating structures are flexible. Currently most of the bottom fixed wind farms are installed in water depths up to 40 meters.[8]

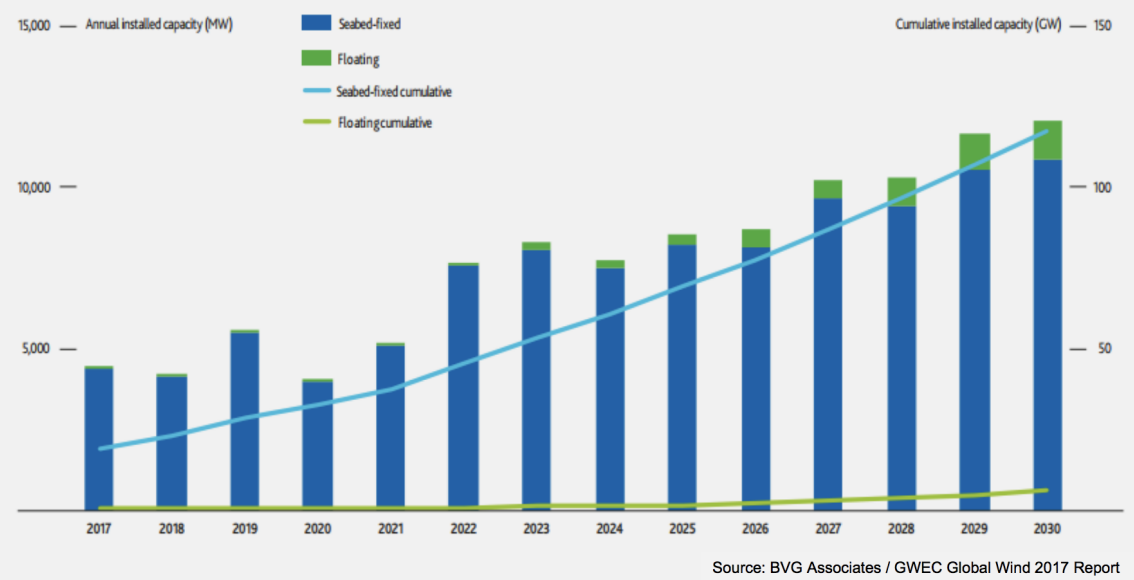

Figure 1.2: Market outlook for Offshore Wind 2030. [8]

When it comes to offshore wind farms, the technology for the tower, nacelle and the blade are similar to the technology used in onshore wind farms. The difference lays in the foundation support structures, this is also where the bottom fixed wind turbines are distinguished from floating wind turbines, which is further explained in the next section. The technology for bottom fixed wind turbines is well developed. While the technology for floating wind turbines is under development with focus on testing and innovation. The market outlook for 2030 presented in Figure 1.2, predicts an increase in the installation for both fixed and floating offshore wind turbines. In 2017 Equinor installed the first floating wind farm in the world, Hywind Scotland, consisting of five pieces of 6 MW wind turbines 30 km outside the coast of Scotland. This was a successful pilot project, and they are currently working on a new project, Hywind Tampen. This is a project consisting of 11 floating wind turbines of 8 MW, which is to electrify oil and gas installations in the North sea [28]. Equinor highlights that 80% of the total potential for offshore wind power is believed to be in deeper waters. After the successful demo project, they have reason to believe that the development of the technology will be rapid[28].

The cumulative capacity of offshore wind and the individual capacity for offshore wind turbines are increasing every year. The development on wind turbine size the last years is described in Table 1.1. In WindEuropes market outlook for 2023, they predict a decrease in the number of turbines installed and an increase in total installed capacity [29]. This means that there will be an increase in the turbine capacity in each turbine. This is cost beneficial as a doubling in turbine size gives

four times more energy [30]. In Table 1.1 numbers for turbines with capacity of 2-15 MW is listed to give an indication of the dimensions for increased capacity.

Table 1.1: The development of the capacity of offshore wind. [1] [2]

Year	Capacity [MW]	Blade length [m]	Blade Weight [tonnes]	Hub Height [m]	Nacelle weight [tonnes]
1999	2	44	10	78	75
2005	5	61.5	17	90	240
2016	8	82	35	138	390
2018	12	107	-	153	-
2020	15	108	-	-	500

Most of the currently operating wind farms are at about 20-30 meters water depth and 20-30 km from shore. In Figure 1.3, the average water depth for offshore wind farms are plotted against the distance to shore, where the size of the bubble indicates the overall capacity of the site. There is also a clear trend for the projects with permits, with both an increased distance to shore and water depth. This are factors that will affect the installation phase in several ways. As the distance to shore increase, there will be a limit where it will be more efficient to bring all components instead of sailing multiple rounds. This will again lead to a need for increased deck capacity for the installation vessels. What installation procedure and vessels that both are feasible and economically favorable is an important factor for further development of the offshore wind market.

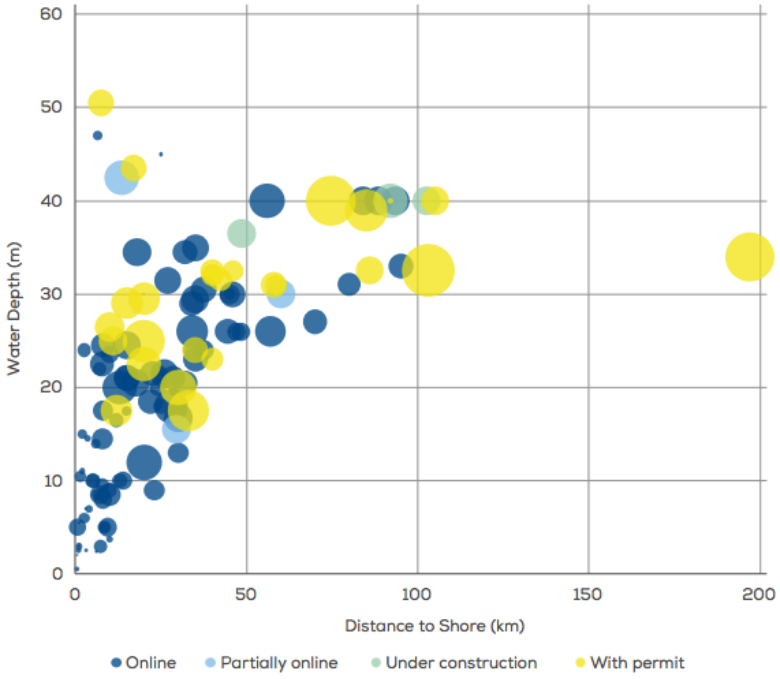

Figure 1.3: Average water depth and distance to shore of bottom-fixed offshore wind farms, organised by development status. [7]

When the capacity and the dimensions increases new challenges follows. The installation process will be more difficult as bigger cranes with larger capacity and higher lifting height are needed. This will affect the installation procedure and which foundation system that is best suited. The operation is more sensitive to environmental conditions and different support structures depends on the water depth. There are many different support structures for offshore wind, which are divided in two groups; floating wind turbines and bottom-fixed wind turbines.

1.1.2 Support Structures

For bottom fixed wind turbines the monopiles foundation is the most common. This is a long tube driven into the seabed with an hydraulic hammer. Because of the simple design, it is cheap to manufacturer, easy to handle and storage which is a big advantages compared to other bottom fixed structures. Monopiles are dominant in the market with a 87% of the market share. Gravity based, jacket and tripod-foundations are other support structure for bottom fixed wind turbines, the respectively holds 2%, 9% and 2% in the total market of bottom fixed wind turbines. The technology used for fixed support structures is based on the oil and gas industry and is well developed. The different support structures are illustrated in Figure 1.4.

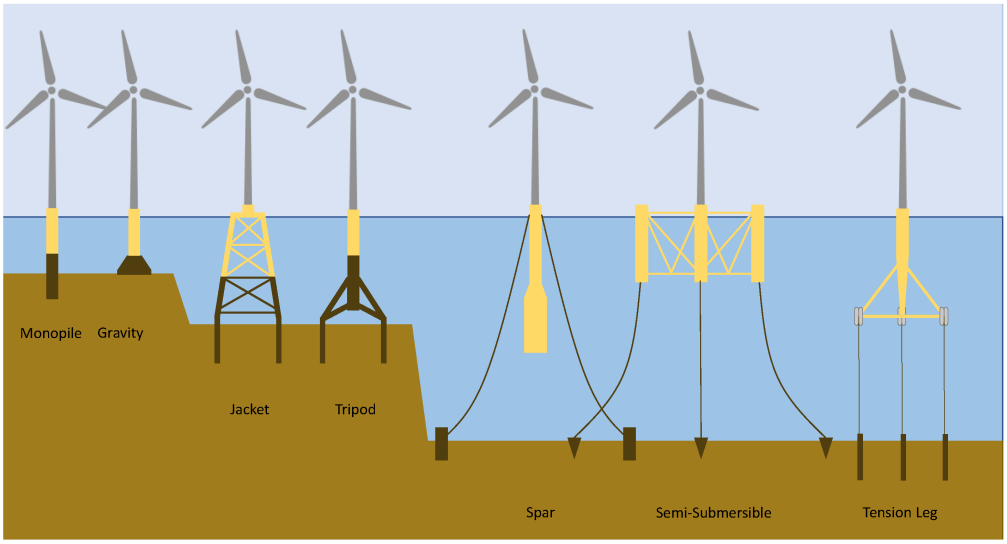

Figure 1.4: Offshore wind turbines with different foundations and water depths [9].

Deeper offshore areas represents 60-80% of the offshore wind potential in Europe. In these areas the wind have a much higher speed and are more stable because of the long distance from shore. The range for the floating wind turbines are 100-900 meter water depth. The big advantage with floating structures is the flexibility related to water depth at installation site. The foundations are floating structures moored to the sea bed by mooring lines. The technology behind floating offshore wind is relatively new, but the floating foundations archetypes are based on the oil & gas industry. There are mainly three types used today, the SPAR buoy, a semi-submersible and a TLP, depicted in Figure 1.4. The technology for floating offshore wind is still in the development phase, and there are several technical challenges for floating offshore wind which needs to be solved for further development. [31]

1.2 Challenges Related to Installation of Offhore Wind Turbine Blades

The challenges in offshore wind are mainly related to costs, specially in the installation phase. About 10-15% of the total cost is from the installation phase [1]. This is due to expensive installation vessels, unexpected delays and very limiting operational requirements and limits. There are several critical points during installation of an offshore wind turbine, but mainly the blade installation is the most constricted procedure. A wind farm objective is to utilize as much wind energy as possible, hence the location is chosen thereafter with consequently high wind velocity and large waves, further from shore and at deeper water depths. This challenges the installation process, and the weather window the operation can be executed in are narrowed down by the wind and sea states.

The turbine size is increasing, in order to increase the generated power and profitability. There are two ways to produce more energy from wind in a given area. Firstly, bigger rotors and blades. Secondly, the wind blows more steadily higher up in the atmosphere, which leads to an increase in the turbines capacity factor for high wind turbines. The capacity factor is a fraction of how much the turbine actually produces and the total potential the wind turbine has. Both of which leading to bigger dimensions of the wind turbine and are challenging the engineering of the installation phase.

Traditionally, the assembly of the offshore wind turbine is done at shore and then the complete assembly are transported to site. In recent time, the assembly at site is commonly used, as the dimensions of the offshore wind turbine are increasing. The most challenging procedure is the blade installation, due to the extreme requirement of precision when connecting the blade to the rotor hub.

Future potential offshore sites for bottom-fixed wind turbines are expected to be at a water depth up to 60 meters. This water depth challenges the feasibility of the commonly used jack-up installation vessel. A floating installation vessel is flexible considering the water depth at site, the vessel is more mobile and the duration of the operation deceases. However, the wave-induced motions of the floating vessel result in a higher relative motion between the blade root and the rotor hub which makes the installation even more challenging.

1.3 Problem Description

EU's goal for the offshore wind industry is to achieve 40 GW installed capacity by 2020 and 150 GW installed capacity by 2030. This means that more than thousand offshore wind turbines must be installed every year. Figure 1.2 shows that the bottom-fixed holds a big share of the installed capacity, and a demand of offshore wind farms with fixed foundation structures, even though floating solutions are likely to enter the market. A consequence of this will be more installations operations for larger wind turbines at deeper water depths.

In addition to the increase in the cumulative capacity of offshore wind, the individual capacity for offshore wind turbines are also increasing. Traditionally, the installation method is to install the rotor, nacelle, tower assembly onshore before it is transported out to the site where the assembly is installed by a crane operations to the foundation. For bottom-fixed wind turbines to be installed at the offshore site, piece by piece. The trend, where the turbine size increases, higher water depths and longer distance from shore will impose new challenges for the onsite installations.

The most common way to install wind turbine blades, the nacelle and tower, is to use a jack-up vessel. A jack-up vessel have four "legs" which can lift the vessel up over the sea surface level and create a stable platform for the on-board crane operations. However, the jack-up vessel is not very mobile and the duration the vessel takes to get in position, lowering its legs and elevating the hull from the sea surface is time consuming and can only be done for small sea states. The increasing water depth for the installation sites will lead to a higher dynamic response in the four legs. Therefore, the consequence of these amplified dynamic responses due to the increased water depths will be interesting to analyse, and check whether or not it is feasible to use a jack-up vessel. As an alternative, it could be interesting to investigate the use of a floating installation vessel for the blade installation. The main challenge for the floating vessel is the wave-induced motion at the crane tip which causes a relative motion between the blade root and the rotor hub.

As mentioned in the previous section, the installation phase for an offshore wind turbine is extremely costly and it is important to find the most efficient method for the installation operation. The objective of the thesis will be to compare the motion responses of the lifted blade during operation when using a jack-up vessel and a SSCV at 60 meters water depth. The analysis will be performed using the simulation software SIMA. The models used in this thesis are based on Y.Zhaos PhD [6] and then modified for deeper water depth.

Firstly, new models in SIMA for 60 meters will be established for the jack-up vessel and the floating installation vessel. The modifications for the jack-up vessel the water depth. Hence, the leg length is increased. In this analysis the cross-section of the legs are kept the same. While, the modifications for the SSCV model are related to the kinematic water depth. The hydrodynamic coefficients are assumed the same for a SSCV in 30 meters and 60 meters water depth.

When the modifications are done for the two models the system behaviour will be identified by regular wave analysis, and the systems natural eigen periods identified. Further, a set of sea states, wind and wave conditions, are defined for the numerical analysis of the two installation systems. An irregular wave analysis is performed in order to find the motion responses in terms of power spectra and statistics. Lastly, a comparison of the motion responses of the vessel and the blade is performed to see the advantages and the disadvantages of the two installation systems. The objective for this analysis is to consider the feasibility of the two installation systems and compare their performance during installation.

Chapter 2

Marine Operations

2.1 General Aspects

A marine operation is a non-routine operation which is related to handling of vessels and structures in the marine environment. The duration is limited and the systems condition is constantly changing, meaning that the structure is not in its normal design condition. Offshore installation procedures, crane and lifting operations are some examples of a marine operation, which will be described in more detailed in this thesis. A marine operation is a complex process and consists of several offshore activities or sub-operations. [32]

When planning and executing a marine operation, practical experience is crucial for a good outcome. New innovations are constantly developing and the experiences are therefore limited. For operations happening for the first time, the need to identify the responses and the safety level is stronger than for routine operations. The normal design condition for a marine structure is determined by its permanent phase, which is important to consider when planning an operation because marine operations represents an intermediate phase for the structure. An example of this is the blade installation for offshore wind turbines. The challenge is that the turbine blades are designed to absorb as much energy from the wind as possible. Hence, it will create additional motion in the system during installation, when it is desirable with as little motion as possible. The challenges are different for every marine operation, and therefore are the specific physical limitations and design criteria dependent on the operation. In addition, every marine operation need to comply with specific rules and regulations. [32]

Specific operational limits for a marine operation are necessary for assessing the operability of the operation, both during the planning and for on-board decision making during the execution phase. Identification of hazardous events and the corresponding consequences are crucial when planning a marine operation. For mitigation and as part of a risk analysis, limits for the response parameters are established to prevent hazardous events such that the marine operation can be executed in a safe manner. An example for a response parameter is the tension in a lifting wire, this is a hazardous event if the wire exceeds its maximum capacity and failure occur. To prevent this, the total tension in the wire must be kept below its maximum capacity at all times, including a safety factor. To assess the tension in the wire, numerical analysis is employed, and from this analysis one can identify which sea states leads to the critical tension. From this, on of the operational limits are established. In other words, the safety criterion for a marine operations is that the responses of the dynamic system, including safety factors should never exceed its allowable limits.

When establishing the operational limits, numerical analysis, documentation, guidelines and experience from similar operation in the past are employed. When establishing the design limit for the significant wave height, H_s, the current practice is to use former experiences, offshore standards, and the α-factor. This approach has not been described properly in literature and scientific papers and is somewhat unclear. Acero, W. et al. (2016) [27], stated that

"*To date, limited work has been carried out to identify critical events and established operational limits based on structural responses, and no systematic methodology seems to have been published.*"

As a response to this observation, Acero, W. et al. developed a systematic methodology, based on operational procedures, for establishing operational limits and assessing the operability for general marine operations. This approach uses numerical analysis to establish critical events and the corresponding response parameters, and transforms the limiting responses into allowable sea state limits.

2.2 Weather Window and The Alpha-factor

During a marine operation it is difficult to monitor the dynamic responses, therefore are these limits transformed and defined by sea states parameters and motion responses of the vessel, which is easier and more practical to monitor during the operation. Hence, the most important factor for whether a marine operation should be executed or not is therefore the environmental conditions (i.e. wave height, wave periods, wind speed and current - depending on the operation). By identifying the operational limits one can find an allowable weather window for the execution of the marine operation. A weather window is an opening in the weather forecast where the environmental conditions does not exceed the operational limits and it is safe to complete the operation. Take the significant wave height, H_s, as an example, the operational limit for the significant wave height is decided so that

$$H_{s,oper} \leq \alpha \cdot H_{s,design} \tag{2.2.0.1}$$

where α is a factor that includes uncertainties in the weather forecast for a weather restricted operation. The value of the alpha-factor is decided such that it reflects on the increasing uncertainty in the weather for operation with long duration and the opposite for short duration operations. The alpha-factor also include the increased uncertainties that occur when weather forecasts reports low wave heights and decreased uncertainties when weather forecasts reports high wave heights. The α-factor considers important parameters as the significant wave height, Hs, the wave peak period, Tp, and the wave direction. Table 2.1, is extracted from Table 4-1 in the DNV-OS-H101 standard [3], and it gives values for the α-factor for different significant wave heights, with a base case in European waters.

Table 2.1: α-factor for the significant wave height, base case [3].

Operational period [hours]	Design wave height [m]			
	$H_S = 1$	$H_S = 2$	$H_S = 4$	$H_S \geq 6$
$T_{POP} \leq 24$	0.65	0.76	0.79	0.80
$T_{POP} \leq 36$	0.63	0.73	0.76	0.78
$T_{POP} \leq 48$	0.62	0.71	0.73	0.76
$T_{POP} \leq 72$	0.60	0.68	0.71	0.74
$T_{POP} \leq 12$	0.55	0.63	0.68	0.72

The required duration of a marine operation is denoted as the reference period (T_R). T_R is a sum of the planned operation time (T_{POP}) and an estimated contingency time (T_C) in case of any contingency situations, which is estimated based on the risk analysis.

$$T_R = T_{POP} + T_C \tag{2.2.0.2}$$

If T_R is lower than 72 hours the marine operation is considered weather restricted. For weather restricted operations, the environmental conditions are measured from reliable weather forecasts and meteorologists on site, which decides if the operations should be executed or not. This means that the characteristics of the environmental condition decides, if the operation can be performed within the planned weather window, are decided by reliable weather forecasts. Figure 2.1 illustrates the weather window for a weather restricted operation. A weather restricted operation can only be performed if and only if $OP_{WF} \leq \alpha \cdot OP_{LIM}$ apply for every critical parameter.

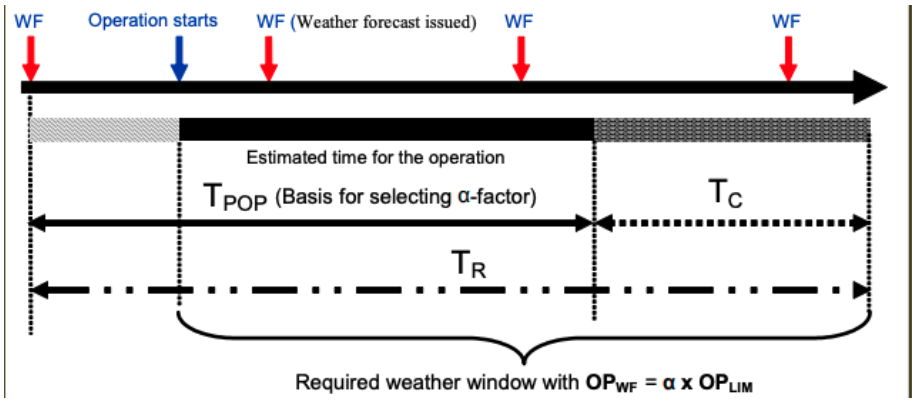

Figure 2.1: Required weather window for marine operations. [3]

On the other hand, if the reference period for a marine operation is longer than 72 hours the operation is considered as an unrestricted operation. For this type of operations, the environmental characteristics are established hence to long term weather statistics and extreme value statistics. The significant wave height for weather restricted operation is determined based on reliable weather forecasts. For unrestricted operations, the significant wave height is dependent on the duration of the operation, on the geographical location the operation will take place. The operational limit for wind velocity are decided based on duration. For an operation with duration less than 30 days, the characteristic wind velocity is the one with a return period of 10 years. Duration of more than 30 days, the return period of 100 years is used for the characteristic wind velocity. Equation 2.2.0.3 estimates the mean wind velocity at a reference height z_r [32].

$$U_m(z, t_{mean}) = U_m(z_r, t_{r,mean}) \left[1 + 0.137ln\left(\frac{z}{z_r}\right) - 0.47ln\left(\frac{t_{mean}}{t_{r,mean}}\right)\right] \tag{2.2.0.3}$$

The focus in this report will be on the mating phase of a single blade installation for an offshore bottom-fixed wind turbine. These operations are especially sensitive for wind, hence the wind velocity and direction must be monitored closely. However, installations of offshore wind turbines are usually weather restricted operations. hence, the operability will be based on the weather forecast [33]. In addition to the significant wave height and wind speed as important environmental conditions, the wave peak period, T_p, and the wave direction are also interesting parameters for installation of an offshore wind turbine due to the motion of the floating installation vessel.

2.3 Crane and Lifting Operations

Crane and lifting operations have increased significance for offshore operations in the recent years. There has been a focus on reducing the installation costs parallel with an increased size of lifted objects. For the offshore wind industry there is a clear trend of increasing size of both the nacelle, blades and tower. This means higher and heavier lifts with following operational constraints. Crane operations are divided in two categories, light lifts and heavy lifts. Light lifts is when the load is small compared to to the crane vessels weight, typically 1-2 % of the vessels displacement. In these cases heave compensation is usually used. Following, heavy lifts are when the load is larger than 1-2% of the vessels displacement [32]. In these cases coupled dynamics have to be considered and heave compensation is not possible. Therefore, it will be stricter constraints and more narrow weather windows. For offshore wind operations the lifts are in general classified as heavy lifts.[32]

When performing an offshore crane operation, there is several constraints and considerations that have to be taken into account. The primary concern during a marine operations is the safety of the cargo and the people. When lifting an object, offshore environmental loads, such as waves, wind and current, will work on the system. This will induce relative motions between the crane, vessel and the lifted object. In principle, this is a 18 DOF problem, but usually both a static and dynamic analysis have to be carried out to ensure a safe operation[32]. For lifting operations the

weather window is usually quite narrow as the operation is sensitive to sudden changes. A wind gust or higher waves can be enough to make the ship capsize, create large snap loads in the ropes or create interference between the lifted object and the ship or humans. To avoid huge snap loads, the ropes are pre-tensioned and the optimal configuration is to have the meta center of the ropes in line with the systems center of gravity[34]. A typical configuration for the crane and the capacity diagram is illustrated in the Figure 2.2.

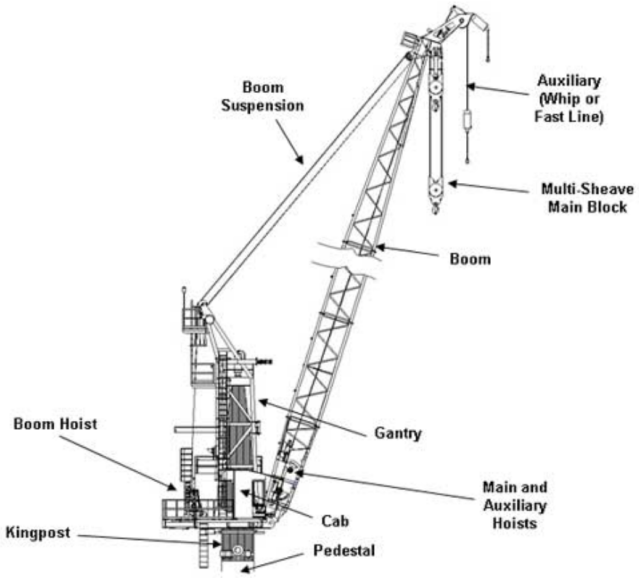

Figure 2.2: Crane configuration.

Another critical aspect of the lifting operation is that the stability is decreasing. When analysing the systems stability, both the static and dynamic stability are of interest for crane operations. The systems static stability is changing when an object is lifted. In the moment when the object is lifted of the deck, the gravitational force will act as all the weight is centered the hook. Therefore, it is essential how high the crane tip is located. If the crane tip is at a high position, this will lead to a rapid increase in the center of mass for the vessel, reducing the metacentric height (GM) and therefore a decrease in the systems stability. A static analysis will determine the allowable crane tip height for a specific case. With regards to the systems stability, the dynamic stability will also play a significant role. As the crane vessel is exposed for wind and wave loads, the system will be in motion and creating heel moments. As the transverse stability is the critical for a ship, the roll motion will be of great importance.[10]

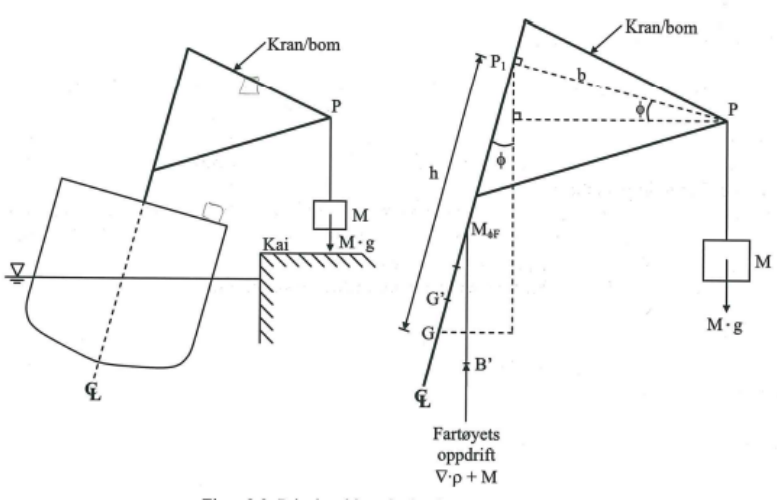

Figure 2.3: Principal sketch of a crane vessel. [10]

The behaviour, such as stability and relative motions, of the crane vessel is highly dependable of what kind of vessel and lifting method that is used. Further in this thesis the cases of a floating crane vessel and a jack-up crane vessels response motions during blade installation of a offshore wind turbine will be analysed and compared.

2.4 Operational Environmental Limits for the Jack-Up Vessel

In general the operational limits are low for the blade installation, and especially during the lowering and retrieval of the jack-up legs. It is found that the limiting sea states for blade root mating are especially low when the wind and wave direction is aligned, and increasing with with misalignment in the wind-wave condition [20]. Further, the study shows that the wave spectral peak period is essential for estimating limiting the sea states. This parameter is significantly influencing the monopiles vibrations, and therefore increasing the relative motions between the crane hook and the hub. This is a critical stage in the operation, and following will the wave spectral peak period be a critical value for deciding the limiting operational weather window [20]. In the following table typical values for the operational limits for installation of offshore wind turbines using a jack-up vessel is listed.

Table 2.2: Operational limits for jack-up vessels in transit and operating condition [4].

	Transit condition		Operating condition	
Capacity [t]	Speed [knots]	Wave height [m]	Wave height [m]	Wind speed [m/s]
800-1500	12	3.0	2.5	16
800	4	2.5	1.65	16

2.5 Operational Environmental Limits for the Semi-submersible

The significant wave height is normally used as the parameter for the operational limit for a regular marine operation. When using a SSCV for the single blade installation, the motion are affected by the incident waves, which will affect the blade motion. Therefore, for this type of marine operation, will the wave period and the wave direction be important parameters when analysing the operational limits, in addition to Hs. In the study *"Assessment of operational environmental limits for offshore single blade installation using response-based criteria"* conducted by Zhao, Y. et al. (2019) [5], the operational environmental limits for a single blade installation on a bottom-fixed offshore wind turbine with a jacket as foundation was analysed by the use of a SSCV. The

analyse was based on a fully coupled numerical model. Table 2.3 shows the results from the study for allowable significant wave heights for varying wind velocities and two different wave periods. The criteria used to decide if the mating attempt should be executed or not is decided by the mating gap. The mating gap is the difference between the blade root radius and the hub radius, and is defined in Equation 2.5.0.1. For the results presented in Table 2.3, the acceptable mating gap, r, is $0.2R_{root}$. The study also proved that when the mating gap radius increased, so did the allowable limits for the motion monitoring phase (step 4). When mating gap radius, r, increased from $0.1R_{root}$ to $0.2R_{root}$ the allowable significant wave height doubled for $T_P = 8$ s and wind velocities, U_{wind}, 6m/s to 12m/s.

$$r = \lambda R_{root} \tag{2.5.0.1}$$

Table 2.3: Allowable limit for the significant wave height, H_s, with different wind velocities, U_{wind}, and wave periods ,T_P [5].

		U_{wind}[m/s]					
		2 m/s	4 m/s	6 m/s	8 m/s	10 m/s	12 m/s
T_P	8 sec	1.72m	1.86m	1.92m	1.92m	1.96m	1.97m
	12 sec	0.31m	0.41m	0.48m	0.51m	0.55m	0.58m

The study also found that the mating attempt is safe to perform for short waves with $T_P \leq 6$ s and $H_s = 3$m and $U_{wind} = 12$m/s. It also shows that when T_P increases, the allowable limit for H_S decreases rapidly. Table 2.3 also shows that for a wave period, T_P, equal to 8 seconds, the allowable limit for the significant wave height is mainly below 1 meter, except for some wind velocities. For $T_P = 12$ s, the allowable significant wave height for the mating attempt is approximately 0.5 meters.

Chapter 3

Installation of offshore wind turbine blades

3.1 Installation methods

3.1.1 General

There are different aspects one have to consider when determining which of the installation methods are best for the specific case. The feasible solution depends on a set of parameters; the environment the installation will take place in, the size of the turbine, crane vessel size and availability, number of lifts and distance from port to offshore site are some of them. Recently, the method of assembling at the offshore site is frequently used as a consequence of the increasing turbine size. Which requires larger deck capacity, higher lifting heights and increased crane capacity.[35]

In general there are six different installation vessels that mainly are used for installation of offshore wind turbines. In Figure 3.1, the most common installation vessels for offshore wind turbines are illustrated. For the different installations methods there are needs for different numbers and types of assisting vessels, which have to be considered in terms of availability and costs. Recently the jack-up crane vessels is the most popular installation vessel for offshore wind turbines, due to the possibility of a stable platform during the crane operations. For the jack-up vessels the water depth is a limiting factor. As new sites at deeper waters is to be explored, the possibility of using a floating installation vessel should be considered. [35]

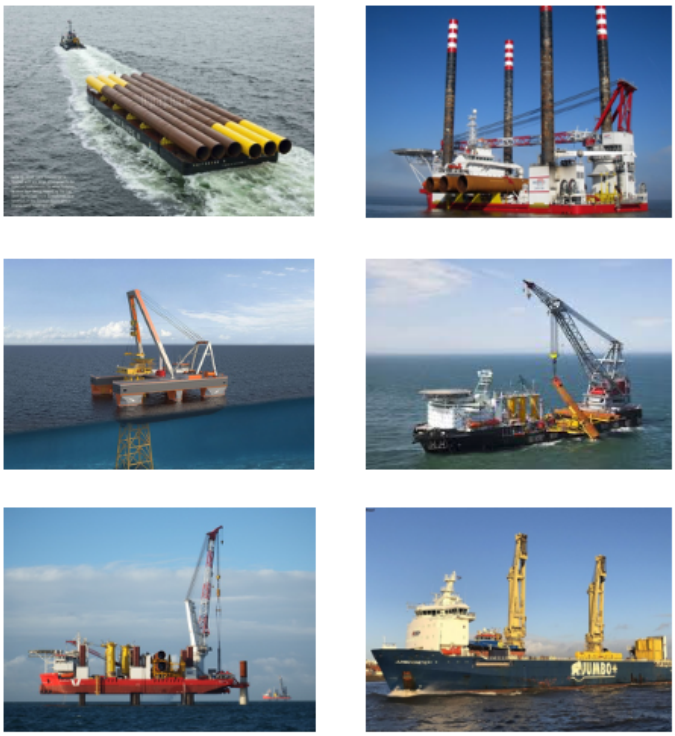

Figure 3.1: Installation vessels used for installation of offshore wind turbines. Top left) Towed Barge [11] Top Right) Jack-Up Crane Barge [12] Mid Left) Semi-Submersible Heavy Lift Vessel [13] Mid Right) Sheer-Leg Crane Vessel [14] Bottom left) Jack-Up Crane Vessel [15] Bottom Right) DP2 Heavy Lift Vessel. [16]

Factors such as turbine size, distance from port, water depth and environmental conditions plays a part in the choice of the installation method. The installation of the different parts of the wind turbine can be done with different type of vessels. Typically a jack-up structure or floating vessel is used for installation of monopiles. Jackets or tripods are most commonly transported on a barge, because of the huge storage demand. For gravity based structures they are usually towed, as the weight of these structures is to heavy for a barge. In Table 3.1, the type of installation vessels used for installation of offshore wind farms in Europe is listed with respective water depths.

Table 3.1: Vessels used in offshore wind farm construction in Europe.

Wind farm	Installation vessel	Water depth
The London Array	Jack-up Crane vessel	25m
Robin Rigg	Jack-up Crane Barge	35m
Walney Extension	SSCV	30m
	Jack-up crane Vessel	
Rampion	Jack-up Vessel	19-40m
Race bank	Jack-up Vessel	12-22m
Borkum Riffergrund 2	Jack-Up Vessel	25m
Arkona Wind Park	Barge + Tug boat	37m
	DP2 Lifting Vessel	
	Jack-up Vessel	
Wikinger	Barge + Tug Boat	42m
	Sheerleg Crane Vessel	
Horn Rev 3	DP 2 Lifting vessel	20m
	Jack-up Crane Vessel	

Table 3.1 show that the jack-up vessels are the most commonly used installation vessel for offshore

wind farms. Further, floating vessel typically is used at sites with greater water depths. There is also different methods for installation of blades in offshore wind farms. Some of which is illustrated in Figure 3.2 and compared with number of lifts. Recently the "single blade installation" method has been the most common. This mainly due to the increase in turbine size. The method requires smaller deck capacity, which is good as the offshore sites recently tend to be located further away from production site. Another benefit is that the blade orientation during installation is flexible, which gives the opportunity of minimizing the energy extraction from the wind during installation.[6]

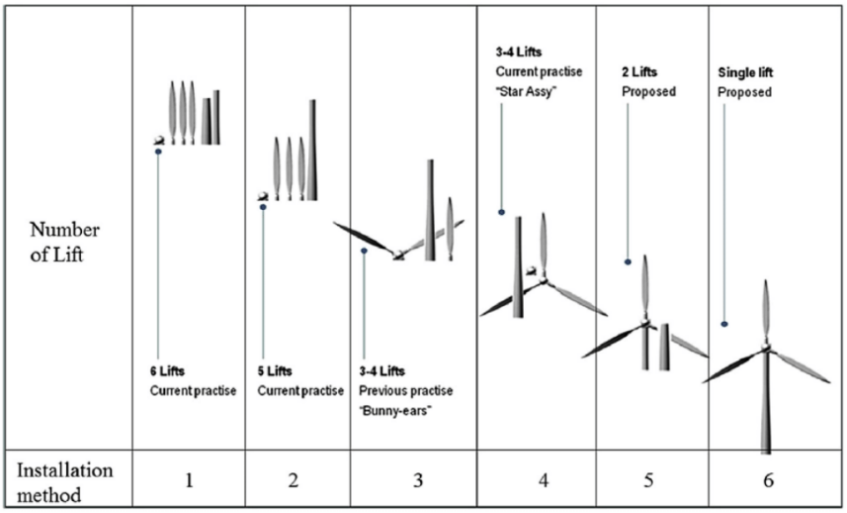

Figure 3.2: Comparison of the different installation methods of wind turbines with number of lifts.

Another aspect that has to be taken into account when choosing installation method is the time efficiency. As explained earlier, the installation has to be planned with regards to the time duration of the operation. If the operation is classified as weather restricted or weather unrestricted, determines a set of rules and regulations the operation has to be planned according to.

Table 3.2: Installation duration and rate for different wind farms in Europe.

Installation Method	# vessels	Duration [months]	# turbines	Installation rate [days/turbine]	Wind farm
Jack-Up Vessel	2	9	58	4.5 (9.0)	Robin Rigg
Jack-Up Barge	2	3	30	3.0 (6.0)	North Hoyle
Sheerleg Crane Vessel	2	1.25	20	1.9 (3.8)	Middelgrunden
DP2 Lifting Vessel	2		49		Horn Rev 3

3.1.2 Single-blade installation

In the following section a "step by step" description of the single blade installation method is provided with associated pictures. This is to provide a greater understanding of the lifting procedure, and to identify the critical stages. Critical stages may change depending on the type of installation vessel that is used. In the pictures below, a jack-up crane vessel is used. However, the general steps for the procedure will be approximately the same regardless of the installation vessel. Overall, the main equipment needed for an offshore single blade installation are the crane vessel, the wind turbine blade and the lifting arrangement. The lifting arrangement for the lifting procedure includes a lift wire, slings, yoke, hook and tugger lines [5]. Even though the steps are general for a jack-up vessel and a floating vessel, there are an important difference between the critical stages which needs to be identified and considered. In Section 3.3 and 3.4 the single blade

installation procedure with the use of a jack-up crane vessel, SSCV and the vessel specific critical stages will be identified and discussed.

Step 1: Lift the blade of the vessel deck

The first step is the lift-of from the vessel deck. This is in general a step that needs to be carefully analysed. As explained in Section 2.7, the lift-off is a critical phase where the system can induce huge motions and/or snap loads in the ropes. In order to reduce the motions, the blade is loaded into the yoke, and then lifted off the deck by the crane winch. The lift off of the yoke is illustrated in Figure 3.3[6].

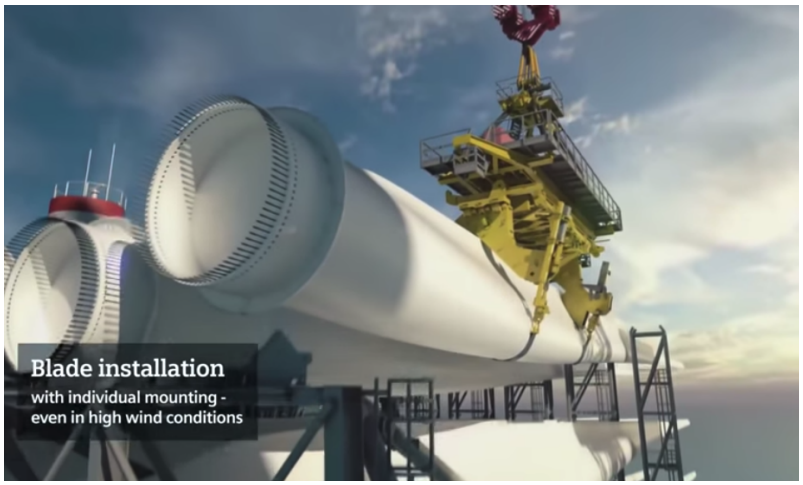

Figure 3.3: Step 1: Lift off from vessel deck. [17]

Step 2: Lift the blade to the hub height

The blade is lifted up to the hub height. The orientation of the blade is monitored by the pre-tensioned tugger lines. For single blade installation the blade orientation is flexible, and the blades can be installed both horizontal mounting, vertical mounting and inclined mounting. The horizontal mounting is generally preferred, as no rotation is required. Step 2 is illustrated in figure 3.5 [6].

Figure 3.4: Step 2: Lifting the blade to hub height. [17]

Step 3: Blade root approach the hub

When the blade is lifted to the installation height, the blade root is approaching the hub by the crane, where the blade is in a safe condition and the risk of impact is minimized.[6]

Figure 3.5: Step 3: The blade root approaches the hub. [17]

Step 4: Monitor the blade root motion

In this step the blade root motions is detected, and if the motions is small enough the mating of the blade and hub can begin. The procedure can not proceed if the motions are to large, in risk of damaging the assets. At the blade root there is a "guide pin" installed, to ensure that the relative orientation is correct for mating. Figure 3.6 shows an illustration of step 4[6].

Figure 3.6: Step 4: Monitor the blade root motion. [17]

Step 5: Mate the blade into the hub

The last step of the single blade installation is the physical mating of the blade root and the hub. This will be done when it is ensured that the motion of the blade root is within the safety limits. In a study by Zhengru, R. et al (2019) [36], the impact loads and consequences were analysed for the mating process. The results showed severe bending and plastic deformations of the guide pin bolt as well as failure of the adjoining composite laminate at the root connection. The final step and a sketch of the blade root with the guide pin is illustrated in Figure 3.7 [6].

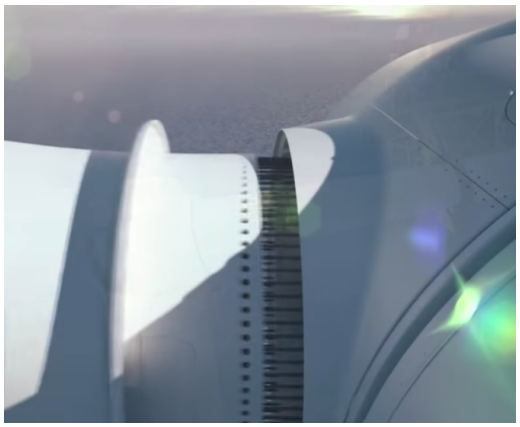

Figure 3.7: Step 5: Mate the blade into the hub. [17]

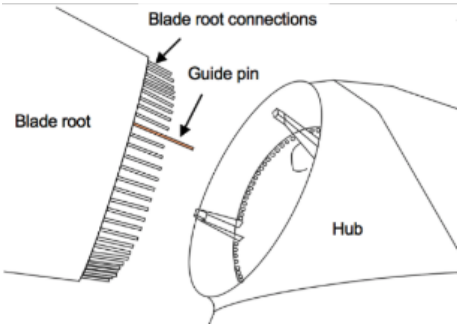

Figure 3.8: Sketch of the blade root and hub.

3.1.3 Critical Events and Limiting Response Parameters

All in all, the blade installation is the most challenging operation, compared with the other operation necessary for installation of an offshore wind turbine. In the blade installation operation, both step 4 and step 5 are considered critical steps among the steps described in Section 3.1.2. As mentioned step 5 will not be able to start if there are to big motions in step 4. The mating phase require high installation precision under rough conditions. At the large lifting height the motion between the turbine hub and the blade root are relatively large. If step 5 fails the risk of damaging the blade or the hub is high. Control and reduction of the blade motion during this phase is essential.

Zhao, Y. et al. (2019) [5] assessed the operational environmental limits for an offshore single blade installation procedure. In the process they identified and analysed the critical events and the corresponding limiting response parameters where. The study used a SSCV for the installation vessel. In the study they identified a critical event as when failure of mating occurred due to exaggerated motion radial to the blade root. The study identified the physical limit as the radial mating gap and the corresponding limiting parameter to be the radial direction for the blade root motion in the hub opening. The mating phase (step 5) would most likely not be successful if the blade root exceeded the mating boundary to often. When the blade root collide with the hub as they connect with each other, radial impacts are much more critical than axial impacts. Radial impact can lead to the critical event of bent guide pins. For this specific critical event, the physical limitation is that there should be no plastic deformation in the guide pins and the radial impact velocity is the limiting response parameter. Figure 3.9 shows an overview of the potential critical events, the corresponding limiting parameters and the allowable limits.

	Operation	Potential critical events	Limiting parameter	Allowable limit
Motion monitoring phase	- Align blade root with hub opening - Monitor blade root motion	- Failure of mating attempts due to excessive blade root relative to hub opening	- Radial motion of blade root relative to hub opening	- Radius of mating gap
Mating phase	- Mate blade root onto the hub	- Guide pins at blade root bent - Wire slack (restrictive)	- Radial impact velocity - Tension in tugger lines	- Established based on FEM analysis - Tugger lines always tensioned

Figure 3.9: An overview over the potential critical events, corresponding limiting parameters and allowable limits for the blade mating process (step 4 and 5). [5]

This thesis will in general study step 4 and step 5, for a jack-up crane vessel and a SSCV. With focus on numerical studies of installation vessels, and the dynamic response and coupled motion during the last two steps of the singe blade installation.

3.2 Installation Systems

The jack-up crane vessel and the SSCV that will be used in this analysis are presented in Figure 3.10 and 3.11, respectively. This section will describe the two installation systems and their challenges and advantages.

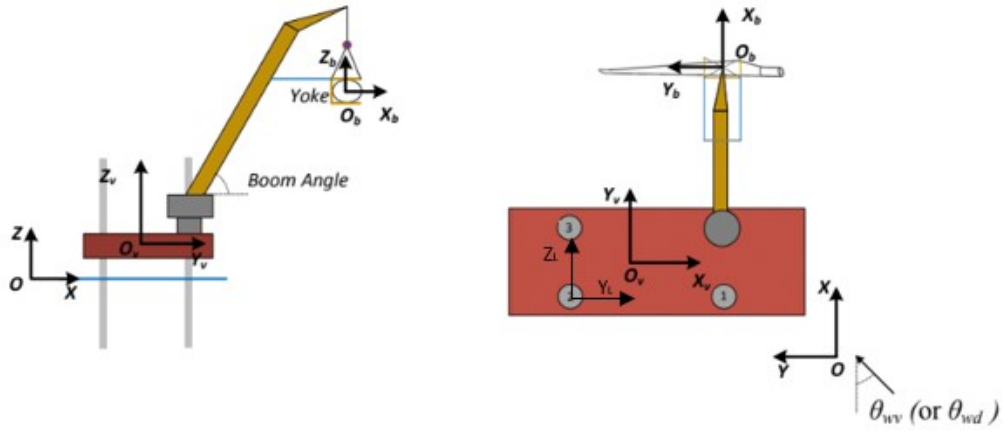

Figure 3.10: Illustration of the jack-up crane vessel. [6]

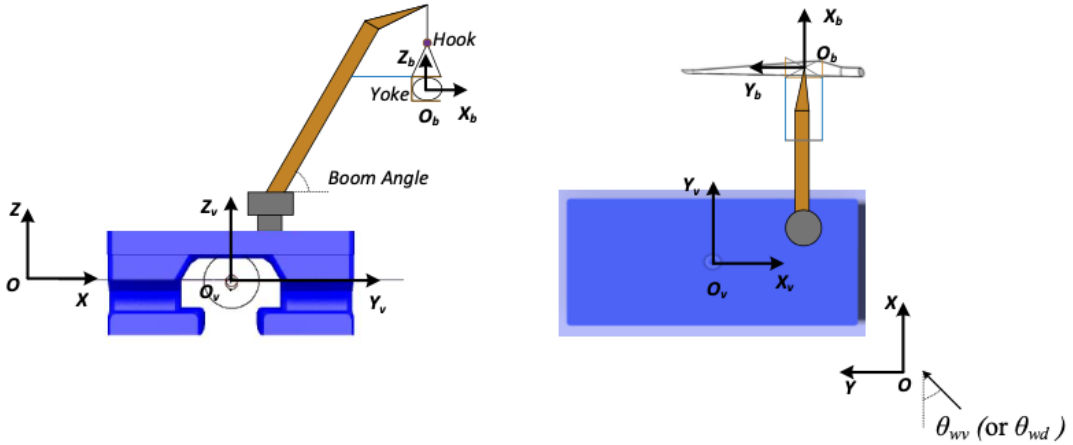

Figure 3.11: Illustration of the SSCV. [6]

3.2.1 The Jack-Up Crane Vessel

This section will introduce the jack-up crane vessel as a installation vessel for offshore wind turbines. In Figure 3.12 and 3.13 a jack-up vessel is illustrated both in transition and in operation. During a voyage the four flexible legs are withdrawn and the vessel is sailing as a normal vessel. During installation the legs are lowered, as illustrated in Figure 3.13 and the hull is above the waterline. This will create a stable platform, and reduce the relative motions in the system. Jack-up crane vessels have in the recent time been increasingly used for installation of offshore wind turbines. They were originally designed to operate in shallow water, at water depths around 30-50 meters[36]. How the jack-up vessel preforms in greater water depths is of huge interest. Fred Olsen Windcarrier,

which has a central role in the jack-up market, states that their jack-up vessels can operate year around in water depths up to 65m [37]. This can contribute to expansion of the offshore wind turbine market, as there will be more and larger areas suited and feasible for offshore wind fields.

Figure 3.12: Jack-up crane vessel in transition. [18]

Figure 3.13: Jack-up crane vessel in operation. [19]

In Table 3.3, the jack-up crane vessels used for installation of offshore wind farms with respective lifting capacity, maximum lifting height and maximum water depth are listed.

Table 3.3: Jack-up crane vessels used in installation of offshore wind farms [6].

Vessel	Max water depth [m]	Crane capacity [t]	Max Lifting height [m]	Wind Farm
Sea Installer	55	900	112	Race Bank (2017)
Bold Tern	60	800	120	Veja Mate (2017)
MPI Adventure	40	1000	105	Rampion (2017)
Seajacks Scylla	65	1500	104	Walney exstension

The procedure for a crane operation using a jack-up crane vessel is described in Figure 3.14. In addition to the procedure described in the previous section, the lowering and retrieving of the legs have to be taken into account. These are in principle time consuming processes, and have to be considered when calculating the time period for the operation. As this is a time consuming and critical process, it will both increase the needed weather window and reduce the operational limits for the operation. As well as the operational limits is stricter when the legs are being lowering and retrieved compared to transit and when acting as a stable platform.

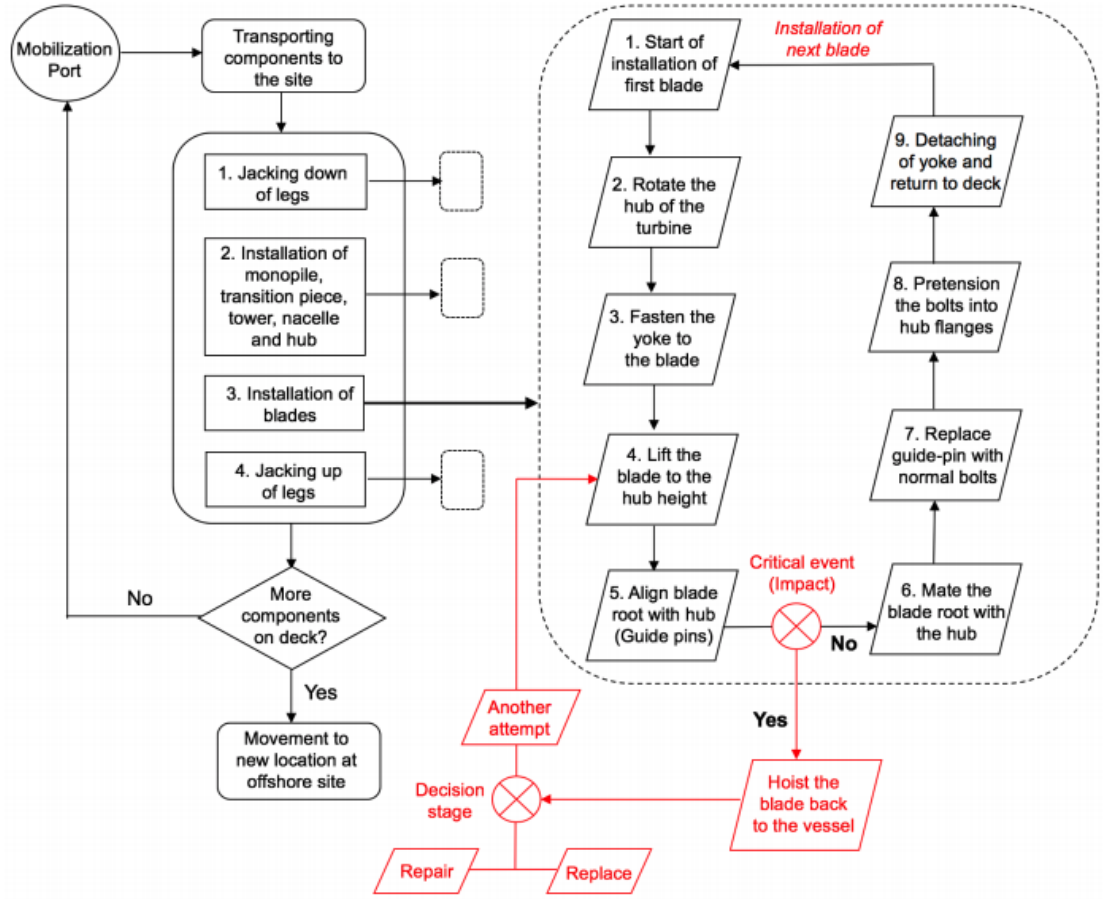

Figure 3.14: Detailed flow diagram describing the blade by blade installation using a Jack-up vessel. [20]

3.2.2 The Semi-Submersible Crane Vessel

The offshore wind turbine operations conducted with a floating vessel today are only installation of monopile foundations, installation of the assembly of the tower, rotor and nacelle and the tower-nacelle-rotor assembly for floating wind turbines. A floating vessel have never installed wind turbine blades. This is because, as mentioned earlier, single blade installation requires high precision and are therefore more challenging than the other components a offshore wind turbine consists of and are expensive operations. However, one may have to start taking use of floating vessels in the blade installation phase as the size continue to increase and the offshore wind turbines will be at deeper waters. Advantages the floating vessels has compared to a jack-up crane vessel are that they are very flexible with respect to water depth, they can operate on both intermediate and deep waters. In addition, they are much faster to relocate and they have more space on deck. However, due to the wave induced motion to the vessel, there are some operational challenges. There are mainly two types of floating installation vessels, the monohull crane vessel and the SSCV. The motion, especially the roll motion, of the SSCV is much smaller then the motion of monohull crane vessel. Hence, the SSCV has a higher operability. The focus on this thesis will therefore be on single blade installation using a SSCV. In the following sections, the configuration and challenges for single blade installation by the use of a SSCV will be described. [38]

The lifting operation for a rotor blade by a SSCV is similar as for the use of a jack-up vessel. Anyhow, the SSCV experiences more challenges and are less operable than the jack-up vessel. This is due to the fact that the floating vessel are directly influenced by the waves, where the jack-up vessel is elevated above the sea surface by its four legs. This wave-induced motion will affect the motion of the blade, which will make the mating phase more difficult, especially at such

large lifting heights. Therefore it is important to do a thorough analysis to obtain the allowable sea states and environmental condition for the installation process.

The SSCV consists of two longitudinal pontoons, which are totally submerged, and six vertical columns that connect the pontoons with the main deck. The SSCVs displacement is $\frac{3}{5}$ more than for a monohull which makes it much more stable and resistant to wave-induced motion. Floating installation vessels are also equipped with a dynamic positioning system or mooring lines to avoid the effects of slowly varying drift motions and to keep the vessel from moving with the wave as much as possible, the SSCV is illustrated in Figure 3.11.

Chapter 4

Numerical Modeling of the Environmental Loads

4.1 General

During operation, the installation system will be exposed to environmental loads. Wind loads will work on the lifted blade as well as the jack-up hull. Further, hydrodynamic loads will act on the legs of the jack-up vessel and on the hull of the floating vessel. The jack-up vessel will also experience soil reaction forces as the legs are penetrating the seabed. In this chapter the numerical modeling of the external loads acting on the system will be described in detail for both the SSCV and the jack-up vessel.

The following figures are comparing the external loads and the structural model for the jack-up crane vessel and the SSCV. In Figure 4.1 the legs of the jack up crane vessel are modelled with a flexible crane and legs with soil interaction. This model is used for the hydrodynamic analysis. The soil-modelling has a big impact om the blade motions when exposed to wave loads. Figure 4.2 is illustrating the model for the SSCV.

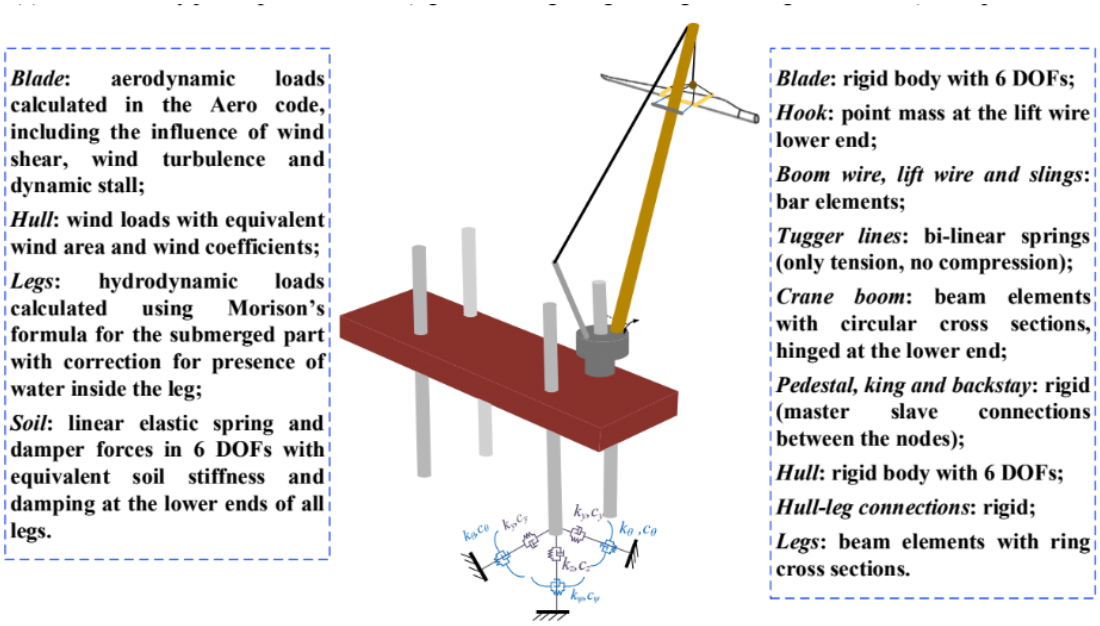

Figure 4.1: Numerical modelling by the jack-up crane vessel. [6]

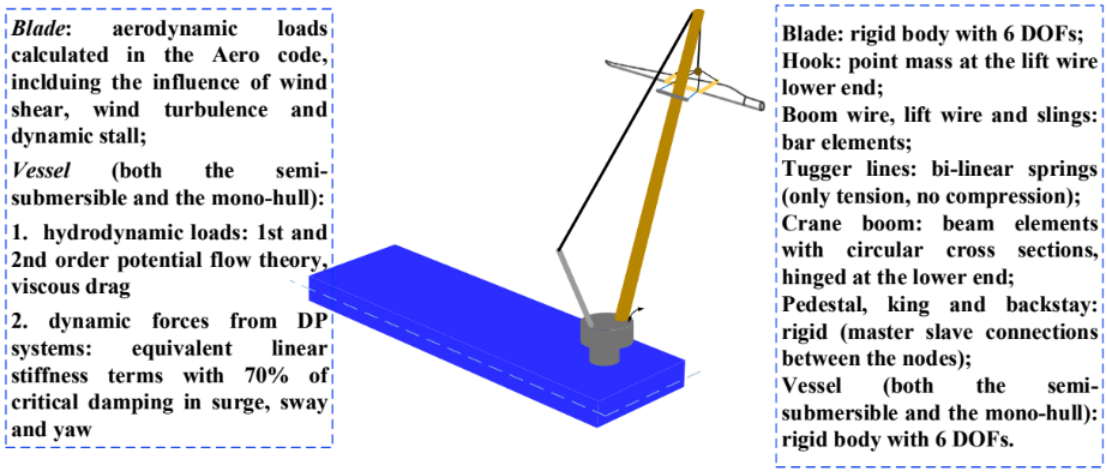

Figure 4.2: Numerical modelling by the SSCV. [6]

4.2 Aerodynamic loads

The aerodynamic loads are due to the wind forces acting on the installation system. Y. Zhao (2018) [6] developed an integrated simulation tool SIMO-Aero for the installation of single wind turbine blades. The code is based on the cross-flow principle, accounting shear forces, wind turbulence and dynamic stall. The aerodynamic loads are considered for the lifted blade and the jack-up hull. The wind loads on the floating vessel is neglected, as the wave forces will be the governing force contribution. For the aerodynamic load calculation the blade is divided into a number of elements which are modeled as foils. Then the aerodynamic loads components, drag and lift, for each element in the local coordinate system are calculated. The total aerodynamic load is the sum of all contributions and is acting in the blade center of gravity in the global coordinate system.

Figure 4.3 illustrates the blade orientation with a local blade element coordinate system, local blade coordinate system and the global coordinate system. The coordinate systems follows the right hand rule. The local blade is denoted O_b with the axis Z_b, Y_b and X_b. Z_b is positive upwards, Y_b is positive towards the blade tip parallel to the blade longitudinal axis and X_b is following the right hand rule. The origin for the local system is in the blades center of gravity. The global coordinate system is denoted O with the three axis Z,Y and X. Z is positive upwards, Y is positive towards tip blade tip and parallel to the longitudinal axis and X is following the right hand rule. The local blade element is a 2D foil and is denoted O_c with the axis X_c and Z_c. The origin for the blade element coincides with the blade elements origin in the X-position for all elements, while the Y-position depends on the location of the element.

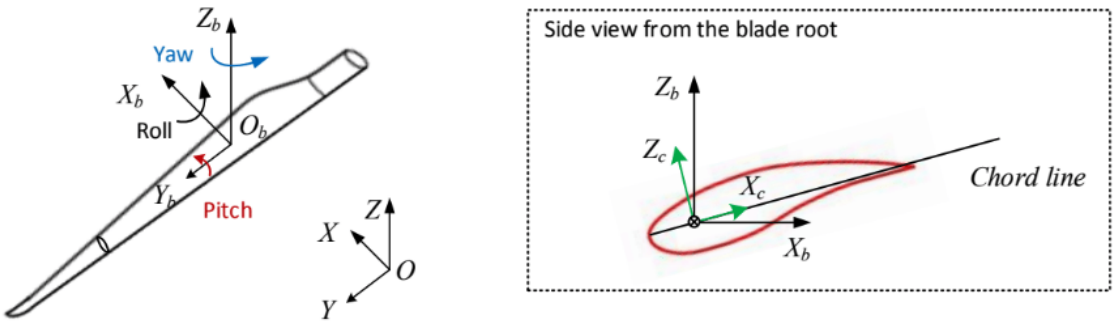

Figure 4.3: Illustration of the blade with three coordinate systems the local blade element, local blade and global coordinate system. [6]

4.2.1 Cross-flow principle

The cross-flow principle is based on the assumption that the blade element suits a 2D approximation. For each element, the aerodynamic load contribution is calculated and then summed up over all the elements to find the total load acting on the blade. In the following Figure [4.4] is the cross-flow principle with associated velocities and coordinate system illustrated.

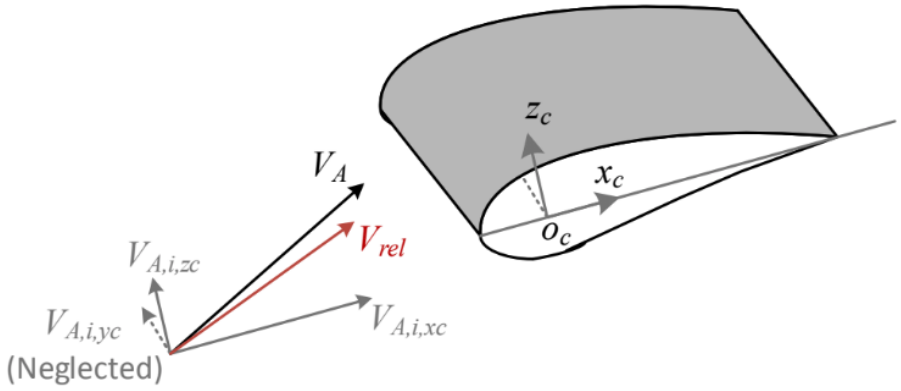

Figure 4.4: Illustration of a blade element with the cross-flow principle. [6]

As illustrated the inflow velocity normal to the blade is neglected, in this case this is the velocity in the local X-direction, following the cross-flow principle. Therefore the relative velocity can be expressed as follows:

$$\mathrm{V}_{rel} = \begin{bmatrix} V_{A,i,xc} & 0 & V_{A,i,zc} \end{bmatrix}^T \tag{4.2.1.1}$$

$V_{A,i,zc}$ and $V_{A,i,xc}$ is the inflow velocities normal to the Z and X axis respectively. This assumption is valid as long as the blade element suits a 2D model [39].

This assumption is valid for a blade during installation [39]. Compared to a blade during operation, it has quite different characteristics. For a rotating blade the rotational velocity has a large contribution to the V_{rel}. However, for a blade during installation the it is mainly the the inflow velocity that contributes to the relative velocity. The relative velocity for each element can be expressed as follows:

$$\mathrm{V}_{\mathrm{A},i} = \mathrm{T}_{GC,i}\left(\mathrm{V}_{\mathrm{WG},i} - \mathrm{V}_i + \mathrm{V}_{\mathrm{IG,i}}\right) \tag{4.2.1.2}$$

Where T_{GC_i} is the transformation matrix from the global system to the local blade element system, V_{WG_i} is the wind inflow velocity, V_i is the blade velocity and V_{IG_i} is the wake induced velocity. Because the blade motion is low during installation, the wake induced velocity will be of marginal significance and can therefore be neglected when calculating the aerodynamic forces on the blade during installation [39]. Following this assumption the relative inflow velocity at the blade element is expressed as following:

$$\mathrm{V}_{\mathrm{A},i} = \mathrm{T}_{GC,i}\left(\mathrm{V}_{\mathrm{WG},i} - \mathrm{V}_i\right) \tag{4.2.1.3}$$

Further, V_{Ai} is used to find the relative velocity V_{rel} which is used for further aerodynamic calculations. The next step in the calculations is to determine the angle of attack α. When you have the angle of attack, the drag coefficient C_D and lift coefficient C_L can be determined. To determine these coefficients, you can either look them up in 2D coefficient look-up tables or used The Beddoes-Leishman dynamic stall model.

4.2.2 Beddoes-Leishman dynamic stall model

The Beddoes-Leishman dynamic stall model was originally constructed in order to calculate the aerodynamic forces on helicopters in 1989 by Leishman and Beddoes, and later in 2006 adopted into calculations for wind turbines. The model consist of three parts, the unsteady attached flow, unsteady separated flow and the dynamic vortex build up and shedding. The unsteady attached flow consist of two contributions. One circulatory component and one impulsive component. The circulatory component is due to the change in the angle of attack while the impulsive component is due to the pitch moment and the rate of change in the angle of attack. Further, the separation of the flow is taken into account. Both due to the low and high pressure side of the foil and in relation to the leading and trail edge of the foil. The third part is the vortex build up and shedding contribution. This contribution is empirically modelled by using the normal force coefficient C_N from the attached and separated flow as an excess circulation. From this the drag coefficient and lift coefficient can be decided and aerodynamic load can be calculated.[6] [39]

When the angle of attack α and both the force coefficients are determined, the total aerodynamic force can be calculated. The contribution from each element is summed up and the total force has its point of attack in the center of gravity of the blade. In Figure 4.5 a flow chart of the total procedure of calculating the aerodynamic forces is described.

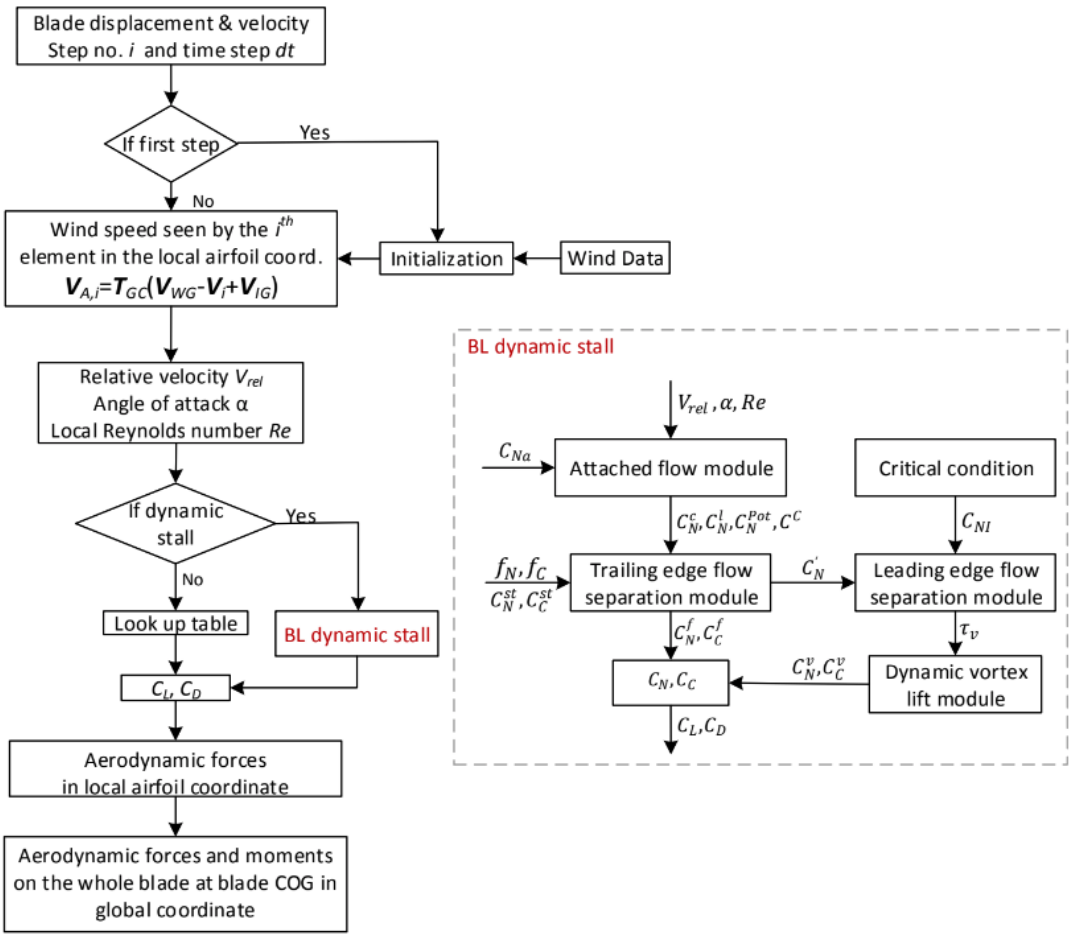

Figure 4.5: Flow chart of the aerodynamic load calculation. [6]

4.2.3 Aerodynamic Loads on the Jack-up Vessel

The wind loads on the jack-up hull have to be taken into consideration during operation. In principle, all components over the sea surface will contribute to the total aerodynamic force on the

system. This will for the jack-up be the part of the legs that's not submerged, the hull structure and the wind turbine components stored on deck.

Equations 4.2.3.1, 4.2.3.2 and 4.2.3.3 are used to obtain the wind load on components in respectively x-direction, y-direction and z-direction. As seen the wind loads are estimated based on a shape coefficient. These are in general hard to obtain correctly for each component. And important factor is that the coefficient is greatly affected by the shielding effects and interaction between the components, and therefore it will not be constant during the entire operation. To obtain wind area and shape coefficient with high accuracy, detailed testing can be conducted, e.g using wind tunnels. For the analysis in this thesis, the contribution from components below the hull baseline is neglected and the components above the hull baseline is considered as a block with equivalent shape and area coefficient. This follows the model in the from Zhao(2019) [6]. This simplification is acceptable as the motions of the jack-up vessel is dominated by wave-induced motions during installation. [6]

$$F_{x,wd} = \frac{1}{2}\rho_{air} C_S A V^2 \cos\alpha \tag{4.2.3.1}$$

$$F_{y,wd} = \frac{1}{2}\rho_{air} C_S A V^2 \sin\alpha \tag{4.2.3.2}$$

$$F_{z,wind} = 0 \tag{4.2.3.3}$$

Where ρ_{air} is the density of air, α is the relative inflow angle for the wind with respect to the hull, as illustrated in Figure 4.6. C_s is the overall shape coefficient, and is constant equal to 1.1. A is the area normal to the wind velocity, and can be calculated by the following equation, using geometrical correlations:

$$A = A_{xn}|\cos\alpha| + A_{yn}|\sin\alpha| \tag{4.2.3.4}$$

Where A_{xn} and A_{yn} is the areas normal to the local x-axis and y-axis respectively.

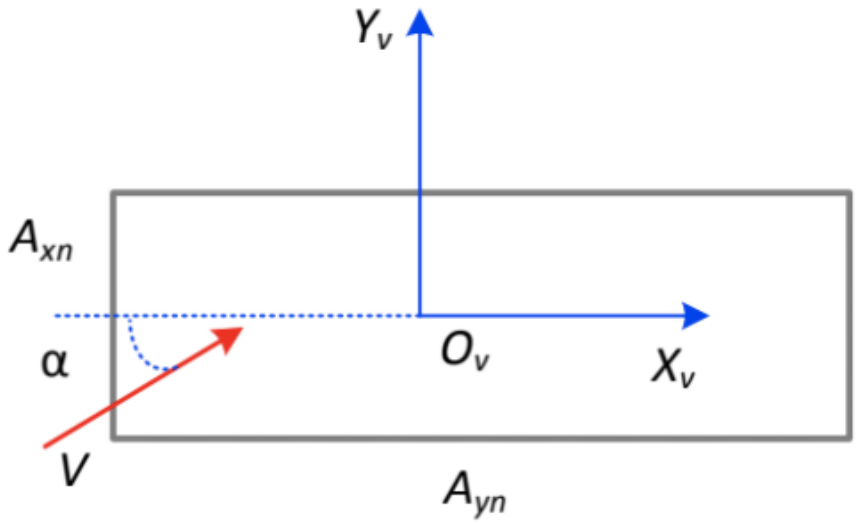

Figure 4.6: Aerodynamic loads on the jack-up hull. [6]

By this the resulting moments acting on the structure can be expressed as in the following equations 4.2.3.5, 4.2.3.6 and 4.2.3.7:

$$M_{x,wd} = -z_c F_{y,wd} \tag{4.2.3.5}$$

$$M_{y,wd} = z_c F_{x,wd} \tag{4.2.3.6}$$

$$M_{z,wd} = x_c F_{y,wd} - y_c F_{x,wd} \tag{4.2.3.7}$$

Where $[x_c y_c z_c]$ is the position vector for the center of equivalent wind block [6].

4.3 Environmental Loads on the Jack-Up Vessel

The jack-up crane hull is elevated during the installation phase, and the hydrodynamic loads are working on the jack-up legs. In this study, the model developed by Zhao et. Al (2018) [21] is used. This is a numerical model for calculation of the response during single blade installation of a wind turbine. The jack-up legs are modeled as beams, taking the structural flexibility and the soil reaction forces into account.

4.3.1 Wave Loads on Jack-up Legs

The wave loads acting on the jack-up legs can be calculated using Morisons equation. Morisons equation is an empirical formula to estimate the loads on a cylinder exposed to waves. The formula is based on the principle of super positioning of two terms. One term which is in phase with the acceleration and related to the mass and added mass of the structure. The other term is in phase with the velocity and is related to the drag forces on the structure. Using both terms Morison's formula is taking second-order forces into account [40]. The jack-up model with acting wave forces is illustrated in Figure 4.7.

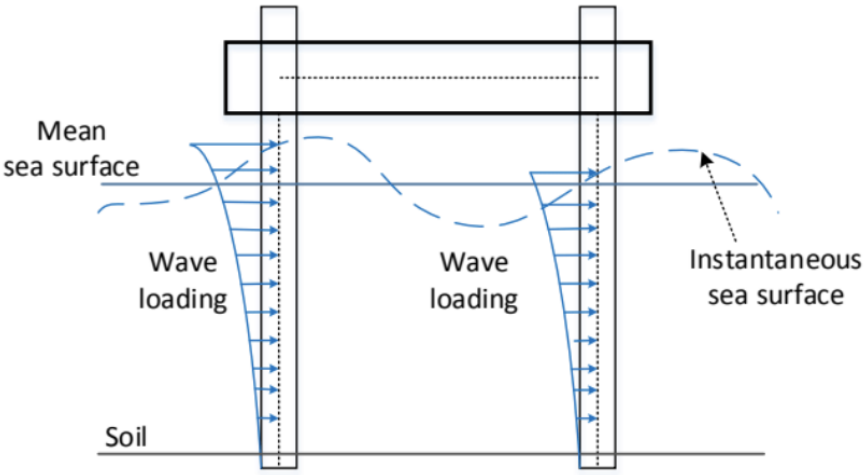

Figure 4.7: Wave loads acting on the jack-up legs. [6]

Equation 4.3.1.1 is Morisons equation as it is expressed in the SIMO-model. The limitations of Morison's equation is that the structure is assumed slender, i.e. D/L<5 which for the case for jack-up legs is true.

$$\begin{aligned} \mathrm{F} = \int_{-h}^{\eta} \Big[& \rho A_{ext} \left(1 + C_A\right) \dot{\mathrm{u}}(z) - \rho A_{ext} C_A \ddot{\mathrm{r}}(z) + \frac{1}{2} \rho D_{ext} C_D |\mathrm{u}(z) \\ & - \dot{r}(z)|(\mathrm{u}(z) - \dot{\mathrm{r}}(z)) - \rho A_{int} \ddot{\mathrm{r}}(z)\Big] \, dz \end{aligned} \tag{4.3.1.1}$$

In Equation 4.3.1.1 the integration limits are "-h", which denotes the sea floor, where "h" is the water depth, and "η" is the height of the wave crest. Further, ρ is the density of water, A_{ext} and A_{int} is respectively the external and internal cross-section area of the leg. C_A and C_D is 2D non-dimensional coefficients for the added mass and quadratic drag, respectively. The vectors u(z) and r(z) is respectively the velocity vector of the undistributed wave field and the response vector of the leg. The last term is taking the effect of water inside the leg into account [21].

4.3.2 PΔ-influence

When the jack-up legs are exposed to the wave loads, a part of the response motion will be a translation in the horizontal plane. The jack-up hull is rigidly fixed to the legs, therefore the hull will follow the motions of the upper part of the legs. This will induce an extra moment working on the structure, as the line of attack of the soil reaction force no longer is in line with the center of the hull-leg connection. Inclination of the legs introduce eccentricity between the hull-leg connection and the soil reaction force. This is another effect that causes extra moment in the hull-leg connections. The P-Δ-effect and leg inclination are illustrated in Figure 4.8.

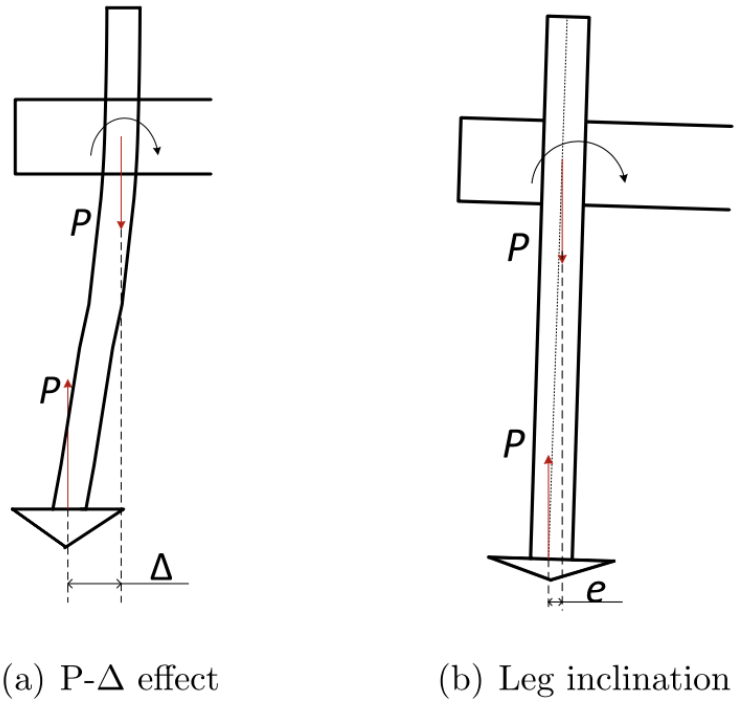

Figure 4.8: Illustration of P-Δ effect and leg inclination. [21]

Both of these effects are taken into account in RIFLEX, by use of the non-linear geometry feature in the finite element model [21].

4.3.3 Soil Structure Interaction Model

The soil-structure interaction will affect the response in the jack-up legs. In Figure 4.9 the part of the leg penetrating the sea bed is illustrated with the model that will be used in the analysis further in this thesis. [6]

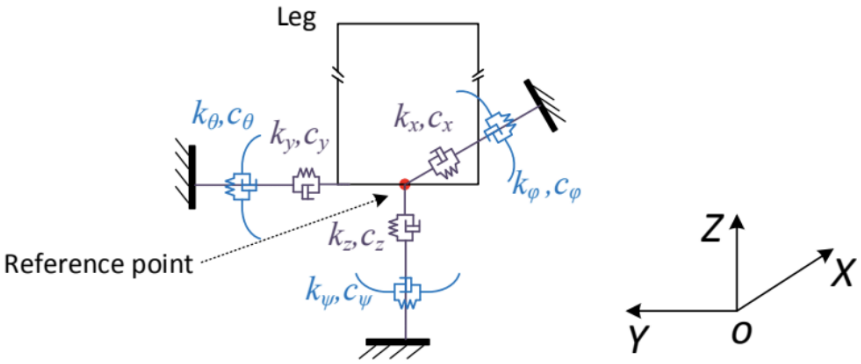

Figure 4.9: Illustration of the the soil interaction model. [6]

In Figure 4.9 the soil-leg interaction is modeled as a combined linear spring and damper model. Because of the frequently re-positioning of the jack-up vessels used for installation of offshore wind turbines, compared to the ones used for installation of offshore platforms, will have shallower soil penetration. A consequence of this is that the operations require lower sea states. As a results of these two factors the soil reaction force will be governed by elastic behavior [41]. By the use of equivalent linear elastic springs and dampers, it is possible to account for site-specific soil characteristics which have been found to be vital for accurate results in the dynamic analysis.

As seen in Figure 4.9, linear springs and dampers with six DOFs in the reference point are used to model the soil resistance force. The reference point is located at the lower end of the jack-up leg, just above the seafloor, where the spudcans are located. The reaction force is derived from the dynamic equation of motion, and expressed as following:

$$\mathbf{F}_s = \mathbf{K_s}\mathbf{X}_{\text{sc}} + \mathbf{C}_{\text{s}}\dot{\mathbf{X}}_{\text{sc}} \tag{4.3.3.1}$$

Where the excitation force $\mathbf{F}_s$ is the soil reaction force. $\mathbf{K_s}$ is the soil stiffness vector for all the six DOFs, without considering coupling effects. The stiffness coefficient will vary with the soil penetration and site-specific soil characteristics. $\mathbf{C}_{\text{s}}$ is the corresponding soil damping vector. $\mathbf{X}_{\text{sc}}$ is the displacement vector in the reference point, including the six DOFs. The dot represent the time derivative of the vector. All the components of the $\mathbf{X}_{\text{sc}}$ vector are written out in the following equation 4.3.3.2:

$$\mathbf{X}_{\text{sc}} = \begin{bmatrix} x & y & z & \phi & \theta & \psi \end{bmatrix} \tag{4.3.3.2}$$

Where x, y and z represent the three translations and ϕ, θ and ψ represent the three rotation motions in a six DOF reference frame at the reference point.

Soil-structure Interaction

It has been found that the jack-up vessel motion is highly dependent on the soil-structure interactions [6]. Zhao (2019) [6] compared the response motion of the jack-up vessels with different models for the soil-interactions. In Figure 4.10 the results Zhao (2019) gained are presented. In Figure 4.10 (a) it is clear that the effect of soil modelling is significant. When modeling the foundation as pinned too large motions occur, as a result of shifting the natural periods of the vessel motions closer to the wave frequency, as seen in Figure 4.10 (b). When using the fixed model, too small motions occur and either of the two models can be verified as accurate [6]. The response is also different in clay and sand. The results in 4.10 shows the importance of site specific modelling of the soil for installation using a jack-up vessel.

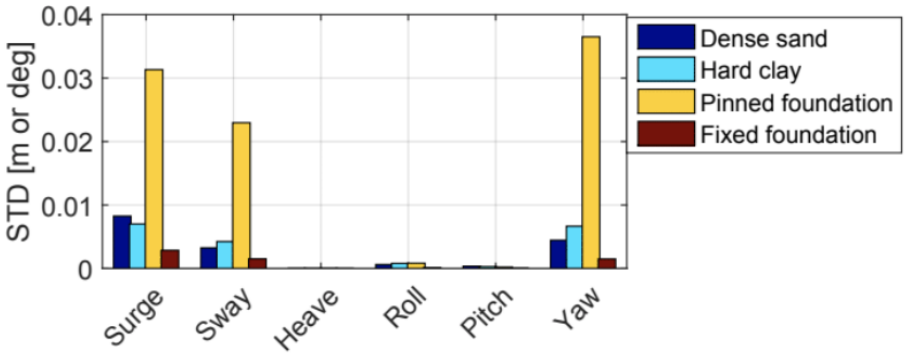

(a) Standard deviations

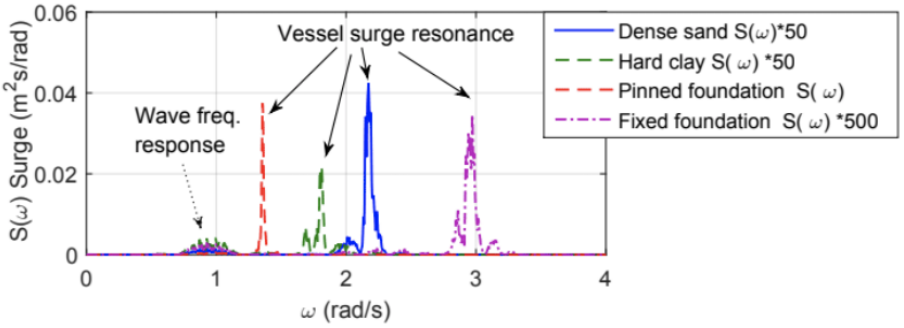

(b) Power spectra of the surge motion [112]

Figure 4.10: Standard deviations and power spectra of jack-up vessel motion with different soil models. [6]

4.4 Hydrodynamic Loads on the SSCV

The wave excitation forces acting on the SSCV are from both first-order and second-order, hydrodynamic forces, and are calculated based on potential flow theory. These wave excitation forces causes the SSCV to move in all six DOFs. The following chapter will describe the different forces acting on the SSCV.

4.4.1 First-order potential flow model

The first-order wave excitation forces are calculated based on the first-order potential flow model. These hydrodynamic forces employs the linear wave theory, frequently called the Airy wave theory. The hydrostatic coefficients added mass, A(ω), the potential damping coefficient, C(ω), and the

first-order wave excitation are dependent only on the frequency and are therefore calculated in the frequency domain. Y. Zhao (2019)[6] stated that the viscous roll damping is found by a damping ratio equal to 3%.

First-order wave theory

Linear wave theory is used to describe the waves. This is a linearised description of propagating gravity waves where the flow is assumed inviscid, incompressible and irrotational. Due to linearity, super-positioning of multiple regular waves with different frequencies are used to model irregular sea.

$$\phi = \frac{g\zeta_a}{\omega}\frac{cosh[k(z+h)]}{cosh(kh)}cos(\omega t - kx) \tag{4.4.1.1}$$

Equation 4.4.1.1 describes the velocity potential according to linear wave theory. ζ_a is the wave amplitude, ω is the wave frequency, g is the gravity, k is the wave number which depends on the wave length, $k = \frac{2\pi}{\lambda}$, where λ is the wave length, L as illustrated in Figure 4.11. h is the water depth and z is distance from sea surface. This equation, together with the dispersion relation $\frac{\omega^2}{g} = ktanh(kh)$ are the basis for the pressure, velocity, acceleration for the linear wave shown in Figure 4.11.

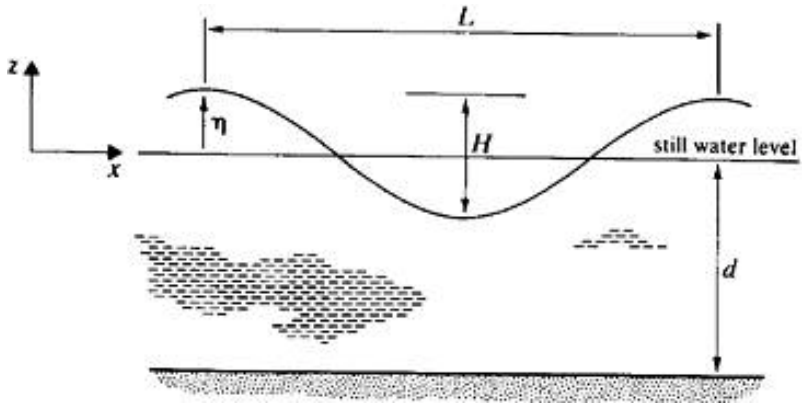

Figure 4.11: A linear wave. [10]

The linear wave theory is characterized by that the output (responses) is proportional with the input (wave excitations). The output is a linear combination of the single inputs. If the input is a harmonic load, then the output will be harmonic oscillations. If this do not apply, the system is non-linear and the outputs depends non-linearly on the input and the linear wave theory does not apply anymore. Linear wave theory can be calculated in the frequency domain since it is only dependent on the wave frequency.

4.4.2 Second-order Hydrodynamic Loads

As a result of the motion from the first-order hydrodynamic loads, the relative motion between the waves and the SSCV causes second-order effects which have an important impact on the SSCVs behaviour. The natural period for a SSCV is typical T $>$ 20 seconds, which means that the low frequencies are important. Hence, the second order effects becomes important to consider. Even though the second-order wave loads are small in magnitude compared to first-order wave loads, they will contribute to higher responses. This is because the SSCV will be exited only of the second-order wave loads as the difference-frequency wave loads might coincide with the natural frequency of the SSCV. The second-order wave loads also have a mean force component, mean wave drift force, which has to be balanced by the mooring system. The second-order wave components will be further described in the following section.

The solution of the second-order problem is mean forces, forces oscillating with difference frequencies wave excitations and with sum frequency wave excitations, in addition to the linear solution. This implies that the difference or the sum of two frequencies describing the wave spectrum are used. The second-order solution keeps all terms in the velocity potential that are either linear with the wave amplitude or proportional with the squared wave amplitude (1^{st}-order and 2^{nd}-order).

Non-linear effects from waves, current and wind interaction with the SSCV are mainly two types of contributions, slowly varying drift forces and mean drift forces. These motions occur more easily in the horizontal plane (therefore drift) because of the mooring lines and due to the large mass of the system. The mooring lines contributes to the restoring forces, which are simplified into equivalent linear stiffness in surge, sway and yaw. To eliminate the slowly varying motion, a system with damping ration 0.7 is applied (large damping) of the vessels damping motion in surge, sway and yaw [6]. These second-order forces exists in all six DOFs, and are important in shallow water.

Mean wave drift forces

Mean wave drift forces are one of the second-order wave force contributions acting on the semi-submersible. The reason a structure in regular incident harmonically oscillation waves is affected by horizontal mean wave forces is mainly because of the relative velocity between the structure and the waves. For a large-volume structure the body surface is sometimes in water and sometimes out of water. By investigating the pressure in one point in the surface zone, one can find that the mean pressure for the structure is non-zero, see Figure 4.12. This means that regular incident wave are modified by the large-volume structure and the vertical motion differs around the waterline and causes the mean pressure to be non-zero. One way to obtain the mean wave drift forces is by the direct pressure integration. By this method, the pressure along the instantaneous wetted surface of the body is integrated by Equation 4.4.2.1.

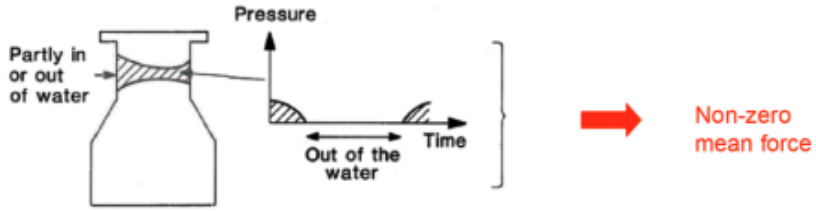

Figure 4.12: The mean value from second-order effects in variation of the wetted body surface. [22]

$$\mathbf{F} = \int_{S_B} p\mathbf{n}dS = -\rho \left(\frac{\partial \phi}{\partial t} + \frac{1}{2}|\nabla \phi|^2 + gz \right) \mathbf{ndS} \tag{4.4.2.1}$$

A semi-submersible will therefore generate mean wave forces which is important to include in the analysis. Second-order loads are also dependent of time, and the motion response can no longer be found by the excitation loads and a transfer function. The calculations has to be done by time domain analysis.

Slowly-varying drift forces

Slow drift forces are amplified oscillation (resonance) excited at low frequencies (difference frequencies) compared with the incident-wave frequency because of non-linear interactions. Generally for moored structures, the restoring forces causes the resonance period to be large for the horizontal motions, and slow-drift motions occur in the horizontal plane. Specifically for a moored semi-submersible, where the water plane area is small, the slow-drift motion can also occur in the vertical plane. The motion in vertical direction is due to the fact that the restoring terms in the

vertical plane are so small, which makes the natural period large. As a consequence slowly-varying drift motions can also occur in heave, roll and pitch. This means that slow-drift motion can occur in all six DOFs.

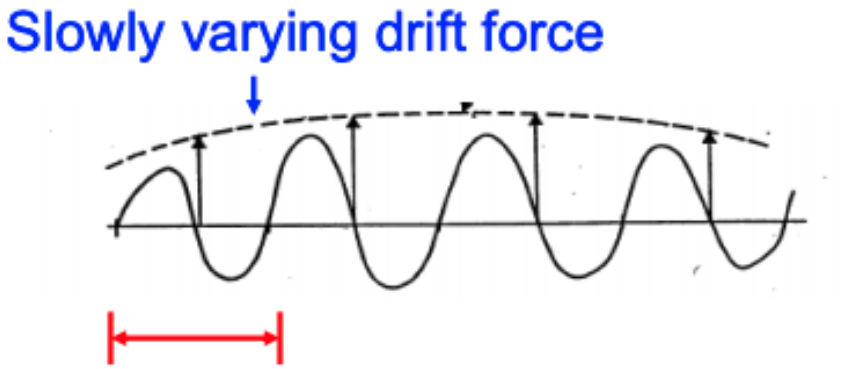

Figure 4.13: A slowly varying drift force. [22]

Figure 4.13 describes where the slow-drift excitation loads come from. These slowly-varying drift forces comes from irregular waves. By locally identify the irregular wave as an approximate regular wave. The second-order effects will cause a mean-drift force and with time, the approximate regular wave will have small changes in both wave amplitude and wave frequency, which will further lead to small changes in the mean-drift force. Therefore, the mean-drift force will slowly vary in time which gives the slowly-varying drift forces caused by irregular waves. [22]

4.4.3 The mooring lines

The SSCV is equipped with mooring lines to avoid drifting from site. The wave-frequency motion of the SSCV is a result from the first order wave loads. Because the mooring lines is designed such that the SSCV natural period is larger than the wave period, the mooring system is not influenced by the first order wave loads. This implies that the first-order wave loads does not excite resonance of the SSCV.

In general the inertial, the damping and the restoring effect from the mooring system influences the slowly-varying motions. Inertial forces will act on the mooring lines together with drag forces from the damping effect and impose a tension acting on the SSCV. This increase the SSCV slowly-varying motion. The stiffness from the mooring system comes from the restoring effects. Normally all these effects are included in the coupled analysis, but for marine operations the most important effect is the restoring effect. This is due to shallow water and therefore short mooring lines and low frequencies, which can be proved by the frequency domain method.

The frequency domain method, which is based on the fact that the response is proportional with the excitation and can be defined by a transformation function, as in Equation 4.4.3.1.

$$X(\omega) = H(\omega)F^{ext} \tag{4.4.3.1}$$

This frequency transformation function is found by the dynamic equation of motion:

$$-\omega^2 \left[M + A(\omega)\right] X(\omega) + +i\omega B(\omega)X(\omega) + C(\omega) = F^{exc}(\omega)$$

Where X(ω) is the response, F^{exc} is the excitation forces and then the transfer function, H(ω, is given by

$$H(\omega) = \frac{1}{-\omega^2 \left[M + A\right] + i\omega B + C}$$

From this and Equation 4.4.3.1, the response is then given by

$$X(\omega) = \frac{F^{exc}}{-\omega^2 [M + A] + i\omega B + C} \tag{4.4.3.2}$$

For very low frequencies, the damping and the mass term becomes negligible, and from this one can see that the restoring forces governs the solution.

For a semi-submersible, the natural period is very large, which means that the important frequencies are low, as mentioned before. Small frequencies gives small wave radiation linear damping. For moored structures, when the total damping gets small, large transverse amplification of the motion will occur near resonance. The presence of the mooring lines will employ large natural periods in the horizontal plane of the moored system. These natural periods will be much larger than the incident-wave period range. As a consequence of this, the resonance can be excited by second-order difference-frequency effects. Figure 4.14 shows the horizontal motions of a moored ship in irregular waves and the force in the anchor lines. The figure compares the waves and the horizontal motion, and from this one can see that the motion is slowly-varying, which can become large, and give large force in the anchor lines. The slowly-drift forces are important when designing the mooring lines.[22]

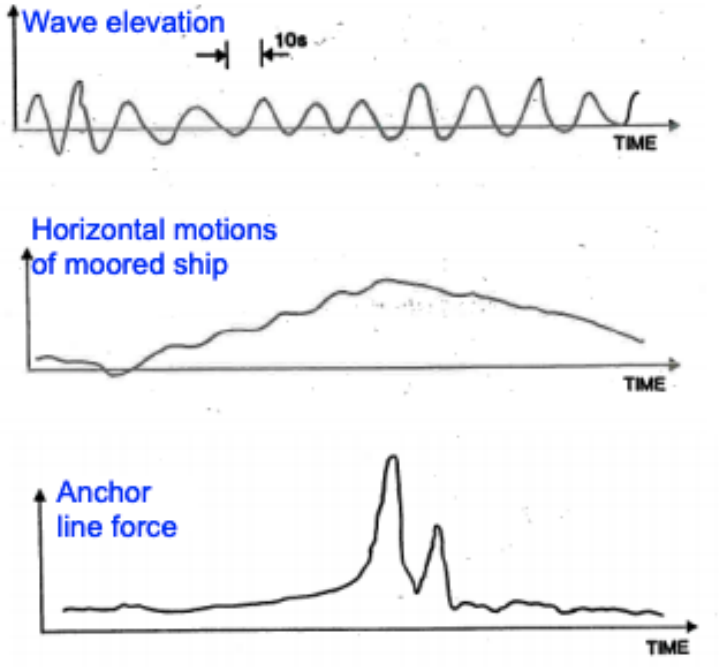

Figure 4.14: Representation of the horizontal motions of the moored ship and the anchor line force. [22]

4.5 Numerical Modelling and analysis of offshore wind turbine installation and guidelines

In order to analyse a marine operation, experience in various disciplines are required. Knowledge within structural mechanics, hydrodynamics, stochastic modeling and probabilistic design are necessary for developing numerical modelling procedure and computer code to simulate an operation [33]. Numerical modelling of a marine operation can give a realistic representation, and can significantly reduce risk during the execution phase because "what-if"-situations can be modelled. A complete marine operation is very challenging to model due to its complexity of several offshore

activities. Today, there exists multiple computer codes and software for simulation of the different aspects the operation, but each software have their own features and every code varies. This means that a combination of various computer codes are necessary to numerically model a marine operation, and the result will be an approximation of the actual dynamic responses.

Numerical modeling of the simulated marine operation can asses the dynamic responses. This can be done in two ways, by applying frequency domain or time domain, depending on the operation type. The frequency domain (FD) analyses the problems with respect to frequency rather than time. This means that the wave loads are defined by wave frequency and given by complex loads. Which means that the load value and phase shift compared with the incoming wave are described by both one real and one imaginary term. This method can be applied for a stationary system that is independent of time. On the other hand, by applying the time domain (TD) approach the structural response is calculated for each time step of the wave. The waves are defined with given wave periods and heights that propagates with time through the structure. Both analysis can be static and dynamic, but the time domain approach demands more computer power. Time domain approach is often used for non-linear systems with properties dependent of time. [42]

There exists different computer codes and digital tools to simulate different aspects of marine operations. The OrcaFlex software conducts dynamic analysis of offshore structures as pipelines, cables and umbilical installations [43]. A similar software, that also analyse pipelines, cables etc., is the OFFPIPE program, which is a finite element method based computer program [44]. DNV has a software package called SESAM, this package consists both of Wamit and Wadam, among many other. Wadam uses the frequency domain approach for hydrodynamic analysis and 3D diffraction theory employing a panel method and Morrison equation [45]. Wamit, on the other hand, analysis wave interactions with complex structures and does a second-order, non-linear analysis [46]. Another software worth mention is the SACS (Structural Analysis and Design Software) [44]. This software does analysis and design of offshore structures in the oil and gas industry and for wind farms. Lastly, the MARINTEK owned software, SIMA. This package includes amongst others, the software SIMO and Riflex. The Riflex software computes static and dynamic analysis of slender marine structures [47]. SIMO is a simulation program for non-linear motions and employs the time domain approach. SIMO simulates motion and station keeping of multi-body systems and other marine operations [48]. The analysis that will be conducted in the next phase of this thesis will use the software SIMA. A coupled analysis between SIMA and RIFLEX will be conducted, where the hydrostatic coefficients are calculated in Hydro-code and the wind forces acting on the turbine blade are calculated in Aero.

When installing an offshore wind turbine, the wind turbine is not in its permanent condition. Safety and efficiency are crucial for the operation, and some guidelines are developed to ensure the safety of the crew and the installation system. Therefore all planning and execution of all marine operations are based on specific regulations and standards. The standards covering marine operations are called VMO standards and include DNV-OS-H101, DNV-OS-H102 and DNV-OS-H201. The aim for these standards is to ensure a probability for structural failure less than $\frac{1}{1000}$ per operation [3]. ISO 29400:2015 [49] and DNVGL-ST-0054 [50] are standards that have been developed in the recent years, specific for installation and transportation of offshore wind turbines.

Chapter 5

Coupled Response Analysis

This section will introduce the method used for the dynamic response analysis of the installation system presented in Section 3.2. A fully coupled SIMO-RIFLEX-Aero method is developed by Y. Zhao (2019) for single blade installation [6]. This chapter gives an overview of the coupled method and structural modeling of the installation system. The external forces acting on the blade installation system are hydrodynamic and aerodynamic loads, which results in relative motions between the blade and the hub during mating as well as tension in the lift wire and tugger lines.

The response analysis will be described for the jack-up vessel as the installation vessel and a SSCV as the installation vessel. For both installation procedures, the blade will be modeled as a rigid body with six DOFs and coupled by a lift wire to the crane tip. The blade as a rigid body is described before the response analysis is described for the jack-up vessel and SSCV respectively.

5.1 General

Systems that are included in a coupled dynamic response analysis are environmental modelling, large volume bodies, slender structures and small-volume bodies. The environmental effects are described by waves, wind and current. For the installation systems analysed in this thesis, the wind force is only acting on the blade and current is neglected. The waves are modelled by regular and irregular waves, which are acting directly on the SSCV and on the four slender legs that keep the jack-up hull elevated above the sea surface.

The large volume bodies are modelled as rigid body motion model with six DOFs, also called a "SIMO-body", and is usually defined as the floater. The interaction effect between the floating SSCV and the waves are described by frequency dependent hydrodynamic coefficients, as inertia, damping and excitation forces. These coefficients are obtained by an external hydrodynamic analysis program. For these frequency dependent coefficients to apply in the coupled dynamic response analysis, which is in the time domain, the coefficients as added mass and damping are converted to a retardation function, and a convolution integral includes the frequency dependent force. This introduces a memory effect in the time domain simulation. The time-domain solution will be described in more detail for both the jack-up vessel and the SSCV later in this chapter.

The slender structures in the system are modelled as many small finite elements, which makes a finite element system, and the FEM applies. The hydrodynamic forces are modelled with Morison equation, where the added mass and drag coefficient are specified for each element. The only slender structures where hydrostatic forces act in the systems analysed in this thesis is the four legs modelled in the jack-up vessel, and will be described in more detailed later in this chapter.

The environmental effects initiate motion in the whole system, which leads to loads in the interacting structures. In a coupled dynamic response analysis, the total loads from the slender structures, mooring lines or the four slender legs on the jack-up vessel, will transfer as a force acting on the

large body, the hull. These forces are able to include both 1st and 2nd order wave forces and a full interaction is included in the dynamic response analysis, because the floater motion and the slender structure motions are obtained simultaneously. The coupling between the hull and crane tip and the blade will be described in detail in a section below. [51].

5.2 Blade Motions

The coupling between the blade and the vessel is equal for both the jack-up vessel and the SSCV, and it is coupled by linear springs between the crane tip and the blade, see Figure 5.1. Where the blade has six DOFs and the crane tip only has three DOFs in the translation directions. The eigen frequencies of the rigid blade motion can be obtained by eigen frequency analysis. This is done by solving the eigenvalue problem. The eigenvalue problem is derived from the dynamic equation of motion, which is expressed in Equation 5.2.0.1.

$$\mathbf{M\ddot{r}} + \mathbf{C\dot{r}} + \mathbf{Kr} = 0 \tag{5.2.0.1}$$

When assuming harmonic loading, r can be expressed, differentiated as in equation 5.2.0.2, 5.2.0.3 and 5.2.0.4. Then the expression for r, $\dot{r}$ and $\ddot{r}$ can be used in equation 5.2.0.1:

$$r = \sin \omega t \tag{5.2.0.2}$$

$$\dot{r} = \omega \cdot \cos \omega t \tag{5.2.0.3}$$

$$\ddot{r} = -\omega^2 \cdot \sin \omega t \tag{5.2.0.4}$$

By assuming free oscillation and neglect the damping, the general eigenvalue problem is found. The determinant is set equal to zero to find the eigen frequency. The general eigenvalue problem and the special eigenvalue problem is expressed in equations 5.2.0.5 and 5.2.0.6 respectively.

$$[\mathbf{K} - \omega^2 \cdot \mathbf{M}]\mathbf{r} = 0 \tag{5.2.0.5}$$

$$[\mathbf{A} - \lambda \mathbf{I}]\mathbf{x} = 0 \tag{5.2.0.6}$$

Where K is the stiffness matrix, M is the mass matrix and ω is the eigenfrequency solved for in the general case. For the special case, Choleskys discretization are used to define a vector "x", to find matrix A, containing both the mass and stiffness properties. This is often simpler with regards to numerical solutions.

5.3 Jack-up Vessel

The installation system using a jack-up vessel is modeled as two rigid bodies, where the jack-up hull and crane are modeled as one rigid body and the blade is one rigid body with six DOFs. Further, the legs are modelled as flexible beams. When the installation system is exposed to external loads, it will lead to response motions. In Figure 5.1 the total installation system is illustrated, describing the modeling and the coupling model between the parts. In the next section both the modeling and the coupling are further described.

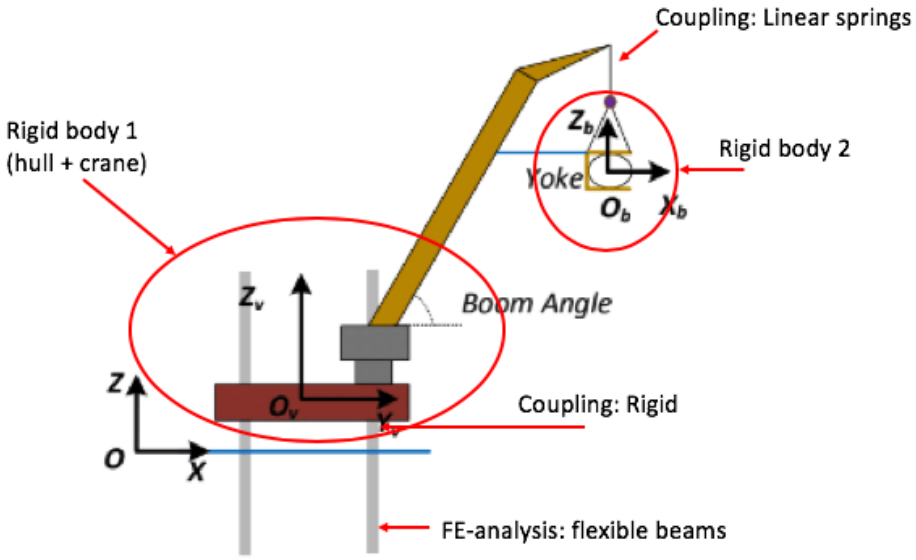

Figure 5.1: Illustration of the jack-up crane vessel model and the coupling.

5.3.1 Coupled Systems and Modeling

The response analysis is done by a coupled analysis of the jack-up structure. The legs are modelled as beams in order to take the structural flexibility into account. The connection between the legs and the hull is assumed to be rigid, this means that the hull will follow the wave induced motions at the legs [6]. Further, the jack-up hull and the crane boom are modeled as one rigid body. The boom wire and slings are represented by bar elements, accounting for axial tension. The lift wire couples the crane and the blade, and is modelled as a linear spring, which accounts for the stiffness in the crane. The relation describing the coupling between the blade and the crane is expressed as the following relation:

$$T = \begin{cases} k\Delta L, & \text{if} \quad \Delta L >= 0 \\ 0, & \text{otherwise} \end{cases} \tag{5.3.1.1}$$

Rayleigh Damping

The damping is a parameter that is hard to obtain exact values for. When analysing slender, marine structures the Rayleigh damping, also called the proportional damping model, is often used. The Rayleigh Damping is therefore a good modeling method for the damping of the jack-up legs. It is a coupling of a proportional relation between the mass and the damping and the stiffness and the damping. The Rayleigh Damping is expressed in Equation 5.3.1.2.

$$\mathbf{C} = \alpha_1 \cdot \mathbf{M} + \alpha_2 \cdot \mathbf{K} \tag{5.3.1.2}$$

With this relationship the damping matrix obtain the same orthogonal properties as the mass and stiffness, with relation to the eigen vectors,Φ, i.e. 5.3.1.3:

$$\Phi_i^T \mathbf{C} \Phi_j = \alpha_1 \Phi_i^T \mathbf{M} \Phi_j + \alpha_2 \Phi_i^T \mathbf{K} \Phi_j = 0 \tag{5.3.1.3}$$

From this the modal damping coefficients can be obtained by the following 5.3.1.4:

$$\bar{c}_i = \Phi_i^T \mathbf{C} \Phi_i = \alpha_1 \bar{m}_i + \alpha_2 \bar{k}_i \tag{5.3.1.4}$$

Further the modal damping is expressed by the damping ratio λ_i and the definition of the eigen frequency $\omega = \sqrt{k/m}$:

$$\lambda_i = \frac{\bar{c}_i}{2\bar{m}_i \omega_i} = \frac{1}{2}\left(\frac{\alpha_1}{\omega_1} + \alpha_2 \omega_1\right) \tag{5.3.1.5}$$

Where α_1 is the stiffness proportional term and damps out the lower mode shapes. α_2 is the mass proportional term and damps out the higher mode shapes. The dynamic response of marine systems is dominated by the lower mode shapes. Therefore, α_1 is commonly set to zero in structural analysis. In Figure 5.2 the damping ratio is graphically plotted as a function of the eigenfrequency. For α_1=0, the linear relationship follows the asymptotic value for the higher frequencies.

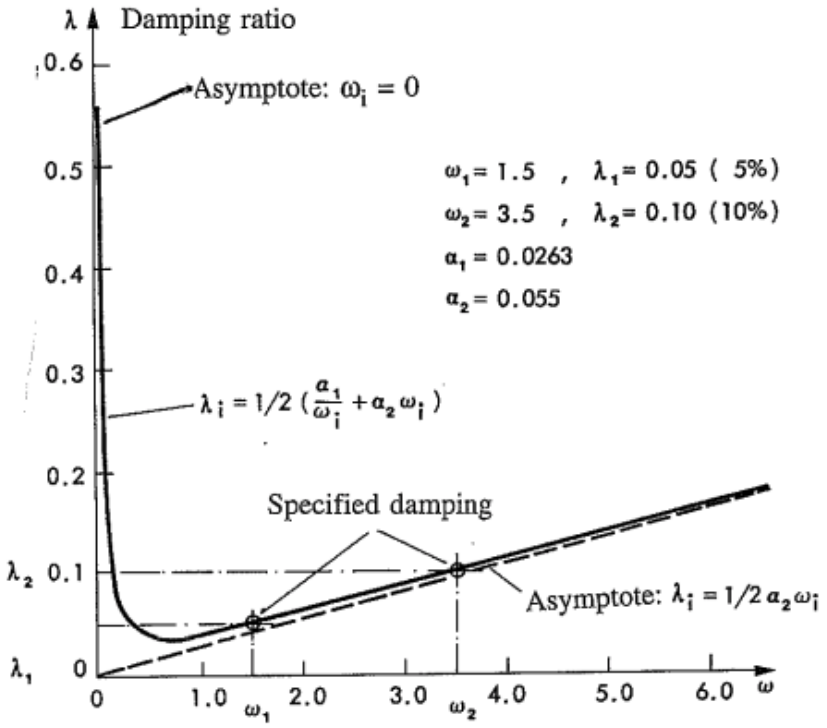

Figure 5.2: Damping as a function of eigenfrequency for proportional damping. [23]

To be sure not to underestimate the response, and get conservation results, the higher frequencies in the spectrum should be used to estimate the damping [23]. Specific for slender structures the coefficients are specified as α_1=0 and α_2=0.005 [6].

Natural periods of the system

The natural periods for the installation system are obtained by a regular wave analysis where the RAOs for the system was found. Since the installation system is a very complex system, the natural periods are found for each part of the installation system separately [6]. The natural periods are a property of the system, describing the characteristics of the response. Therefore the natural period of the system is often found before doing the response analysis, in order to have an indication of the frequency range for the response.

5.3.2 Dynamic Time Domain Analysis

The response of the jack-up installation system is found by a time-domain non-linear finite element analysis. This is done by applying iterative methods to solve the equation of motion. The dynamic equation of motion for a spatially discretized finite element system model can generally be expressed as following:

$$\mathbf{R^I}(\mathbf{r}, \ddot{\mathbf{r}}, \mathbf{t}) + \mathbf{R^D}(\mathbf{r}, \dot{\mathbf{r}}, \mathbf{t}) + \mathbf{R^S}(\mathbf{r}, \mathbf{t}) = \mathbf{R^E}(\mathbf{r}, \dot{\mathbf{r}}, \mathbf{t}) \tag{5.3.2.1}$$

Where:

- $\mathbf{R}^I$: Inertia Force Vector
- $\mathbf{R}^D$: Damping Force Vector
- $\mathbf{R}^S$: Internal Structural Reaction Force Vector
- $\mathbf{R}^E$: External Force Vector
- $\mathbf{r}$, $\dot{\mathbf{r}}$, $\ddot{\mathbf{r}}$: Structural Displacement, Velocity and Acceleration vectors

This is a nonlinear response analysis, as the relative motions between the external loads and the installation system are taken into account. The external loads working on the jack up structure are the hydrodynamic loads acting on the legs and the aerodynamic loads acting on the hull and the blade, these are thoroughly described in Chapter 4. To find the response, numerical time integration methods can be used. This can be done both by non-linear time domain analysis and linearized time domain analysis.

For the non-linear time domain analysis the incremental form of the dynamic equilibrium equation is obtain by considering two configuration within a short period of time. The expression will be as following 5.3.2.2:

$$\left(\boldsymbol{R}^I_{t+\Delta t} - \boldsymbol{R}^I_t\right) + \left(\boldsymbol{R}^D_{t+\Delta t} - \boldsymbol{R}^D_t\right) + \left(\boldsymbol{R}^S_{t+\Delta t} - \boldsymbol{R}^S_t\right) = \left(\boldsymbol{R}^E_{t+\Delta t} - \boldsymbol{R}^E_t\right) \tag{5.3.2.2}$$

In equation 5.3.2.2 the increment external loading is balanced by the increments of damping, inertia and stiffness over a time interval, Δt. For numerical solutions, the nonlinear incremental equation of motion is linearized by introducing the tangential mass, stiffness and damping at each time increment. The linearized incremental equation of motion is expressed as following:

$$M_t \Delta \ddot{r}_t + C_t \Delta \dot{r}_t + K_t \Delta r_t = \Delta R^E_t \tag{5.3.2.3}$$

Where $\mathbf{M}_t$, $\mathbf{C}_t$ and $\mathbf{K}_t$ is representing the tangential mass, damping and stiffness respectively, computed at a time t. $\Delta\dot{\mathbf{r}}$, $\Delta\ddot{\mathbf{r}}$ and $\Delta\mathbf{R}^E_t$ are the incremental displacement, velocity and external loading respectively. They are expressed as following.

$$\begin{aligned}
\Delta \boldsymbol{r}_t &= \boldsymbol{r}_{t+\Delta t} - \boldsymbol{r}_t \\
\Delta \dot{\boldsymbol{r}}_t &= \dot{\boldsymbol{r}}_{t+\Delta t} - \dot{\boldsymbol{r}}_t \\
\Delta \ddot{\boldsymbol{r}}_t &= \ddot{\boldsymbol{r}}_{t+\Delta t} - \ddot{\boldsymbol{r}}_t \\
\Delta \boldsymbol{R}^E_t &= \boldsymbol{R}^E_{t+\Delta t} - \boldsymbol{R}^E_t
\end{aligned} \tag{5.3.2.4}$$

It is assumed that the displacement and velocity at current time increment, the external loading at current and the next time increment is known. Then different integration methods can be applied, where an acceleration is assumed between the two time steps. The most common methods used are average acceleration, linear acceleration Newmarks method. The accuracy depends on the integration method and the integration step. Step-by-step time integration will then give the total response over a time period. [23]

5.4 The Semi-submersible Crane Vessel

The installation system consist of two rigid bodies. The floating semi-submersible and the crane are modeled as one rigid body with six DOFs, the blade is modeled as another rigid body with six DOFs, similar to the jack-up vessel. Different from the jack-up vessel is that the hull experiences the incident waves, and the vessel and the crane-tip experiences the same wave-induced motion. The relative motion between them are neglected, as the crane is fixed. The coupling between the crane-tip and the blade is the lift wire, modeled as a linear spring. This spring accounts for the stiffness in the crane in the same way as described in Section 5.3.1 for the jack-up vessel. The coupling between the blade and the crane is therefore also described with Equation 5.3.1.1 for the SSCV.

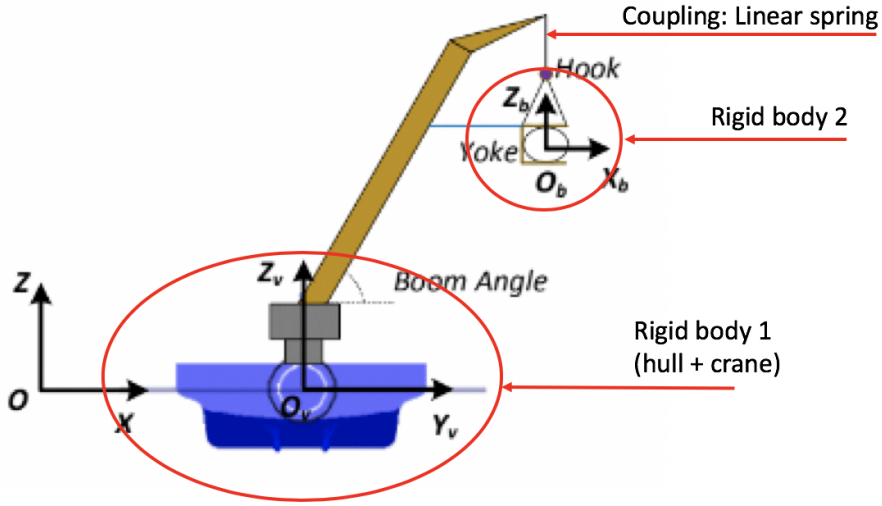

Figure 5.3: Illustration of the SSCV model and the coupling.

The coupled installation system is modelled and analysed with the software SIMO. SIMO is used for dynamic analysis for non-linear rigid-body motions in the time domain. The coupled system of the floating vessel and the blade in Figure 5.3 consists of total twelve DOFs and are influenced by the forces described in Chapter 4. In the following sections, the modeling and the responses for a floating installation system will be further described.

5.4.1 Numerical Modeling

The objective is to find the maximum response in the blade. This response is a coupled solution between the blade and the SSCV. The blade response is studied in Section 5.2. An eigenvalue analysis is conducted to identify the frequency range where the high responses can be expected. Further, the coupled response for the installation system is found by direct integration of the dynamic equation of motion in the time domain. As mentioned earlier, the added mass, the potential damping and first order wave excitations are obtained in the frequency domain because they only depend on the frequency and are further used in the time domain using the convolution integral. For a sinusoidal motion, the equation of motion is given by Equation 5.4.1.1 [52].

$$\mathbf{M}\ddot{\mathbf{x}} + \mathbf{C}\dot{\mathbf{x}} + \mathbf{D_1}\dot{\mathbf{x}} + \mathbf{D_2}\mathbf{f}(\dot{\mathbf{x}}) + \mathbf{K}(\mathbf{x})\mathbf{x} = \mathbf{q}(\mathbf{t}, \mathbf{x}, \dot{\mathbf{x}}) \tag{5.4.1.1}$$

- $\mathbf{M} = \mathbf{m} + \mathbf{A}(\omega)$
- $\mathbf{A}(\omega) = \mathbf{A}_\infty + \mathbf{a}(\omega)$
- $\mathbf{A}_\infty = \mathbf{A}(\omega = \infty)$

- $\mathbf{C}(\omega) = \mathbf{C}_\infty + \mathbf{c}(\omega)$
- $\mathbf{C}_\infty = \mathbf{C}(\omega = \infty) \equiv 0$

$\mathbf{M}$	Frequency dependent mass matrix
$\mathbf{m}$	Mass matrix for the whole structure
$\mathbf{A}$	Frequency dependent added mass matrix
$\mathbf{C}$	Frequency dependent potential damping matrix
$\mathbf{D}_1$	Linear damping matrix
$\mathbf{D}_2$	Quadratic damping matrix
$\boldsymbol{f}$	A vector function where every element is given by $f_i = \dot{x_i}\lvert\dot{x_i}\rvert$
$\mathbf{K}$	Coupled hydrostatic stiffness matrix
$\mathbf{x}$, $\dot{\mathbf{x}}$, $\ddot{\mathbf{x}}$	Position, velocity and acceleration
$\mathbf{q}$	Excitation force vector

The coupled hydrostatic stiffness includes the stiffness of the ship, the stiffness from the mooring lines and the coupling between the vessel and the blade. The excitation force is a sum of every force contribution included in the analysis, see Equation 5.4.1.2. The contributions are wind $\mathbf{q_{WI}}$, first and second order wave excitation forces, $\mathbf{q^{(1)}_{WA}}, \mathbf{q^{(2)}_{WA}}$, current drag forces, $\mathbf{q_{CU}}$, and any other excitation forces $\mathbf{q_{ext}}$.

$$\mathbf{q}(\mathbf{t}, \mathbf{x}, \dot{\mathbf{x}}) = \mathbf{q_{WI}} + \mathbf{q^{(1)}_{WA}} + \mathbf{q^{(2)}_{WA}} + \mathbf{q_{CU}} + \mathbf{q_{ext}} \tag{5.4.1.2}$$

For the SSCV analysed in this thesis, the wind contribution $\mathbf{q_{WI}}$ only acts on the blade, not on the hull and the loads from the current are assumed so small that they are neglected. The first order wave excitation force, $\mathbf{q^{(1)}_{WA}}$, is from the linearised propagating gravity waves, and the second order wave excitation forces, $\mathbf{q^{(2)}_{WA}}$, are from the mean wave drift forces and slowly-varying drift forces. Even though the excitation forces typically are from a wave spectrum from a stationary process, is the responses non-stationary because of the non-linearized system, as described in Chapter 4.

The hydrostatic coefficients listed above are frequency dependent and found in the software HydroD. The hydrostatic coefficients for the model of the SSCV used in this analysis are identified for a water depth of 30 meters. However, the difference between the hydrostatic coefficients for the SSCV for 30 meter and 60 meter water depth are assumed so small, so a new analysis in HydroD are not conducted in this thesis.

Time Domain analysis

The dynamic responses is obtained by the time domain method since the dynamic properties are changing with time during the operation. This means that the responses are not linearly dependent on the excitations, and the dynamic system is non-linear with a non-stationary resulting process. The response is found by time integration of Equation 5.4.1.3 for every twelve DOF.

$$(\mathbf{m} + \mathbf{A}_\infty)\ddot{\mathbf{x}} + \mathbf{D_1}\dot{\mathbf{x}} + \mathbf{D_2}\mathbf{f}(\dot{\mathbf{x}}) + \mathbf{K}(\mathbf{x})\mathbf{x} + \int_0^t \mathbf{h}(\mathbf{t} - \tau)\dot{\mathbf{x}}(\tau)d\tau = \mathbf{q}(\mathbf{t}, \mathbf{x}, \dot{\mathbf{x}}) \tag{5.4.1.3}$$

Where the retardation function, $\mathbf{h}(\tau)$, is computed by the Fourier transform of the frequency-dependent added-mass and damping.

$$\mathbf{h}(\tau) = \frac{1}{2\pi}\int_{-\infty}^{\infty} \mathbf{c}(\omega) + \mathbf{i}\omega\mathbf{a}(\omega)\mathbf{e}^{\mathbf{i}\omega\mathbf{t}}\mathbf{d}\omega = \frac{1}{2\pi}\int_{-\infty}^{\infty} \mathbf{H}\left(\omega\right)\mathbf{e}^{\mathbf{i}\omega\mathbf{t}}\mathbf{d}\omega \tag{5.4.1.4}$$

Equation 5.4.1.4 shows that the frequency-dependent added mass en potential damping is incorporated into the retardation function $\mathbf{h}(\tau)$ and by convolution it is transformed to the time domain where the analysis is conducted.

Chapter 6

Numerical modelling in SIMA

6.1 General

The single blade installation for an offshore wind turbine is a challenging process. The margins are small, and if something goes wrong the consequences will be extremely expensive and hazardous. By establish the dynamic response during installation by advanced numerical simulation, one can ensure safety and installation efficiency. This chapter will firstly describe the detailed modelling of the jack-up Vessel and the SSCV from Y. Zhaos PhD [6]. Further, describe the fully coupled SIMO-RIFLEX-Aero code used to analyse the single blade installation of an offshore wind turbine using the two installation systems. Lastly, the set up of the SIMO program system and file communication will also be shortly described.

6.2 Installation Systems

This section will describe the installation systems that are used in the coupled analysis in SIMA. First the crane and blade configuration is described. This will be the same for both the jack-up vessel and the SSCV. Following, the global and local coordinate systems will be described. Further, the jack-up vessel and the SSCV will be presented with main dimensions and vessel specific considerations. The models used in this thesis are from Y. Zhaos PhD with some modifications [6].

6.2.1 Blade and Lifting Arrangement

In Figure 6.1 the pedestal crane is illustrated. This is a typical configuration for offshore cranes, and will be used in both installation vessels. The crane system consists of the boom, a wire system, boom supports and a lattice boom. The boom wire is connected to the pedestal through the backstay, for extra support. The crane is connected to the vessel by the crane support. The main parameters of the crane are presented in Table 6.1, and the position of the crane tip for the respective vessels are listed in Table 6.2, where the position is given relative to the coordinate system to the respective vessel.

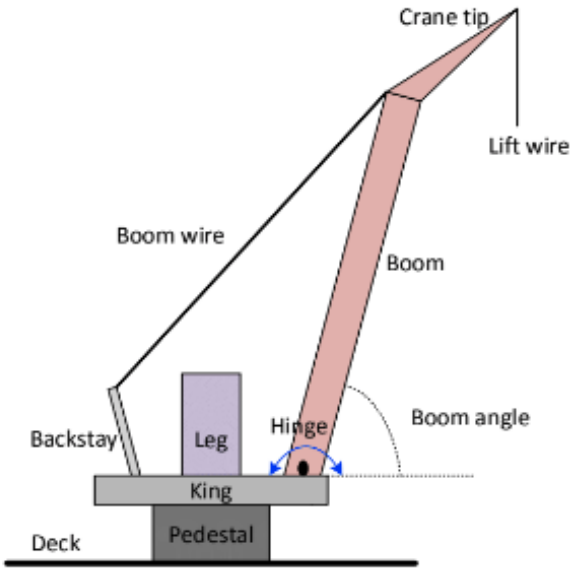

Figure 6.1: The pedestal crane configuration. [6]

Table 6.1: Main parameters of the crane.

Parameter	Value	
Boom length	107.6	m
Crane boom angle	67.6	deg
No. of boom wires	2	[-]
Boom wire stiffness	9048	kN/m
Boom wire damping	90.5	kNs/m

Table 6.2: Crane tip position on the vessels.

Crane tip position on the vessel	(x,y,z) [m]
The Jack-Up Vessel	(34.2, 49.3, 133.2)
The Semi-submersible	(66, 65.3, 144.9)

For the DTU 10MW wind turbine, which will be analyzed in this thesis, the turbine blade is installed at a hub height of 119 meter above the mean sea surface. The yoke, i.e., the configuration physically attached to the object that is to be lifted, is connected with four slings to the hook. A pair of the slings are usually connected to the jib hook and two are connected to the main hook. This gives greater flexibility in the lifting configuration, compared to having only one hook. Two horizontal tugger lines are connected from the yoke to the crane support, in order to achieve extra motion control of the lifted object. Pretension are deployed to the tugger lines in order to prevent slack in the lines, and keep tension through the entire operation. Figure 6.2 illustrates the tugger line system. The main properties of the blade and the lifting system are presented in Table 6.3, where the position of the center of gravity of the turbine blade is listed relative to the blade root.

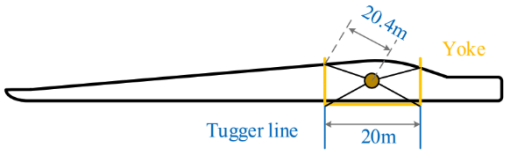

Figure 6.2: Illustration of the turbine blade and the tugger line system. [6]

Table 6.3: The blade and the lifting system.

Parameter	Value	
Hook mass	10	tons
Yoke mass	47	tons
Blade mass	41.67	tons
Blade length	86.37	m
Blade COG	26.2	m
Installation height	119	m
Tugger line arm length	10	m

6.2.2 Coordinate Systems

The jack-up crane vessel configuration is illustrated in Figure 6.3 and the SSCV in Figure 6.4 with the global earth fixed coordinate system and the local coordinate systems for the hull, the crane tip and the blade.

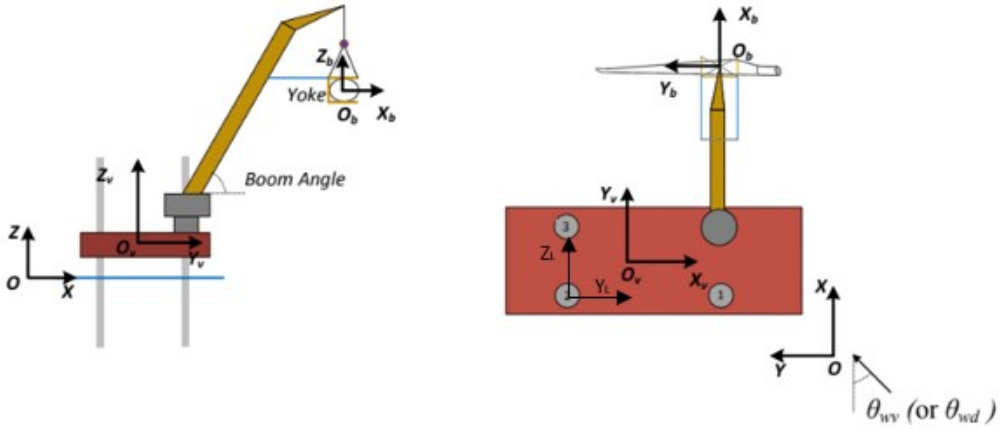

Figure 6.3: Configuration of the Jack-up crane vessel. [6]

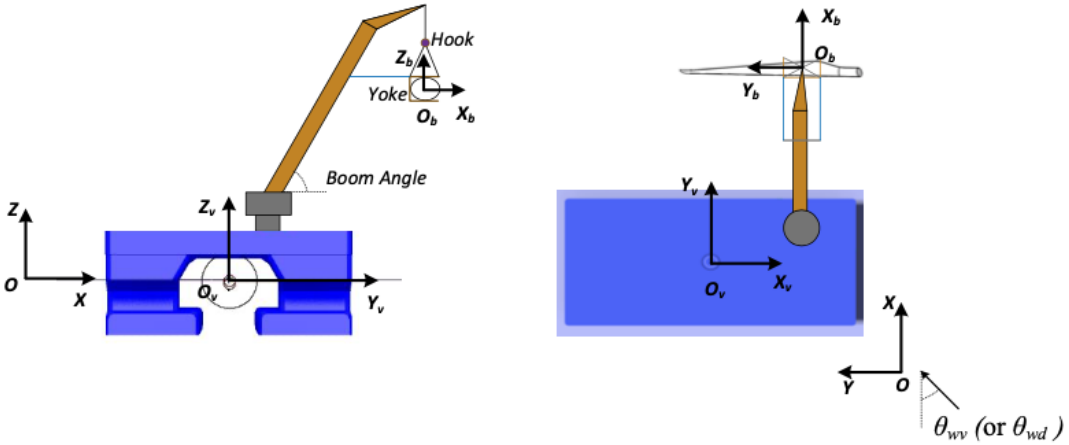

Figure 6.4: Configuration of the SSCV. [6]

The coordinate system used for the analysis of the blade installation consists of three coordinate systems, O (XYZ), O_v (x_v,y_v,z_v) and O_b (x_b,y_b,z_b), the global coordinate system, the vessel-related

coordinate system and the blade-related coordinate system, respectively. The origin of the vessel-related coordinate system is located in the center of the water plane area of the SSCV and in the geometrical center of the hull for the jack-up, where the x_v follows the vessels longitudinal direction, y_v follows the right hand rule and z_v is straight upwards. The blades O_b, has its origin located in the blades centre of gravity, where y_b follows the blade longitudinal direction at rest with positive direction towards the blade tip, x_b follows the right-hand rule and z_b is normal to the x_b-y_b plane and is positive upwards. When the blade is at rest the blades coordinate system is parallel with the global coordinate system. θ_{wd} is the relative wind angle, which describes the angle between the incident wave direction and y_b direction in the blades coordinate system. The wave direction is also an important factor to include, and in Figure 6.4 and 6.3 the incident wave angle is denoted as θ_{wv} and describes the angle between the wave direction and positive X direction in the global coordinate system O. In addition the legs of the jack-up structure are defined as illustrated in Figure 6.3. The local leg z_L axis is parallel with the global x axis, and the local leg y_L axis is defined parallel in the opposite positive direction with the global Y axis. Further, the origin of the local leg coordinate system, O_L is located in the center of the leg. [38]

6.2.3 Geometry of the Vessels and Main Parameters

The main parameters for the jack-up vessel are shown in Table 6.4. The only change from Y. Zhaos model is that the legs are modelled for 60m water depth instead of 30 meters. The jack-up vessel configuration is presented in Figure 6.3. The natural periods of the jack-up system are listed in 6.5.

Table 6.4: The main parameters of the Jack-Up Vessel.

Parameters	values	
Hull length	132	m
Hull width	39	m
Hull depth	9	m
Displacement during transportation	2.20×10^4	m^3
Total elevated load	1.69×10^4	tons
Leg length	112	m
Leg diameter	4.5	m
Leg spacing - x-direction	68.3	m
Leg spacing - y-direction	30.6	m
Airgap	7.2	m
Leg below hull	67.2	m

Table 6.5: Natural Periods of the jack-up structure.

	Leg - x_g	Leg - y_g	Double Pendulum	Crane boom: 1st mode
ω_n [rad/s]	1.3	1.4	0.5	1.9
T_n [s]	4.83	4.49	12.0	3.31

The main parameters for the SSCV are shown in Table 6.6, the configuration is presented in Figure 6.4 and the SSCVs natural period obtained in Section 7.2.2 are presented in Table 6.7.

Table 6.6: The main parameters of the SSCV.

Parameter	Value	
Length	175	m
Width	87	m
Operational Draught	26.1	m
Displacement	1.638×10^5	m^3

Table 6.7: Natural Periods of the SSCV obtained by the RAO in Section .

	Surge	Sway	Heave	Roll	Pitch	Yaw	Double Pendulum
ω_n [rad/s]	0.0670	0.0635	0.2732	0.3491	0.3492	0.067	0.5
T_n [s]	93.8	98.9	23.0	18.0	18.0	93.8	12

6.3 SIMA

SIMA is a MARINTEK workbench which gives complete solutions for simulation and analysis of marine operations and floating systems. The software perform a non-linear time domain analysis. One is able to model the system internal in SIMA, and perform engineering analysis of the marine operation, do a feasibility evaluation and identify challenging scenarios that can occur during a marine operation. The SIMA package includes, among others, the SIMO and RIFLEX package. [24]

6.3.1 Program Structure

Figure 6.5 presents the flowchart that illustrates the layout of the program system and how the files communicate between modules. The three main modules are inpmod, stamod and dynmod. The files in between are file systems for communication between the modules. The program structure is similar for both SIMA and RIFLEX.

- **INPMOD:** The input data manipulation, input generation, and interface to external sources of data. Describes the geometry, boundary conditions etc.
- **STAMOD:** Reads the input data, conduct the static analysis and define the static equilibrium and initial condition.
- **DYNMOD:** The dynamic response calculation using time domain analysis

The modules **OUTMOD** and **S2XMOD** are for the post-processing internal in SIMA or for export of the results.

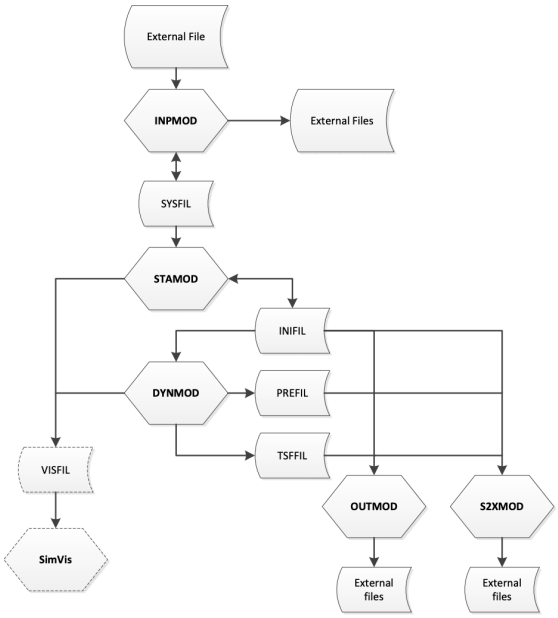

Figure 6.5: Layout of the SIMA program system and file communication between modules. [24]

6.3.2 Coupled Simulation Method

In this analysis a fully coupled SIMO-RIFLEX-Aero simulation code has been used. Figure 6.6 illustrates an overview of the coupled simulation method, which role each program has and how it is coupled. The Aero-code calculates the aero dynamic forces and moments acting on the turbine blade. It is integrated to SIMO through an external dynamic link library (DLL), and provides SIMO with the aerodynamic loads acting on the blade, and SIMO then calculates the blade rigid body motion at the blades COG. The wind field used in Aero is simulated in TurbSim, as a stochastic, full-field turbulence flow. The combination of SIMO and RIFLEX allows for a detailed modeling of the installation system and system mechanical coupling. The SIMO program gives a flexible modelling of complex multi body system, and for the installation systems used in this thesis the vessel and blade are modelled as two separate rigid bodies. It simulates motion response and station-keeping behaviour. RIFLEX, on the other hand is a computer program for analysis of flexible risers and slender structures, using FEM, and simulates the structural responses. Dynamic analysis in both SIMO and RIFLEX comprises linear and non-linear time-domain analysis. A SIMO-RIFLEX coupled simulation provides both motion response of the bodies and the structural response in the slender structures. The SSCVs hydrodynamic coefficients as the added mass, the damping and the stiffness are calculated in HydroD, which is a SESAM software that conducts hydrodynamic analysis in the frequency domain. The hydrodynamic coefficients are then converted by a retardation function described in Section 5.4.1, and into the time-domain which the SIMO-software uses. [24]

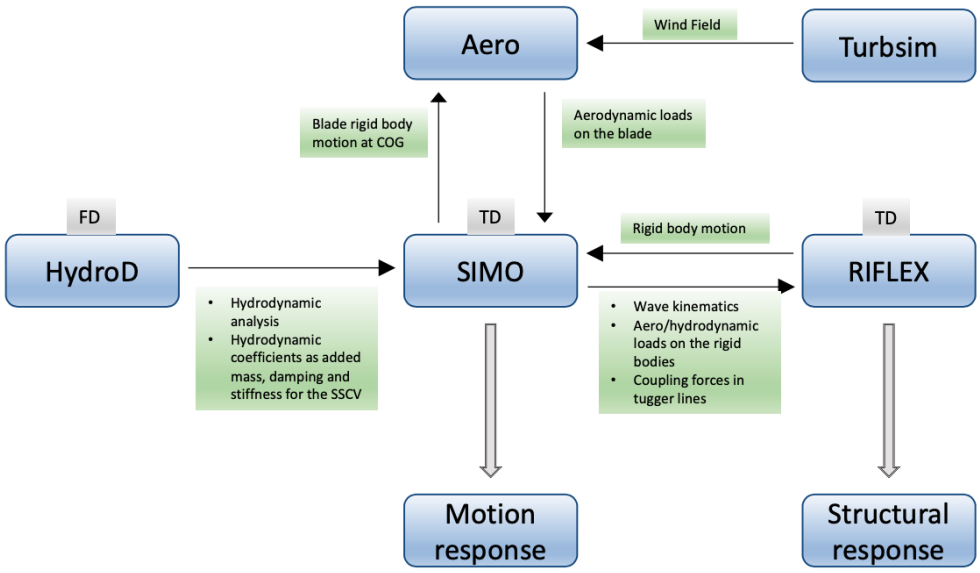

Figure 6.6: Flowchart of the coupled simulation method in SIMA.

Chapter 7

Results

7.1 General

This chapter will present the results from the coupled dynamic response analysis conducted in SIMA for both the jack-up vessel and the SSCV. The results are extracted from SIMA and further evaluated and post-processed in MATLAB. Firstly, the system properties are identified for the two installation systems. Further, the response statistic are analysed for the vessel, crane tip and blade. This is done for three conditions; regular wave loads, irregular wave loads and irregular wind and wave loads. Regular and irregular waves are described in Section 4.4.1. Figure 7.1 and 7.2 shows the installations system with respective coordinate system, which is described in Section 6.2.2. The body motions will be referred to by their respective local coordinate system.

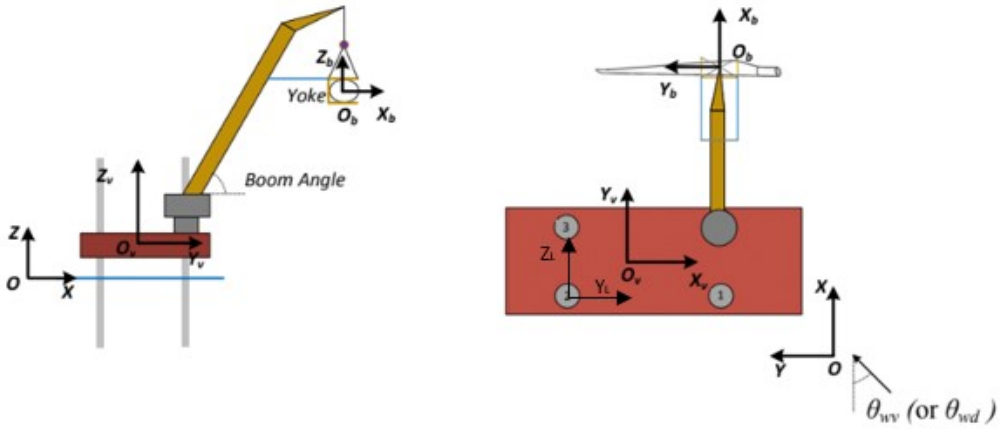

Figure 7.1: Illustration of the jack-up crane vessel analysed in the calculations. [6]

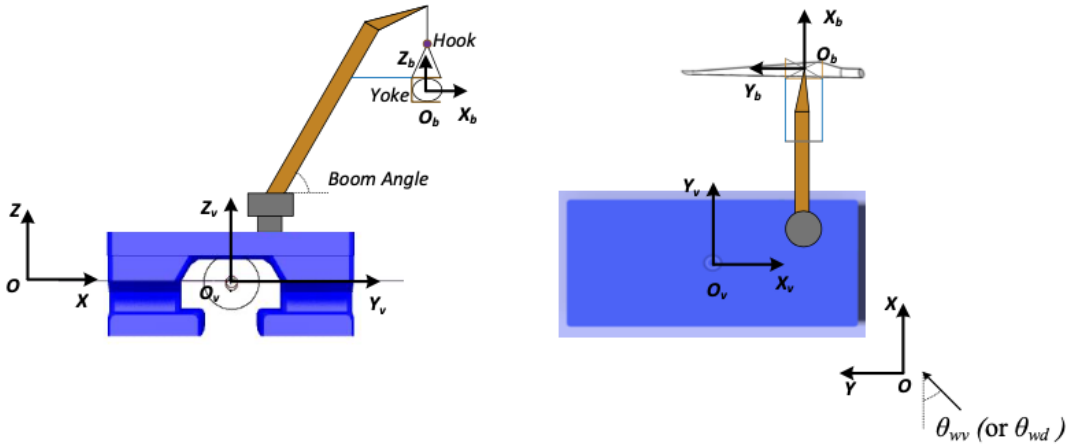

Figure 7.2: Illustrations of the SSCV analysed in the calculations. [6]

7.2 Regular Wave Analysis

The regular wave analysis is conducted both for the jack-up vessel and the SSCV and is presented in this section. The main purpose for the regular wave analysis is to find the system properties by obtaining the equivalent response amplification operator, RAO. This is done by running simulations with a constant wave elevation and different wave periods. Then the response amplitude is divided by the wave amplitude. For the regular wave analysis it is important to remove the transient part of the simulation and only use responses in steady state condition to obtain correct results. In this report a total simulation length of 1000 seconds is preformed, then the the last 600 seconds is used to obtain the equivalent RAO. Firstly, the system properties are found by obtaining the RAOs. Secondly, the response statistics are described.
In Figure 7.3 a time series of the wave elevation and the vessel response in surge and sway are illustrated. As expected, the time series show that the response motion follows the same period as the propagating waves. It is also seen that the vessel response has reach steady state after about 300 seconds. This illustrates why the transient part of the response has to be removed, and verifies that steady state is reached within 400 seconds. Hence, the analysis can be done for the last 600 seconds of a total simulation time of 1000 seconds.

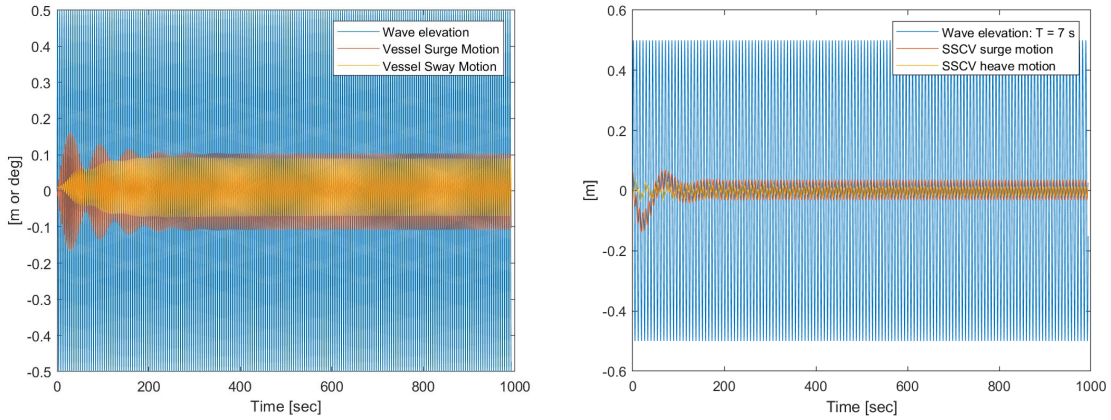

(a) Jack-up (b) SSCV

Figure 7.3: Time series for jack-up vessel and the SSCV showing the transient and the steady state period of the simulated time period.

7.2.1 Jack-up

In the following section the results from the regular wave analysis of the jack-up structure are presented and described. First, the RAO of the lower leg, vessel and blade are found. This is done for both a wave elevation of 1 meter and 4 meters in head sea. Then the response for the vessel and the blade in six DOFs is compared for different wave directions.

RAO of Bending Moment in Jack-up Legs

The bending moment in the legs are found in the lower part of the legs where they penetrate the sea floor. The RAO for both H = 1 m and H = 4 m are presented in Figure 7.4 and 7.5.

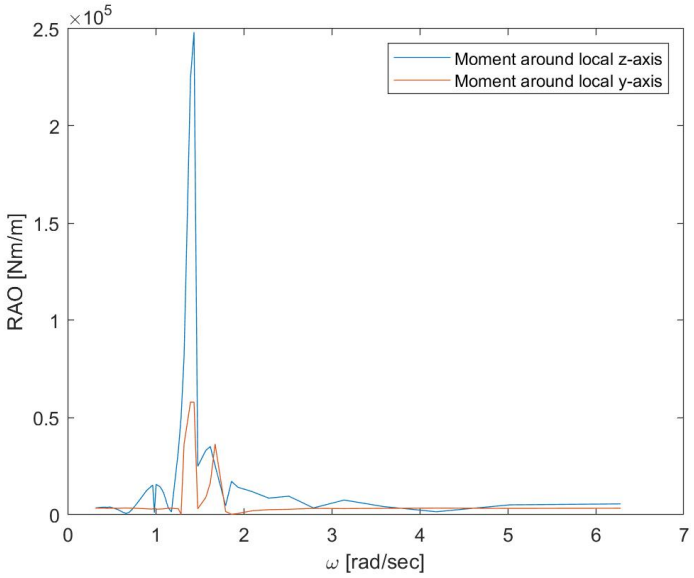

Figure 7.4: RAO of the bending moment in the lower leg; head sea θ_{wv} =270 deg, H = 1 m.

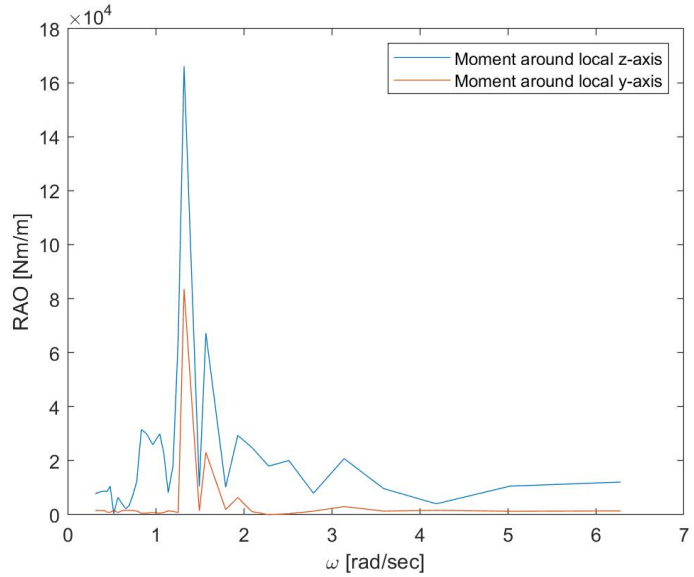

Figure 7.5: RAO of the bending moment in the lower leg; head sea θ_{wv} =270 deg, H = 4 m.

As expected the moment around the local z-axis, when following the coordinate system described

in Figure 6.3, is the dominant in head sea. The natural period of the legs are at 4.375 seconds, where the largest bending moment occur. It is in general the first mode that are of interest.

The response in the legs are important for the jack-up structure, as these are the only part of the structure experiencing wave forces. The coupling between the legs and the hull is modelled as rigid, which means that the vessel is moving with the legs. The hull is affecting the natural period of the legs, as it is a large mass on top of the legs which will increase the natural period. For the cases in Figure 7.4 and 7.5 the moments will mainly induce surge and sway motion on the vessel, the rotations are expected to be present but small. As the water depth is relatively large, the expected natural periods larger than in shallower water as the length of the legs are increased without changing the cross-section.

RAO of Vessel and Blade motion

In Figure 7.6 the RAO for the vessel is plotted in six degrees of freedom in head sea with incident waves of H= 1 m. As expected, the surge RAO is the greatest of the translations. For the rotation, yaw is dominant which is induced from the moment in the legs both around local z-axis and local y-axis.

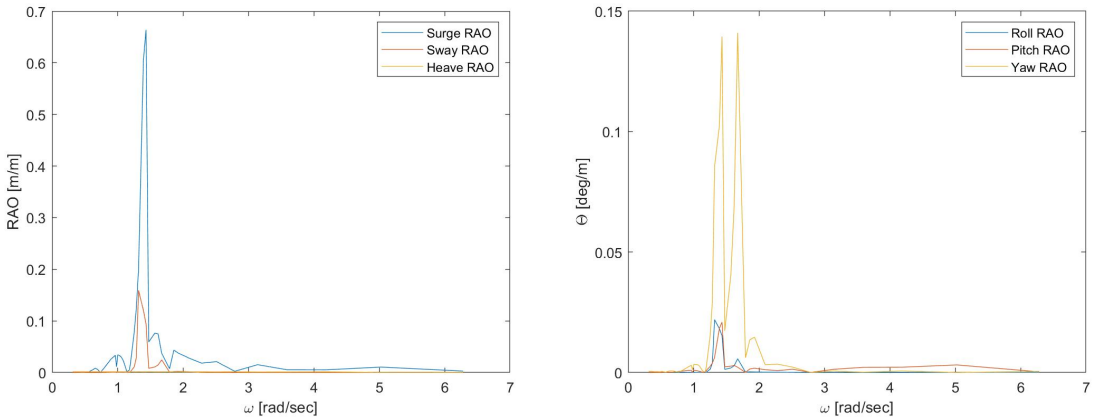

(a) Translations (b) Rotations

Figure 7.6: RAO of the jack-up vessel motion for the six DOFs; H=1m, head sea θ_{wv}=270deg.

Figure 7.7 show the RAO of the vessel for waves with H = 4 m. The surge motion is dominant as for H = 1 m, and at about the same magnitude. Both the sway response motion and the yaw response motion are strongly increased compared to H = 1 m. This coincides with the change in bending moment from H = 1 m to H = 4 m. The modes are excited at the same frequencies, which is a validation of the analysis. The system properties are not changing due to change of the external loads.

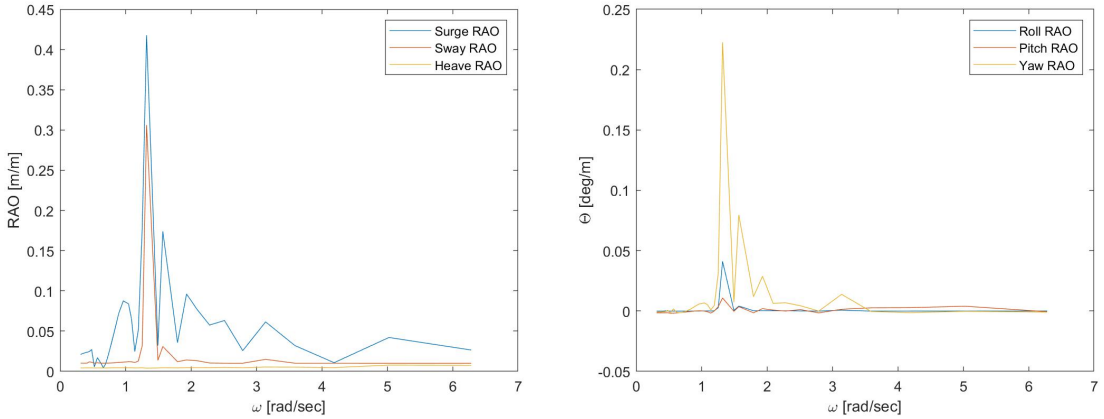

(a) Translations (b) Rotations

Figure 7.7: RAO of the jack-up vessel motion for the six DOFs; H=4m, head sea θ_{wv}=270deg.

In Figure 7.8 the blade RAO is illustrated. It is the blade sway and roll motion that is dominating as expected in head sea. For both the sway RAO and roll RAO there are two peaks. One that coincide with the natural period of the leg and one at 3.75 seconds which might be the second bending mode of the crane boom. At T = 12 s another resonance effect is induced. This is the pendulum motion, which appears as roll motion for the blade.

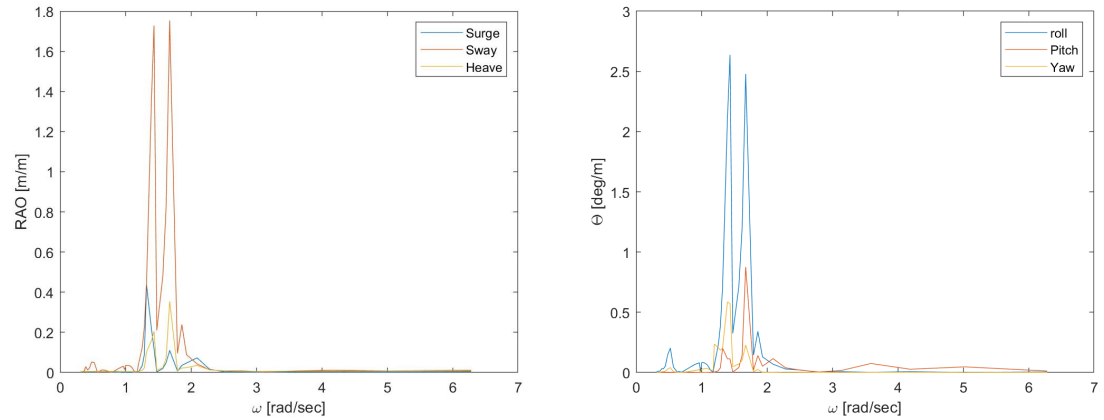

(a) Translations (b) Rotations

Figure 7.8: RAO of the jack-up blade motion for the six DOFs; H =1 m, head sea θ_{wv} = 270 deg.

In Figure 7.9 the blade RAO with incident waves with wave height of 4 meters are illustrated. The response, when the wave elevation is 4 meters for the peaks that were dominating in the former case, is still excited for the same frequencies, as expected. The change is that the blade surge and pitch RAO are strongly increased. As for the vessel response, H = 4 m increase the energy in the system, but the properties remains.

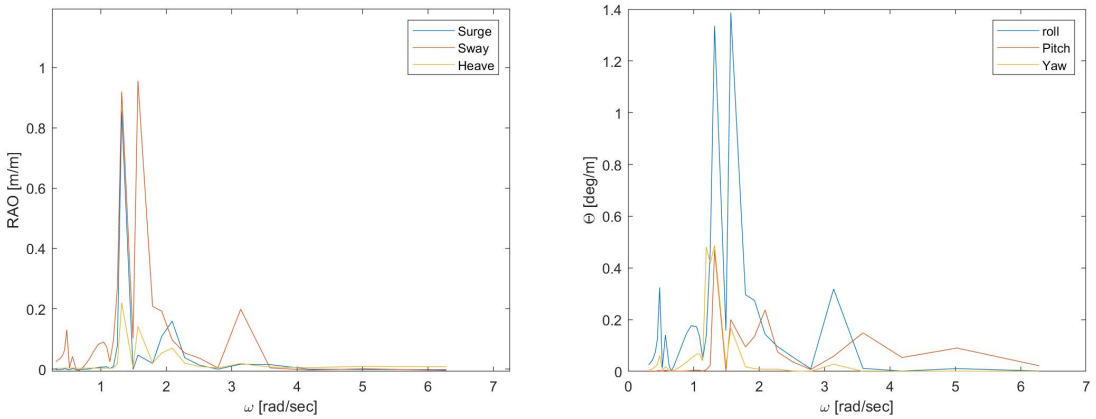

(a) Translations (b) Rotations

Figure 7.9: RAO of the jack-up blade motion for the six DOFs; H=4m, head sea θ_{wv}=270deg.

Wave Direction Comparison

Figure 7.10 illustrates the vessel and blade response when exposed to different wave directions. As expected the vessel surge motion is the greatest in head sea and the vessel sway motion is the greatest in beam sea. The jack-up vessel experiences no heave motion in this sea state as it is a fixed platform. When comparing the rotations the roll motion is the dominant for all the wave directions. Further, in quartering sea the yaw response motion is relatively high. The blade response is in general ten times larger than the respective vessel response, and the head sea condition induces the greatest motions on the blade. The largest blade response is the sway and roll motion, which respectively is 0.0015 meters and 0.034 degrees.

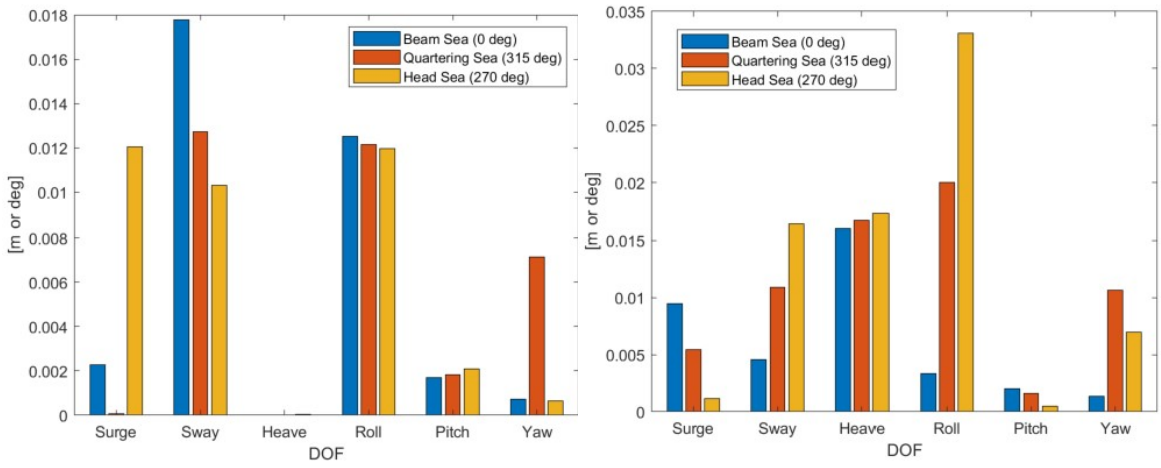

(a) Vessel (b) Blade

Figure 7.10: Maximum motion response of the jack-up; beam sea $\theta_{wv} = 0$ deg, quartering sea $\theta_{wv} = 315$ deg and head sea $\theta_{wv} = 270$ deg, H = 1 m, T = 7.3 s.

7.2.2 The Semi-Submersible Crane Vessel

This section will present the regular wave analysis of the SSCV. Firstly, the RAO is found for H= 1 m and H= 4 m in head sea, both for the vessel and blade response. Further, the responses in all six DOFs are compared with different wave headings for both the vessel and the blade motions.

RAO of the Vessel and the Blade motion

Figure 7.11 show the RAO of the SSCV in all six DOFs in head sea and H = 1m, for wave periods in the range between 5 and 125 sec. The peaks obtained in the RAOs are typically related to resonant motions and the system natural periods. The surge and heave resonance is clearly shown in Figure 7.11 (a). The sway resonance is not as significant as heave and surge due to the heading of the propagating waves. The pitch is excited at two different frequencies, hence the two peaks, see Figure 7.11 (b). The peak to the left occur at the same frequency as the heave resonance, which means that the pitch motion is induced by the heave resonance. The peak occurring to the right, is the pitch resonance motion to the vessel, which is also shown in the surge and heave motion in Figure 7.11 (a).

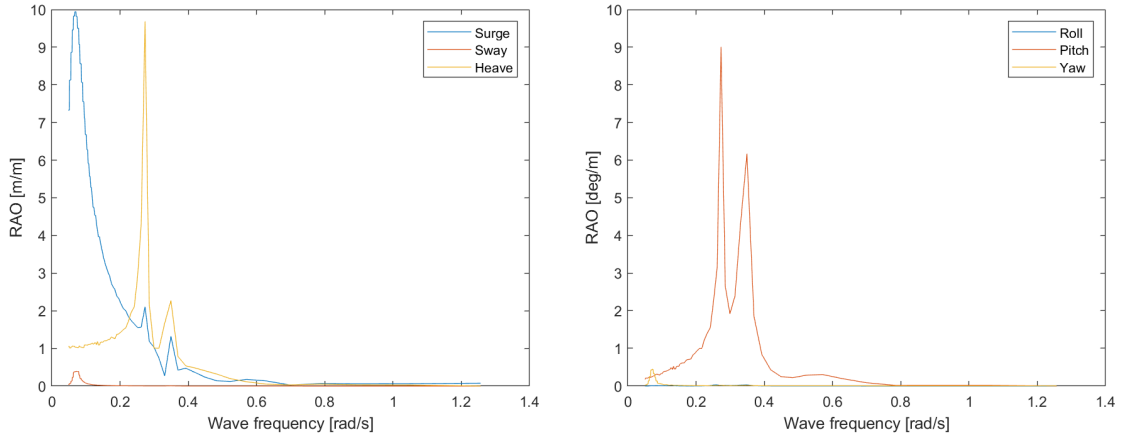

(a) Translations (b) Rotations

Figure 7.11: RAO for the SSCV; H = 1 m, head sea $\theta_{wv} = 270$ deg.

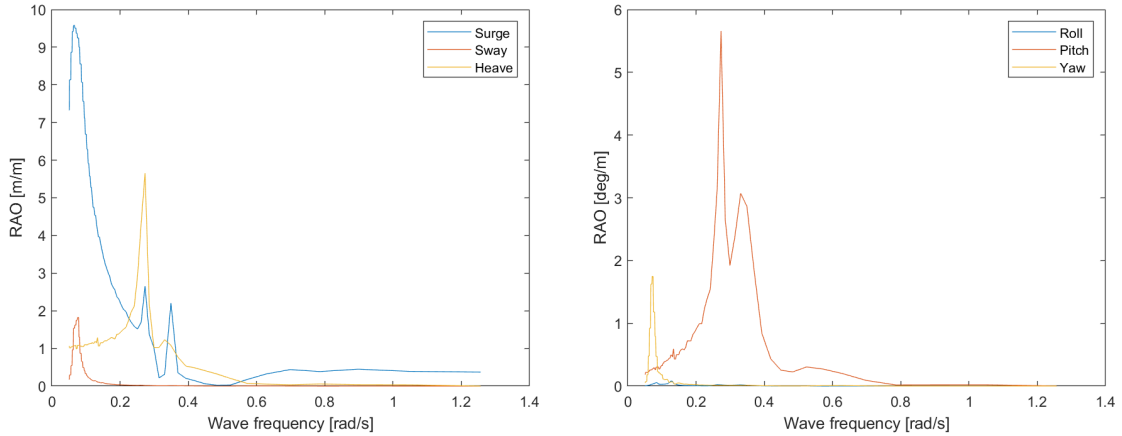

(a) Translations (b) Rotations

Figure 7.12: RAO for the SSCV; H = 4 m, head sea $\theta_{wv} = 270$ deg.

Figure 7.12 shows the RAO for the vessel with a wave height of 4 meters. Compared to Figure 7.11 the peaks occur at the same frequencies, but the amplitudes have some variations.

Figure 7.13 presents the RAO for the SSVCs blade motion in all six DOFs in head sea for H = 1m. Similar to the obtained RAO for the vessel, the resonant periods can be identified for the blade. The RAO for the blade have peaks at the same frequencies as the vessel, which is due to the coupling between the vessel and the blade. However, the blade has an additional peak, which

is the pendulum resonant motion, which appears as roll motion for the blade. Figure 7.14 present the RAO of the blade with H= 4 m. The peaks occur at the same frequencies for the translation and rotational motions, but are highly amplified in pitch and yaw motion.

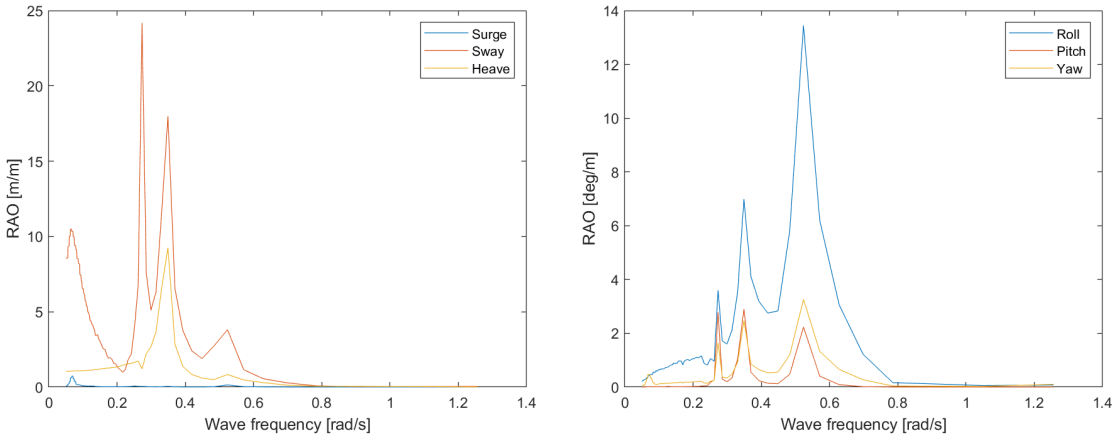

(a) Translations (b) Rotations

Figure 7.13: RAO for the SSCV blade; H = 1m, head sea $\theta_{wv} = 270$ deg.

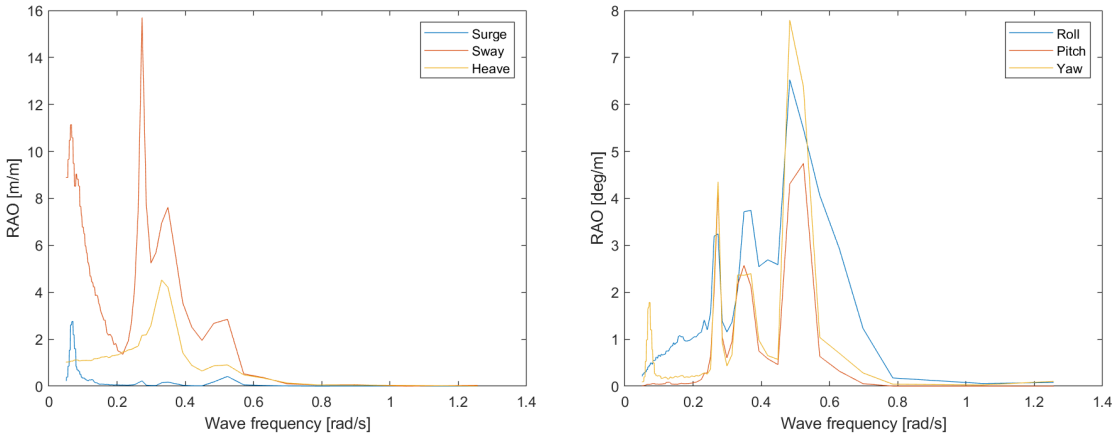

(a) Translations (b) Rotations

Figure 7.14: RAO for the SSCV blade; H = 4m, head sea $\theta_{wv} = 270$ deg.

Wave Direction Comparison

Figure 7.15 presents the responses of the SSCV and the blade when the wave direction is varying for all six DOFs. The responses are connected to the local coordinate system related to the respective body illustrated in Figure 6.4. For the SSCV, the sway-, roll- and yaw- motions are large in beam sea, as expected. In head sea the surge- and pitch motion is largest. The sway- and yaw-motion are extremely small for the vessel in head sea, which can be explained by the SSCVs moment of inertia. This is also why the motions are larger in beam sea than in head sea for the SSCV. The blade have the largest responses in beam sea, which is expected due to the vessel motions.

From the plot, it shows that the blades roll motion is independent of the wave headings, which can be explained by the geometry of the blade, the blade is extremely long compared to wide, so the rotation around the local x-axis will always be present. Similar to the vessel, the blade response in beam sea are generally larger than for head sea and quartering sea. The plots also shows that the blade have generally larger motions than the SSCV.

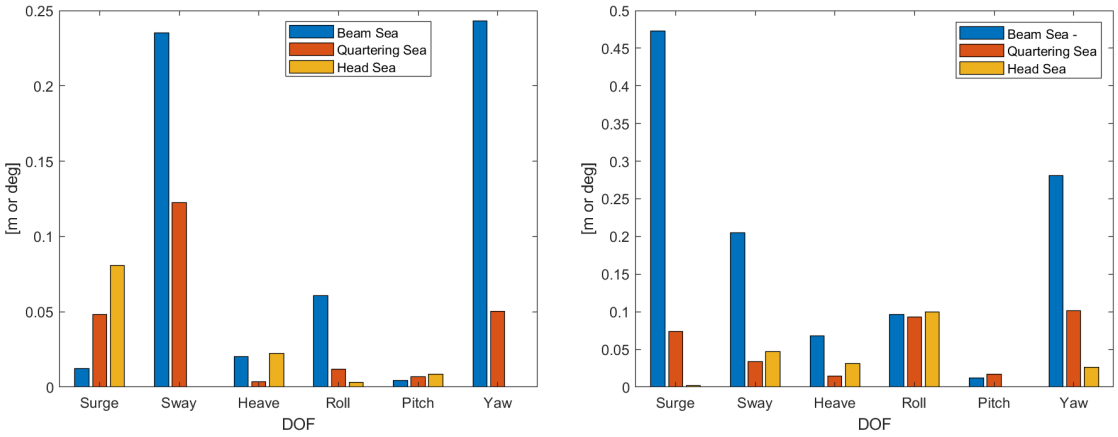

(a) Vessel (b) Blade

Figure 7.15: Maximum motion response of the SSCV and the blade; beam sea θ_{wv} = 0deg, quartering sea θ_{wv} = 315deg, head sea θ_{wv} = 270 deg, H = 1 m; T=7.3 s.

7.3 Jack-up vessel: Irregular wave analysis

In the following sections are the irregular analysis of the jack up structure when exposed to wave loads presented. There are mainly four cases that will be analysed, in Table 7.1 the parameters for these cases are listed. Firstly, the system properties will be presented. Secondly, the statistical response for the four cases will be presented.

Table 7.1: Cases for irregular analysis

	H_s [m]	T_p [sec]	θ_{wv} [deg]
Case 1	1.0	[5 6 7 8 9 10]	0, 270, 315
Case 2	0.5	6.8	0, 270
Case 3	1.0	7.3	0, 270
Case 4	1.5	7.7	0, 270

Figure 7.16 illustrate the wave loads. In Figure 7.16 (a) the time series of the wave and the blade surge response is plotted. In Figure 7.16 (b) the wave spectrum and the blade surge response spectrum is plotted. The peak frequency of the wave spectrum is 0.87 rad/s, which is correct when Tp is 7.3 seconds.

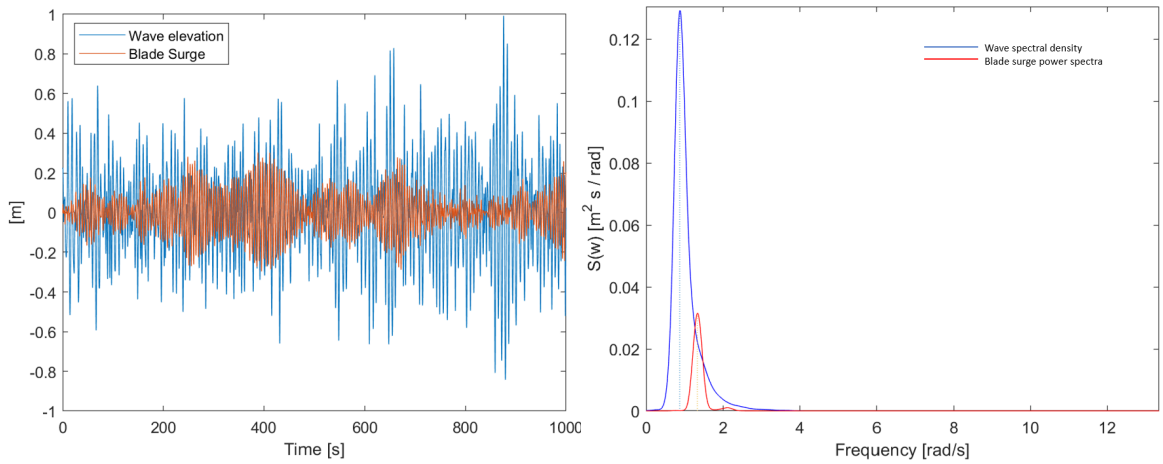

(a) (b)

Figure 7.16: Time series and wave spectrum; Hs = 1 m, Tp = 7.3 s, beam sea $\theta_{wv} = 0$ deg.

7.3.1 System Properties

Vessel

In Figure 7.17 the power spectra is illustrated in beam sea and head sea. The vessel sway motion is excited for a frequency of 1.3 rad/s while the vessel surge motion is excited at a frequency of 1.4 rad/s. This is due to the jack-up leg bending mode in respective direction. As expected, the vessel sway motion is largest of magnitude in beam sea and following coupled roll and yaw motion are induced. In head sea, the vessel surge motion is the dominant motion and following coupled yaw motions are induced. There is no pitch motion, this is due to a combination of the geometry of the hull and in general small motions. When comparing the two directions, beam sea gives the largest response motions.

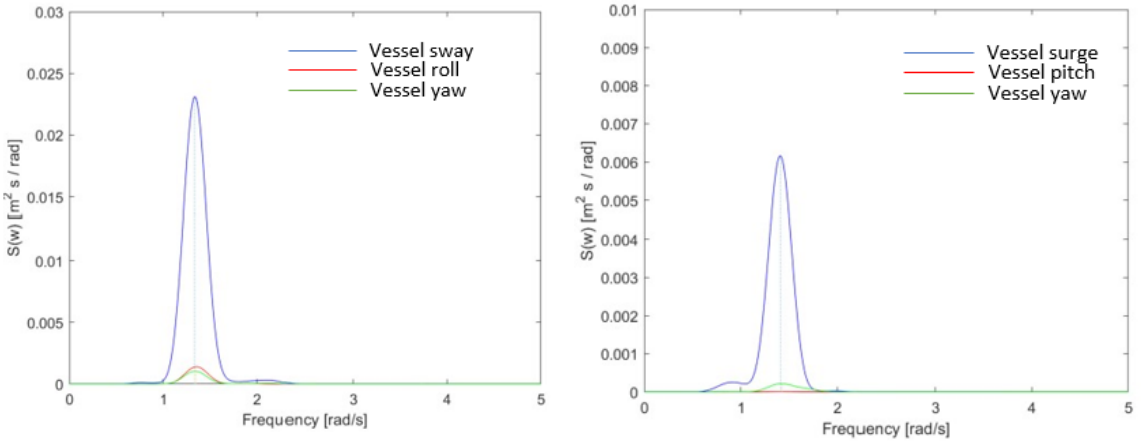

(a) Beam sea $\theta_{wv} = 0$ deg (b) Head sea $\theta_{wv} = 270$ deg

Figure 7.17: Power spectra of the jack-up vessel motion; Hs = 1 m, Tp = 7.3 s.

Crane tip Response

In Figure 7.18 the power spectra of the crane tip motion is illustrated in beam sea and head sea. As the crane is modelled as a fixed beam connected to the hull body, the crane follow the vessel motion. For beam sea the vessel sway induced motions occur, with the natural frequency of 1.3 rad/s. This gives motions in global x-direction for the same frequency. In head sea, motions in

global y-direction and global z-direction are induced by the vessel surge motion, at a wave frequency of 1.4 rad/s. Further, the response motion in the global x-direction is exited by the vessel motion at a frequency of 1.3 rad/s.

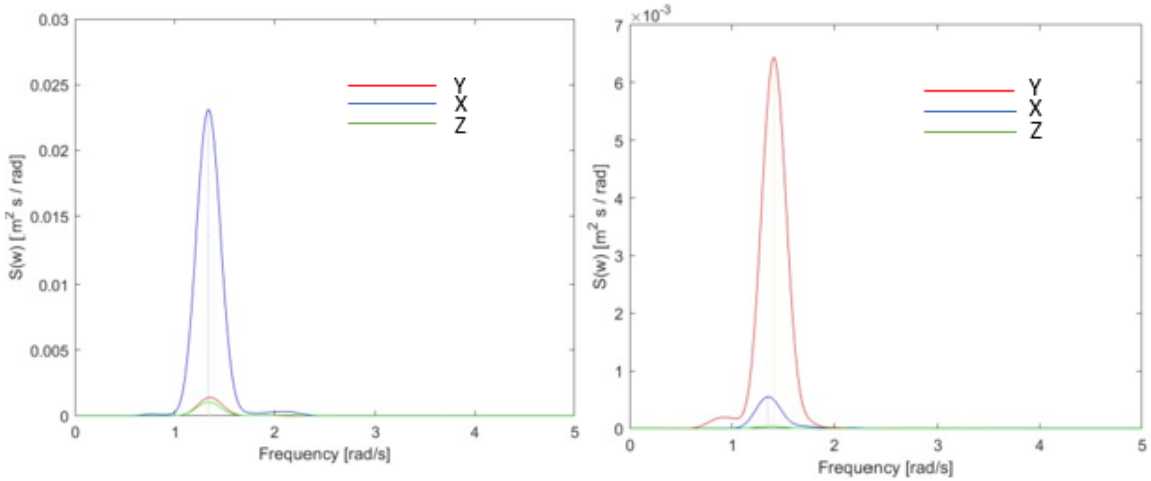

(a) Beam sea $\theta_{wv} = 0$ deg

(b) Head sea $\theta_{wv} = 270$ deg

Figure 7.18: Power spectra of the jack-up crane tip motion; Hs = 1 m, Tp = 7.3 s.

Blade Response

The two Figures 7.19 and 7.20 show the power spectra of the six DOFs for the blade. The arrows indicate how the blade motion is induced by the leg and crane vibrations. With wave loads as the only external load, the blade motion mainly is caused by the vessel motion. The blade is also excited around the pendulum natural frequency. The natural frequency of the first bending mode of the crane boom is 2 rad/s and the double pendulum induced resonance is at a frequency of 0.5 rad/s. In general, the motion response that is of significance in this case is the blade surge-, roll- and pitch motion.

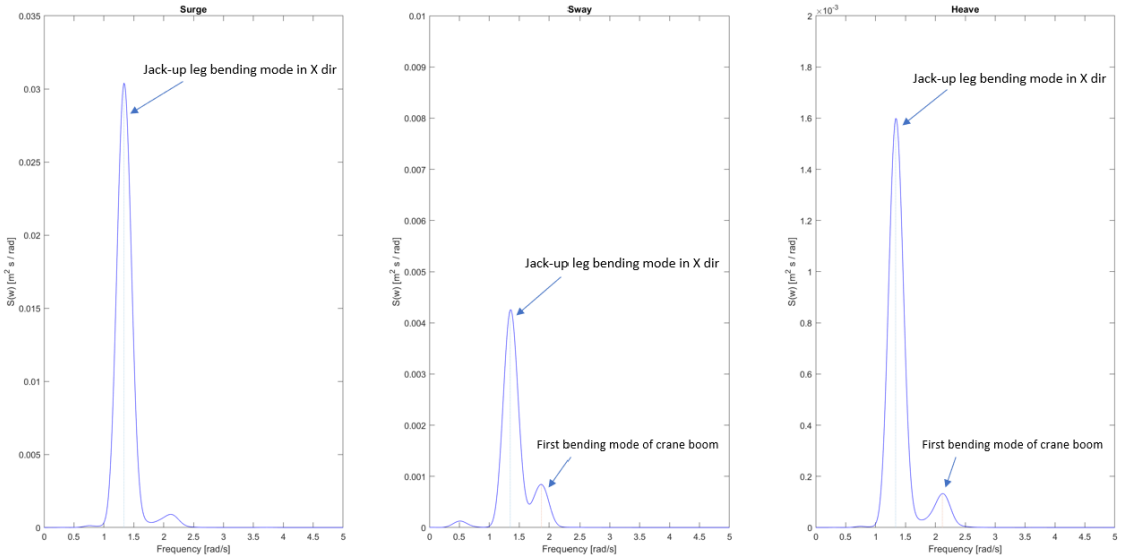

Figure 7.19: Power spectra of the jack-up blade translations; beam sea $\theta_{wv} = 0$ deg, Hs = 1, Tp = 7.3 s.

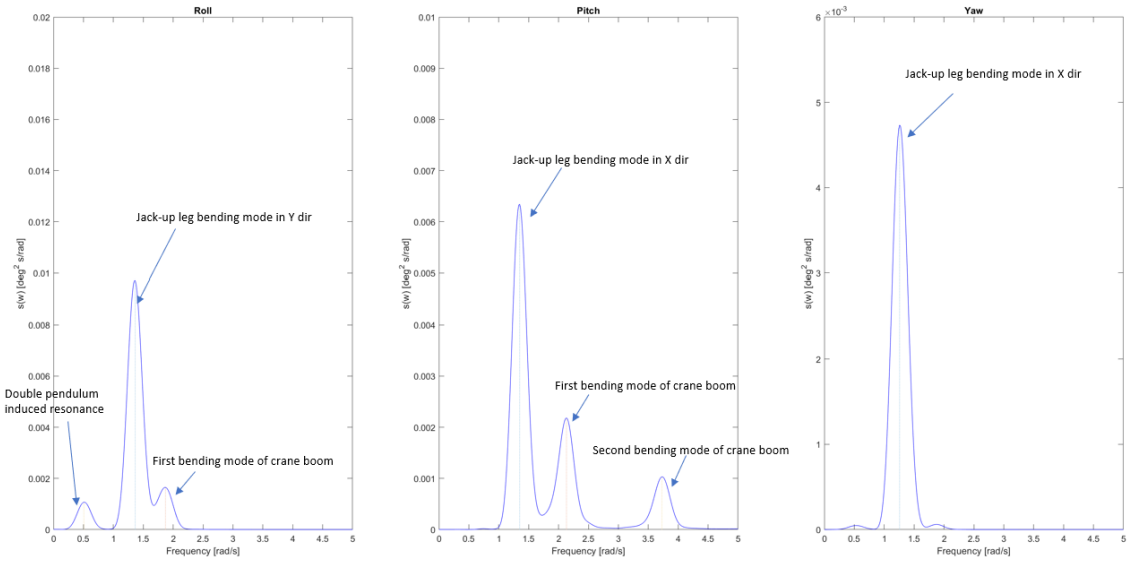

Figure 7.20: Power spectra of the jack-up blade rotations; beam sea $\theta_{wv} = 0$ deg, Hs = 1, Tp = 7.3 s.

In Figure 7.21 and 7.22 the power spectra for the blade motion in six DOFs in head sea is plotted. Firstly, it is seen that the natural period of the jack-up legs bending mode in the global y-direction that is excited. This frequency is 1.4 rad/s due to the change of wave heading. In general, head sea induce less energy in the system compared to beam sea.

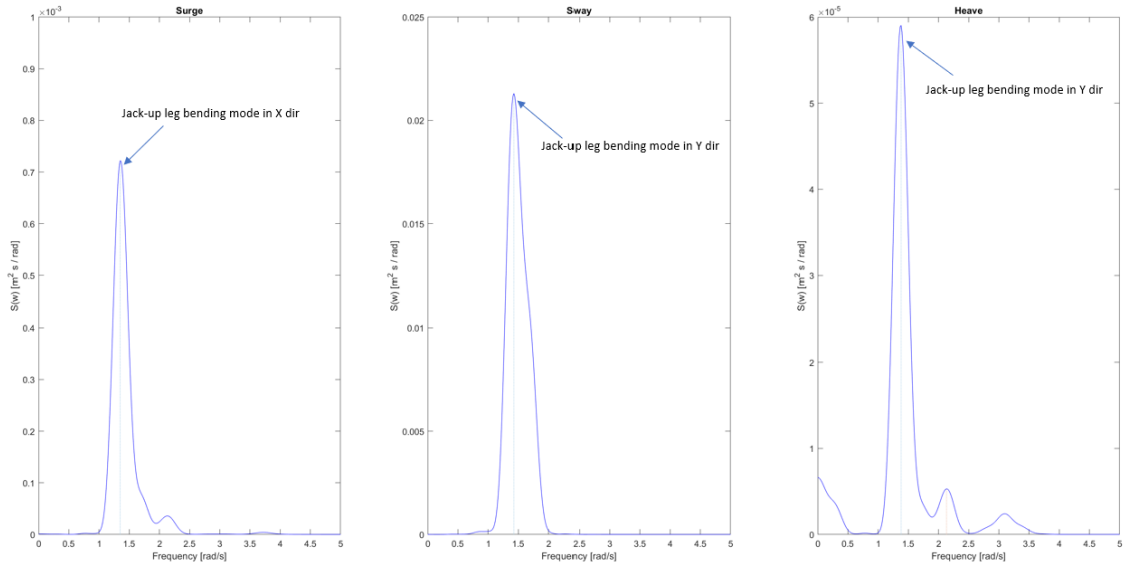

Figure 7.21: Power spectra of the blade motion translation; Head sea $\theta_{wv} = 270$ deg, Hs = 1 m, Tp = 7.3 s.

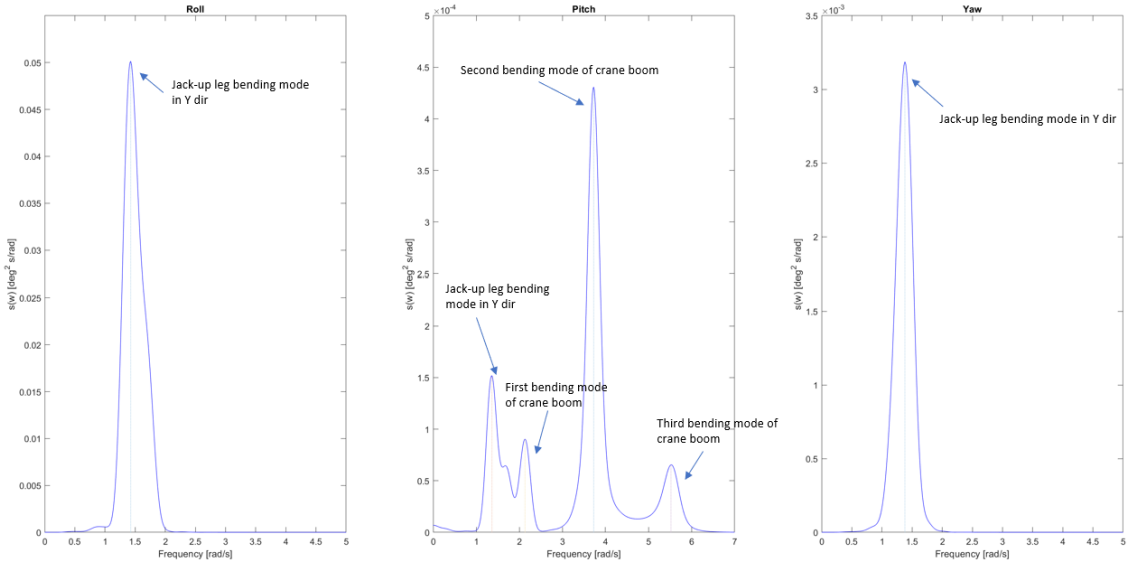

Figure 7.22: Power spectra of the blade motion rotation; head sea $\theta_{wv} = 270$ deg, Hs = 1 m, Tp = 7.3 s.

7.3.2 Response Statistics

Case 1

In Figure 7.23 the standard deviation of the vessel, crane tip and blade response motion is compared for varying peak periods. Firstly, the general magnitude of the response motions are about doubled in beam sea compared to head sea. Further, the largest response is for the case with T=5 s. As found in the previous chapter the jack-up leg bending mode is about 5 seconds, the case with a peak period close to the natural period gives the greatest response.

In Figure 7.23 it is seen that the response for the blade is larger than the crane tip, which again is larger than the vessel response. This is due to that the crane tip response are due to both leg bending and crane boom bending. The blade also have pendulum motion, which increase the response.

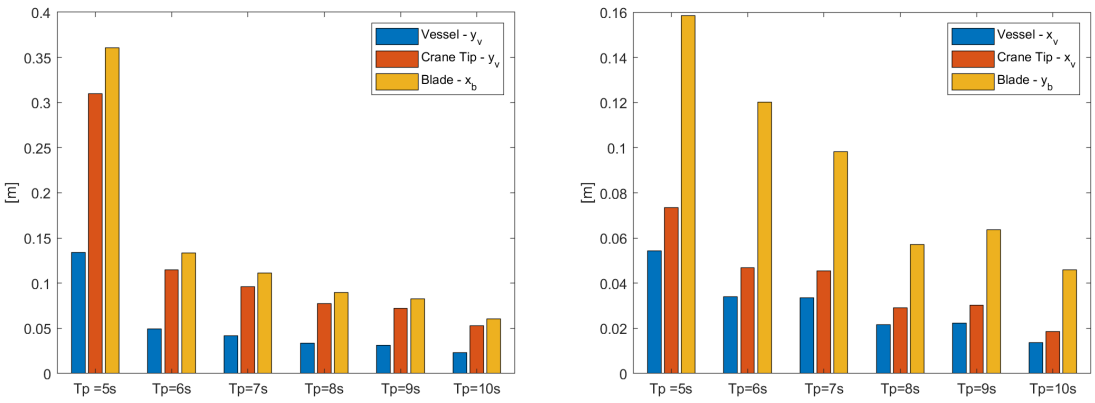

(a) Beam sea (b) Head sea

Figure 7.23: Standard deviation of the jack-up vessel, crane tip and blade motion for varying Tp; beam sea $\theta_{wv} = 0$ deg, head sea $\theta_{wv} = 270$ deg, Hs = 1 m.

In quartering sea, the blades dominant response motion is in the local y-direction. The blade sway motion is in general about twice as big as the response motions. Also in this case the response is

largest for a peak period of 5 seconds, closest to the natural period, and decreasing for increasing peak periods. The largest blade motions is seen in head sea. The blade motion in beam sea are reduced due to tugger lines.

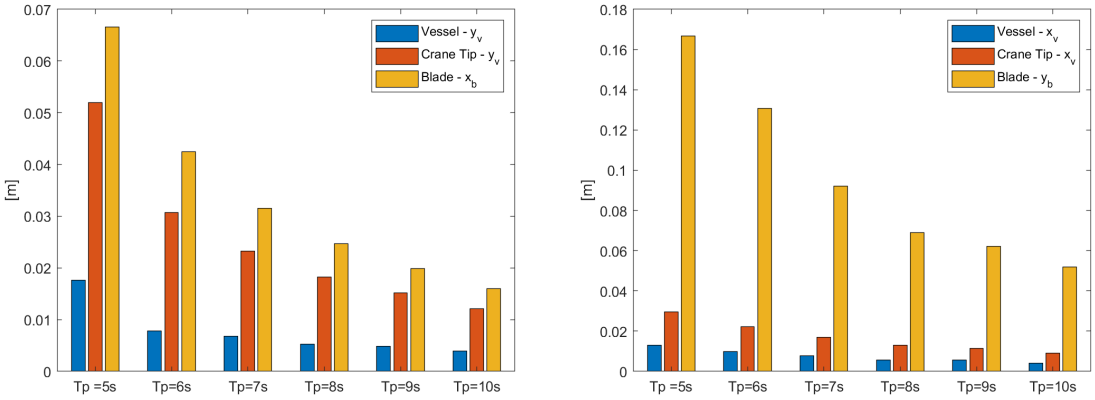

(a) Motion response in global x-direction

(b) Motion response in global y-direction

Figure 7.24: Standard deviation of the jack-up vessel, crane tip and blade motion for varying Tp; quartering sea $\theta_{wv} = 315$ deg, Hs = 1 m.

From the comparison of the three wave directions, it is beam sea that induce the motions of the greatest magnitude on the installation system.

Case 2, 3 and 4

In Figure 7.25 the standard deviations of the vessel, crane tip and blade motion are illustrated for waves propagating in beam sea and head sea. The response increase with the increase of the wave height and peak period. Compared to case 1, the response is increasing for increasing peak periods. This indicates that the increase of the wave height has a greater impact on the structure response than the spectral peak period. This presupposes that the wave period is outside the resonance range.

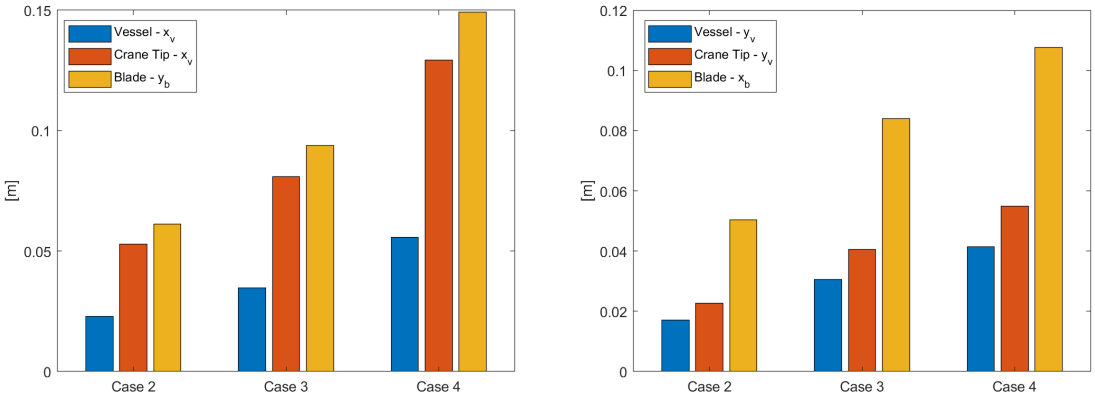

(a) Beam sea $\theta_{wv} = 0$ deg

(b) Head sea $\theta_{wv} = 270$ deg

Figure 7.25: Standard deviation for the jack-up vessel, crane tip and blade motion for case 2, case 3 and case 4.

The standard deviation of the crane tip motion in the x_v-, y_v and z_v-direction is compared in both beam sea and head sea. The standard deviation in y_v-direction is the largest in beam sea and the responses in x_v-direction is largest for head sea. The overall response in beam sea condition is about twice as large as for head sea.

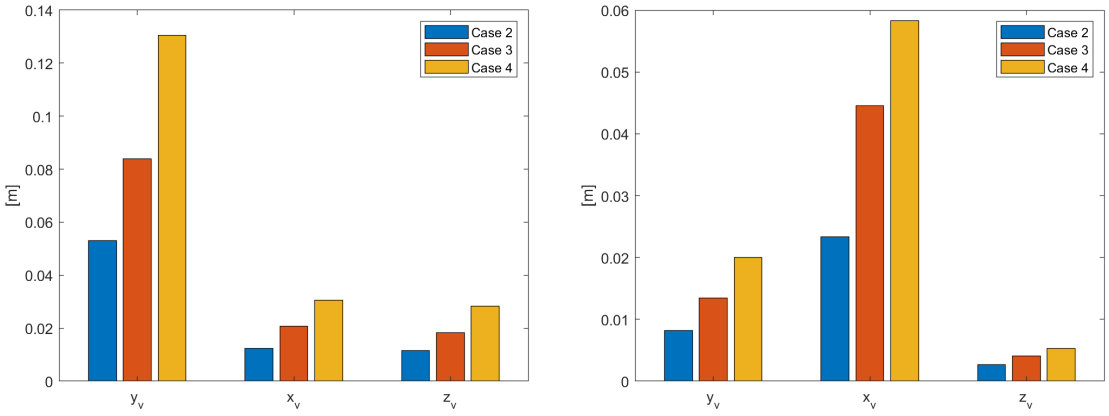

(a) Beam sea $\theta_{wv} = 0$ deg (b) Head sea $\theta_{wv} = 270$ deg

Figure 7.26: Standard deviation of the jack-up vessels crane tip motion for case 2, case 3 and case 4.

In Figure 7.27 the standard deviations are presented for the six DOFs of the blade in case 2, case 3 and case 4 for beam sea and head sea. For the blade, vessel and crane tip, case 4 gives the largest response motion. In beam sea the surge motion is dominant, but there are in general relatively high motions for all six DOFs. In head sea the response are governed by the sway and roll motion.

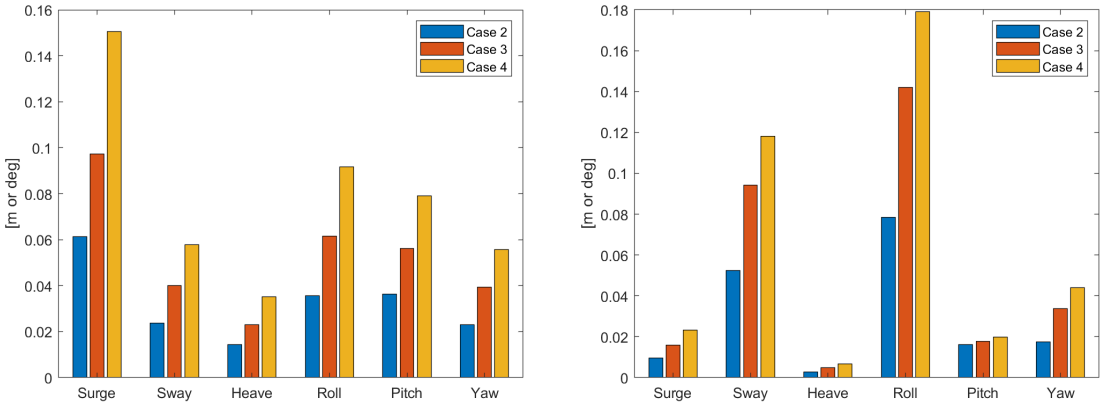

(a) Beam sea $\theta_{wv} = 0$ deg (b) Head sea $\theta_{wv} = 270$ deg

Figure 7.27: Standard deviation of the jack-up vessels blade motion in all six DOFs for case 2, case 3 and case 4.

7.4 The Semi submersible: Irregular wave analysis

This section will present and describe the results obtained by the irregular wave analysis without wind for the SSCV. The different cases analysed for the semi-submersible crane vessel are the same as the cases for the jack-up vessel, and are presented again in the table below.

Table 7.2: Cases for irregular analysis for the SSCV.

	H_s [m]	T_p [sec]	θ_{wv} [deg]
Case 1	1.0	[5 6 7 8 9 10]	0, 270, 315
Case 2	0.5	6.8	0, 270
Case 3	1.0	7.3	0, 270
Case 4	1.5	7.7	0, 270

Firstly, the system properties for the vessel, crane tip and blade will be presented by power spectra. For this analysis Hs=1 m and Tp=7.3 s has been used for beam and head sea. Lastly, the response statistics for every case and response parameter will be described in detail.

Figure 7.28 (a) show the time series of the wave elevation together with the blade surge motion in beam sea. It shows that the blade motion is not proportional with the wave elevation, which means that the system is non-linear. Figure 7.28 (b) show the wave spectral density with the power spectra of the blade surge motion.

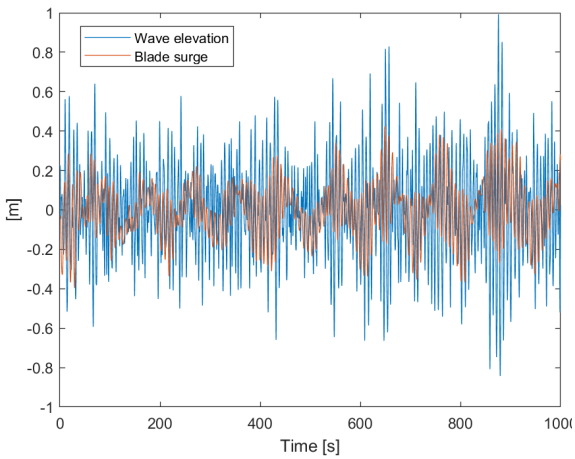

(a)

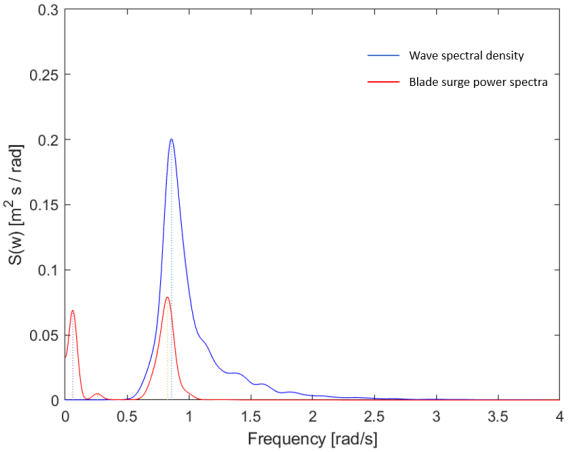

(a)

Figure 7.28: Time series and wave spectral density; Hs=1m; Tp=7.3sec, $\theta_{wv} = 0$ deg.

7.4.1 System Properties

Vessel

Figure 7.29 shows the power spectrum for the vessel motions in sway, heave, roll and yaw in beam sea. The resonance frequency for sway and yaw is at about $\omega \approx 0.065$ rad/s, which is in the same range as found in the regular analysis. At $\omega \approx 0.27$ rad/s, the vessel experiences heave resonance. For the roll motion, there is a peak for the same frequency which means that this peak is induced from the heave resonant motion. The wave frequency response which occur around $\omega \approx 0.86$ rad/s, corresponds to the spectral peak period Tp = 7.3 s.

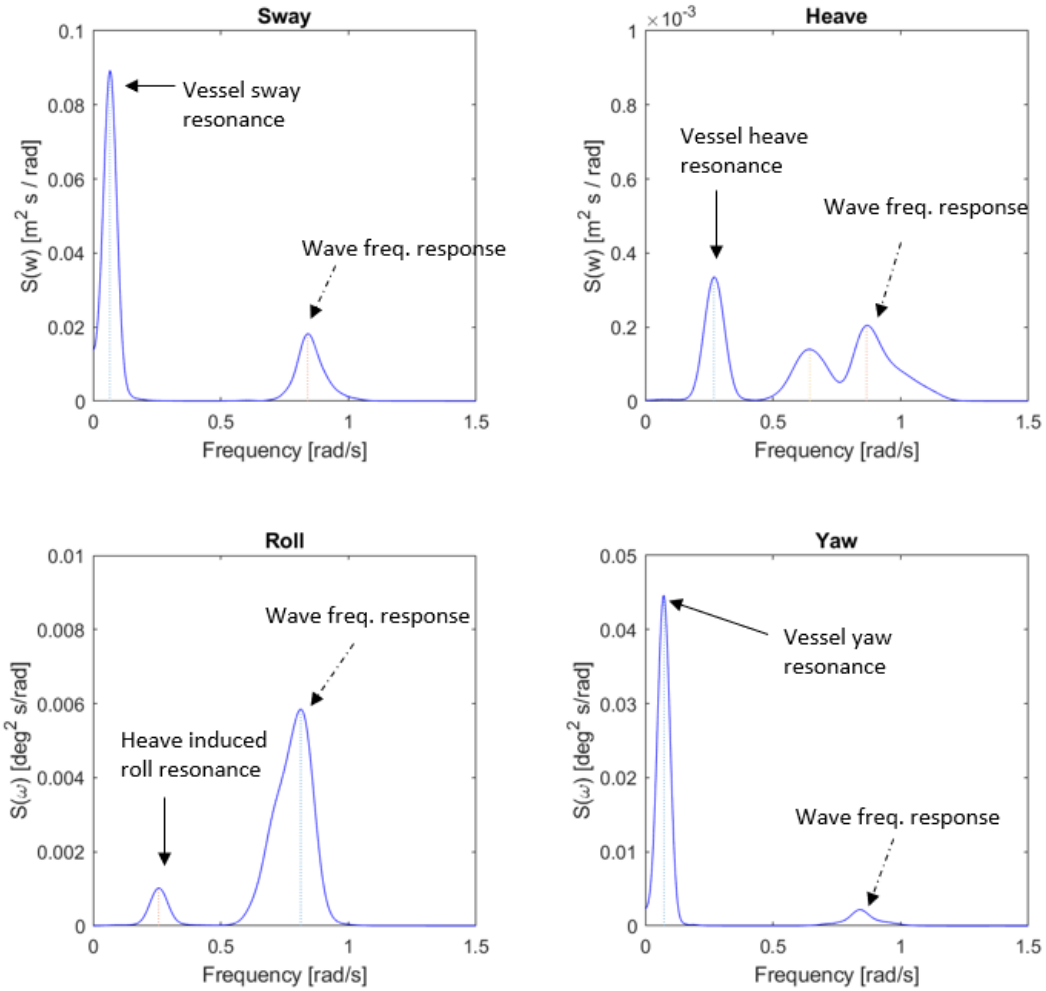

Figure 7.29: Power spectra of the SSCVs vessel motion; Hs=1 m, Tp=7.3 s, beam sea $\theta_{wv} = 0$ deg.

Figure 7.30 shows the vessels surge, heave and pitch motion in head sea. The vessel surge resonance is in the same frequency range as found in the regular analysis. At the same frequency as for the vessel heave resonance, an excited motion in pitch motion is induced.

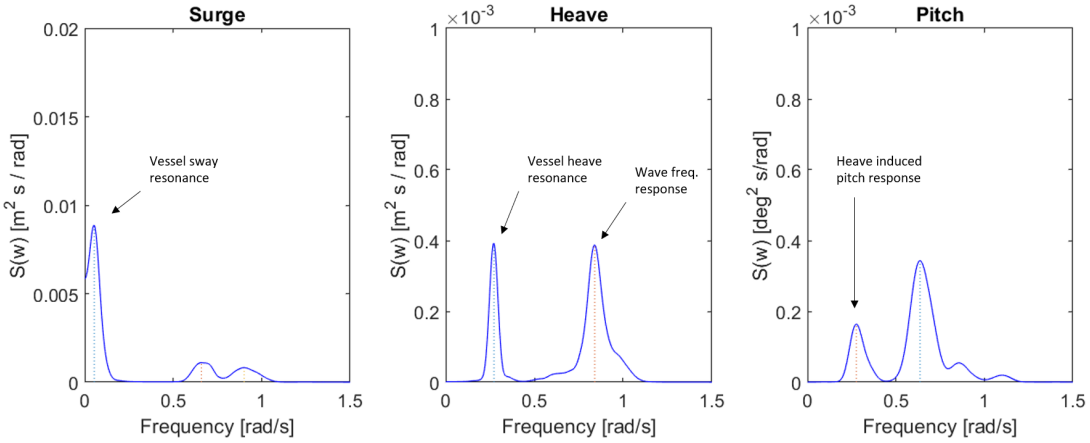

Figure 7.30: Power Spectra for SSCVs vessel motion; Hs=1 m, Tp=7.3, head sea $\theta_{wv} = 270$ deg.

Crane tip

Figure 7.31 presents the power spectra of the crane tip motions in head sea and beam sea. For both wave directions the crane tip motion is excited at a frequency approximately equal to 0.075 rad/s. These excitations occur close to the SSCVs natural period in surge and sway.

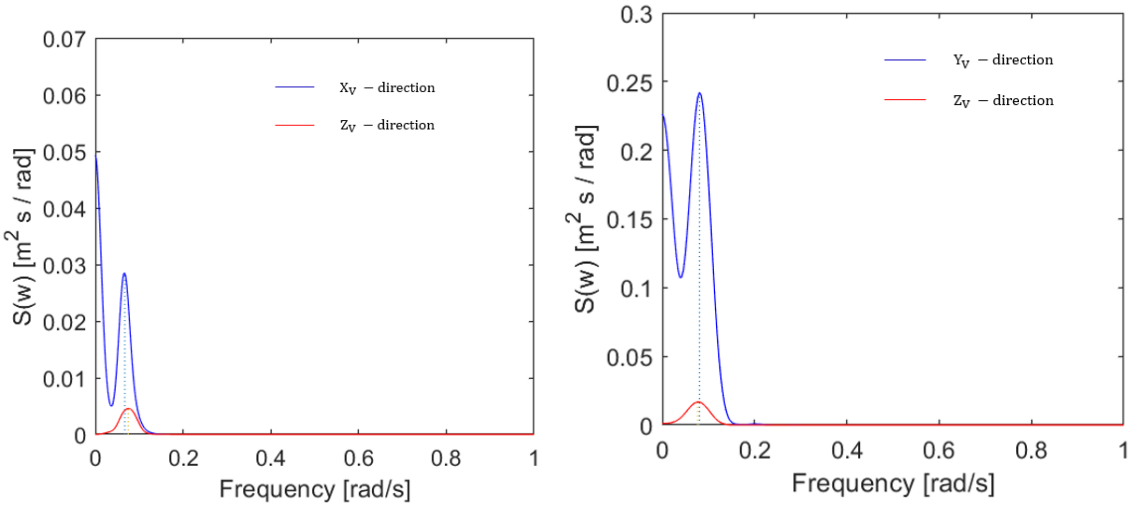

(a) Head sea, $\theta_{wv} = 270$ deg

(b) Beam sea, $\theta_{wv} = 0$ deg

Figure 7.31: Power spectra of the SSCVs crane tip motion; Hs=1m; Tp=7.3sec.

Blade

The resonance motions for the blade in beam sea are shown for all six DOFs in Figure 7.32. The figure shows how the blade motion is induced by the vessel motion. The pendulum resonance for the blade occur in the roll power spectrum at $\omega = 0.5$ rad/s. The reason for this is that the two tugger lines in x-direction significantly reduces the blades pitch motion, as seen for the power spectra for the pitch motion in Figure 7.32. Since they don't act in the global y-direction, the roll motion is not reduced by the tugger lines and pendulum resonance can occur for T = 12 s.

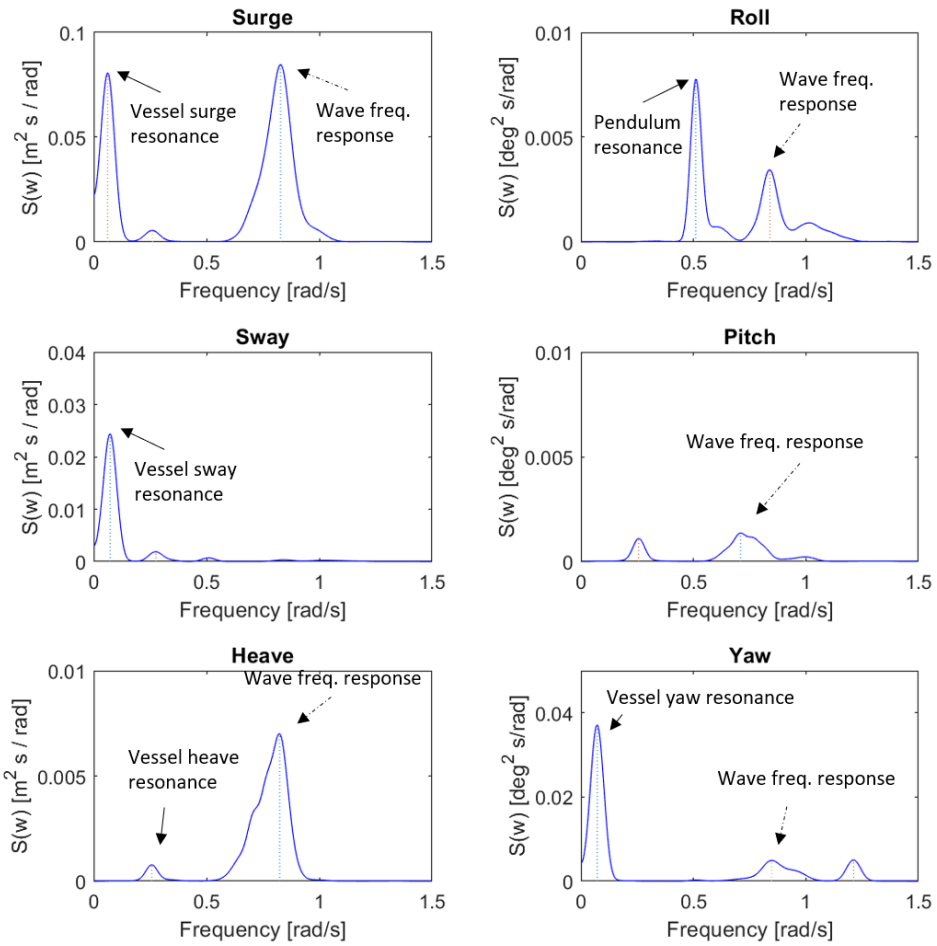

Figure 7.32: Power spectra of the SSCVs blade motion in all six DOFs; beam sea $\theta_{wv} = 0$ deg, Hs=1 m, Tp=7.3 s.

Figure 7.33 show the power spectra of the roll motion in head sea, and the pendulum resonance occur at the same frequency as the pendulum motion in beam sea.

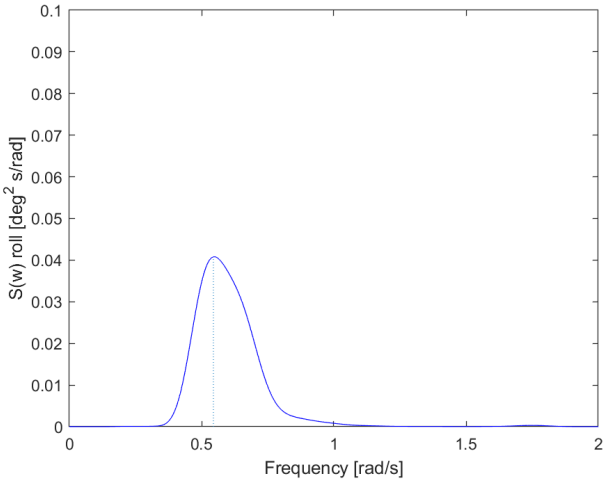

Figure 7.33: Power spectra of the SSCVs blade roll motion; head sea θ_{wv} =270 deg; Hs= 1 m; Tp=7.3 s.

7.4.2 Response Statistics

Case1

The first case analyses the responses for different T_p in head sea and beam sea. Figure 7.34 shows the standard deviation of the vessel, crane tip and blade responses for Hs=1 m. The plots shows that the responses for the crane tip and blade are highly dependent on the peak period in beam sea, and the responses increases as the peak period increases. Short peak periods or high frequency waves does not contribute to large wave-induced motions for the SSCV in head sea. The blade motion increases as the wave period approaches the blade pendulum resonance frequency, Tp = 12 s. Figure 7.34 (a) and (b) also show that the blade only experience a resonant pendulum motion in head sea and not beam sea, due to the existing tugger lines in global x-direction.

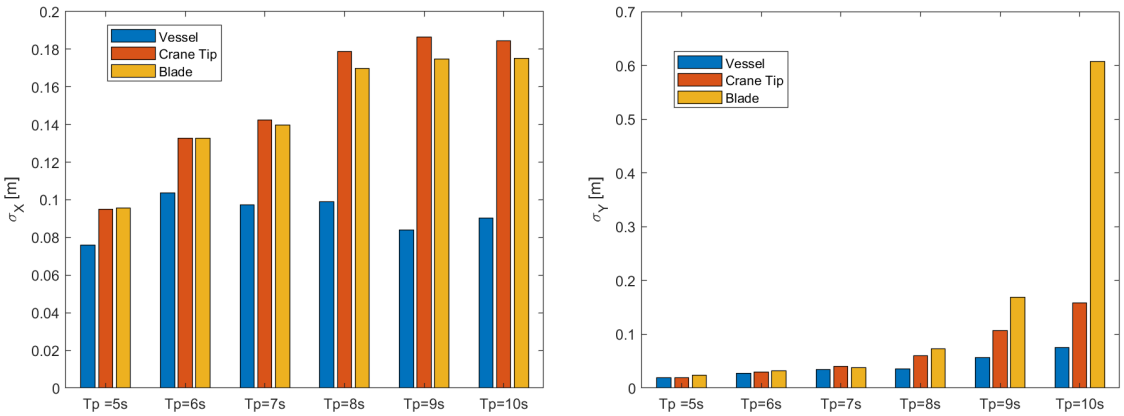

(a) Response in global x-direction; Beam sea, $\theta_{wv} = 0$ deg.

(b) Response in global y-direction; Head sea, $\theta_{wv} = 270$ deg.

Figure 7.34: Standard deviation for the SSCVs vessel, crane tip and blade motions for varying Tp; Hs = 1 m.

Figure 7.35 presents the responses in global x- and y-direction for increasing Tp in quartering sea. Also here, the responses increase with increased Tp, especially for the crane tip and the blade. From Figure 7.34 and Figure 7.35, it is clear that the motions are larger in beam sea, as found in the regular wave analysis.

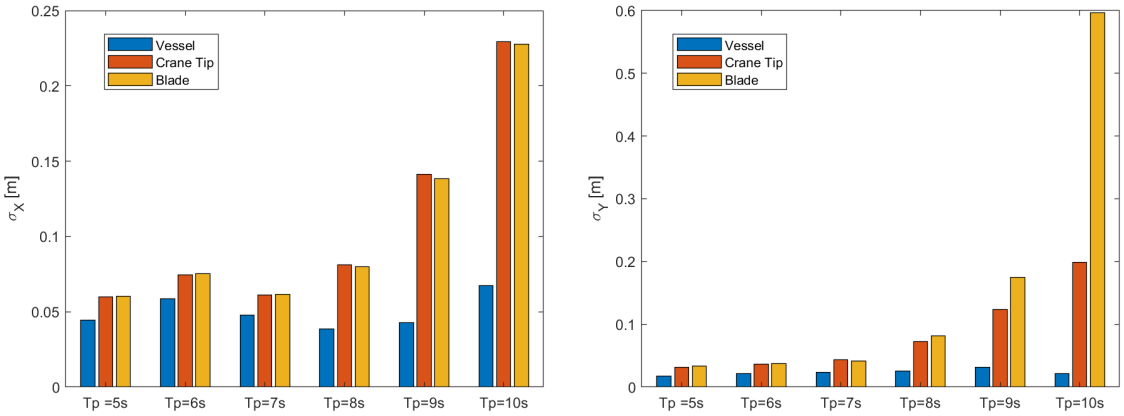

(a) Response in global x-direction;

(b) Response in global y-direction;

Figure 7.35: Standard deviation for the SSCVs vessel, crane tip and blade motions for varying Tp; quartering sea $\theta_{wv} = 315$ deg, Hs = 1m.

Case 2, 3 and 4

Figure 7.36 show the standard deviations for the vessel response, crane tip response and the blade response in beam and head sea for case 2, 3 and 4. The response motions are larger for case 4 than case 2 because of the larger significant wave height and larger peak period. The two plots also shows that the crane tip motion is larger than the vessel motion, even though the crane is fixed with respect to the vessel. Crane operations at large heights tends to have a larger translation motion than the vessel, as the vessel rotations contributes to the crane tip motions.

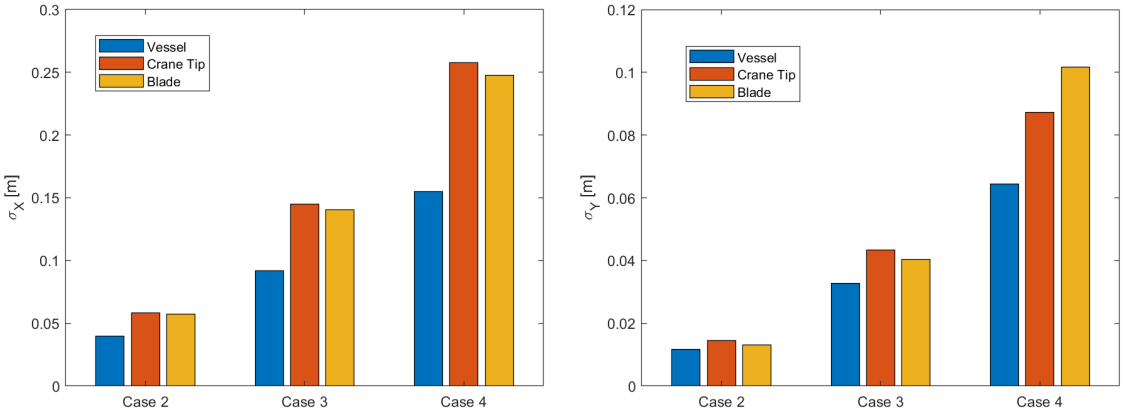

(a) Response in global x-direction; Beam sea, $\theta_{wv} = 0$deg.

(b) Response in global y-direction; Head sea, $\theta_{wv} = 270$deg.

Figure 7.36: Standard deviation for the SSCVs vessel, crane tip and blade motion for case 2, case 3 and case 4.

In this analysis the crane is assumed fixed, so the crane tip motion is mainly induced from the wave loads acting on the vessel. Figure 7.37 shows the standard deviations for the crane tip translation motions for case 2, 3 and 4 in both head and beam sea. The responses increases when Hs and Tp increases. Figure 7.37 shows that the crane tip motion is larger for all cases in beam sea than the response in head sea. The crane sway motion in head sea, remains small for all three cases, while the heave response in head sea for case 4 deviates from case 2 and 3. The latter also apply for the heave response in beam sea, see Figure 7.37 (b).

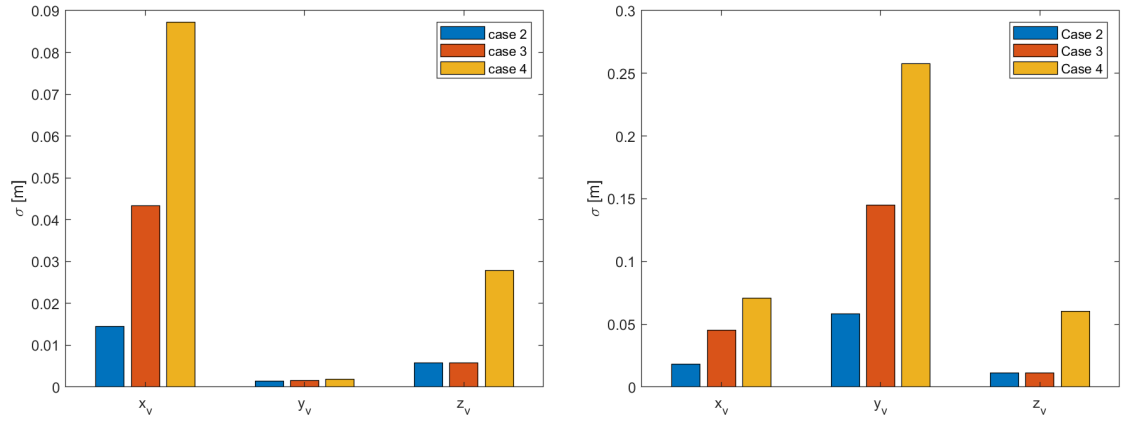

(a) Head Sea, $\theta_{wv} = 270$ deg

(b) Beam sea, $\theta_{wv} = 0$ deg

Figure 7.37: Standard deviation for the SSCVs crane tip motion in the vessel related coordinate system.

Low Tp only have marginally contribution to the response compared to the significant wave height. This is however, when Tp is outside the wave resonant range for the vessel. When Tp is within the resonant range, the contribution from Hs becomes trivial. This is seen by comparing the crane tip response in vessel related y-direction, presented in Figure 7.37 (b), with the crane tip response in Figure 7.34 (a) in Section 7.4.2. The observed standard deviation from the crane tip response is $\sigma_{y_v} = 0.2579$ m when Hs=1.5 m and Tp=7.7 s, and $\sigma_{y_v} = 0.1845$ m for Hs=1 m and Tp=10 s.

In Figure 7.38 the standard deviations of the blade motion in head and beam sea are presented. Figure 7.38 (a) shows that the surge and pitch motion of the blade does not change much from case to case, when both Hs and Tp increases in head sea. A tendency seen in the previous cases for the SSCV motion and the crane tip motion is that there are generally larger responses in beam sea than in head sea. For the blade response, the roll motion in head sea is larger than the roll motion in beam sea according to the standard deviations shown in Figure 7.38 (a) and (b), this is due to the working tugger lines in the global x-direction.

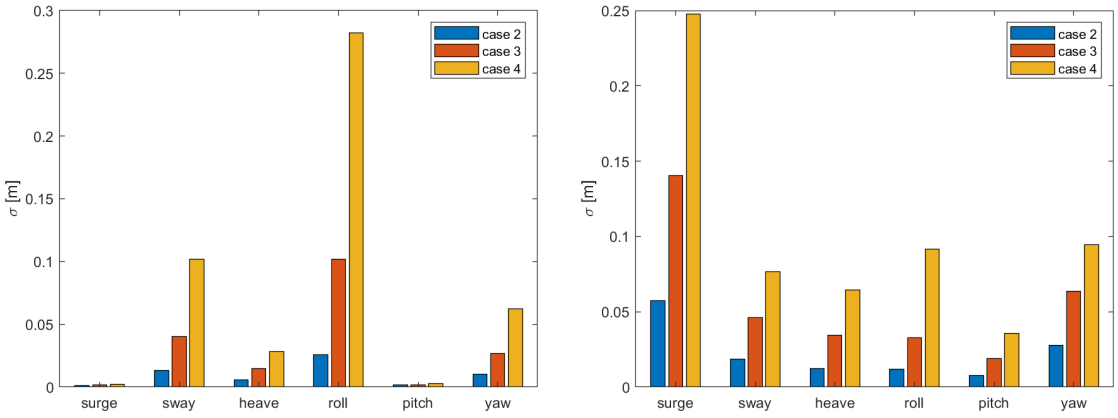

(a) Head sea, θ_{wv} =270 deg.

(b) Beam sea, θ_{wv} =0 deg.

Figure 7.38: Standard deviation of the SSCVs blade motion in six DOFs for case 2, case 3, case 4.

7.5 Jack-Up Vessel: Irregular Wave Analysis with Wind Loads

This section present the results from the wave + wind analysis of the jack-up vessel. The following section will firstly describe the properties of the system and secondly the statistical response results. There are mainly two environmental conditions that are considered. These will be mentioned as case 1 and case 2. Table 7.3 present the fixed and running variables for these cases.

Table 7.3: Parameters for the two main cases considered for the wave and wind analysis.

	Hs [m]	θ_{wd} [deg]	Fixed variables	Running variables
Case 1	1.0	0	θ_{wv}, U_w	Tp
Case 2	1.0	0	Tp,U_w	θ_{wv}

In Figure 7.39 the time series of the wind velocity and a time series of the blade roll motion are plotted. In the figures it is seen that the wind velocity varying with a mean value of 7 m/s.

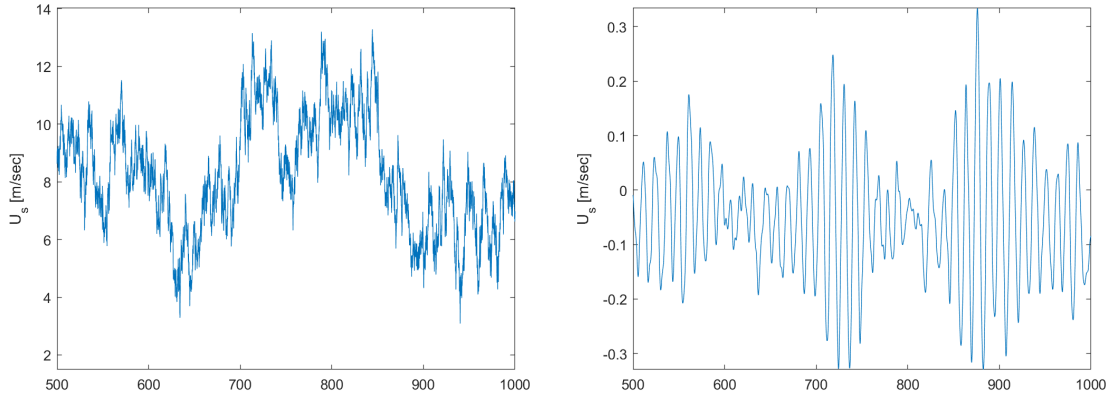

(a) Wind speed

(b) Blade roll response

Figure 7.39: Time series of the wind speed and the jack-ups blade roll motion; Hs = 0 m, U_s = 7 m/s, θ_{wd} = 0 deg.

Figure 7.40 illustrates the blade response motion for the six DOFs when exposed to only wind loads. The roll motion is the dominating response motion. This is due to the double pendulum response motion that can be seen as roll motion. Compared to the response motion for only waves, the blade now experience some heave motion.

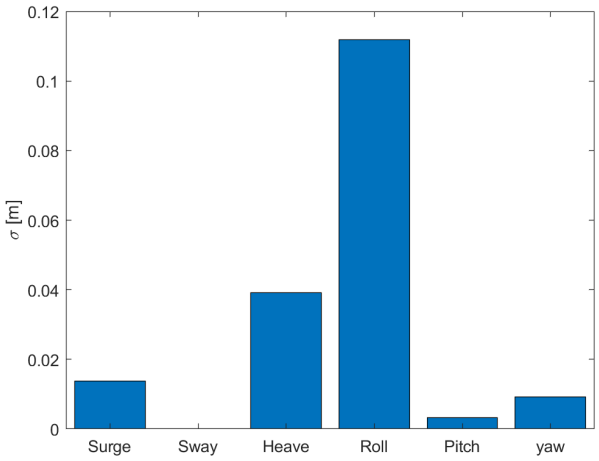

Figure 7.40: Standard deviations for the jack-up blade six DOFs exposed to wind loads only; Hs = 0 m, U_s = 7 m/s, θ_{wd} = 0 deg.

7.5.1 System Properties

The power spectra for the blade is presented in Figure 7.41 and 7.42. They present two combinations of wind and wave direction, head sea and beam sea. Further, the responses of both wind and wave loads and only wave loads are compared in the figures.

Figure 7.41 illustrates that there is more energy in the system when exposed to both wind loads and waves loads, compared to only wave loads. The system is excited at a frequency of 0.5 rad/s when exposed to wind loads in global x-direction. This is the double pendulum response, which was identified in the regular and irregular result sections. The pendulum motion of the blade increased when wind loads included. Further, it is seen that the excitation frequency for the case with wave and wind loads is 1.3 rad/s while the case of only wave loads have an excitation frequency of 1.4 rad/s. The dominating response motions correlates with the expected motions for the wave direction, which means that the wave direction has a greater impact on the system compared to the wind direction.

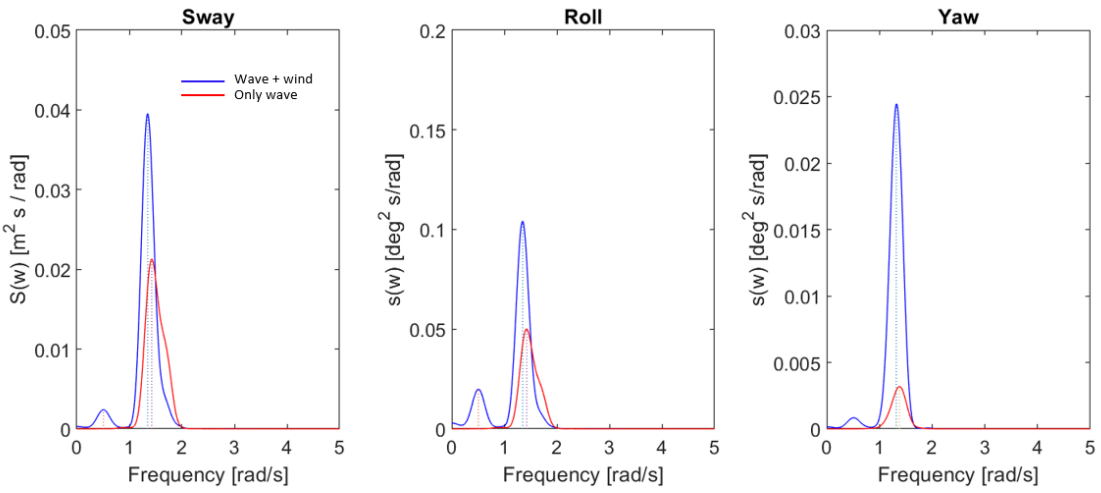

Figure 7.41: Power spectra of the blade sway, roll and yaw motion with wind and with out wind; Hs = 1 m, Tp = 7.3 s, head sea θ_{wv} = 270 deg, θ_{wd} = 0 deg.

In beam sea the responses for surge and pitch nearly coincide, as seen in Figure 7.42. For the yaw excitation, there is a response larger for the case of no wind but of small magnitude. Compared to head sea, Figure 7.41, the resonance periods for the case of wind and wind+wave analysis now coincide. This is expected as the wave and wind direction in this case is in the same direction.

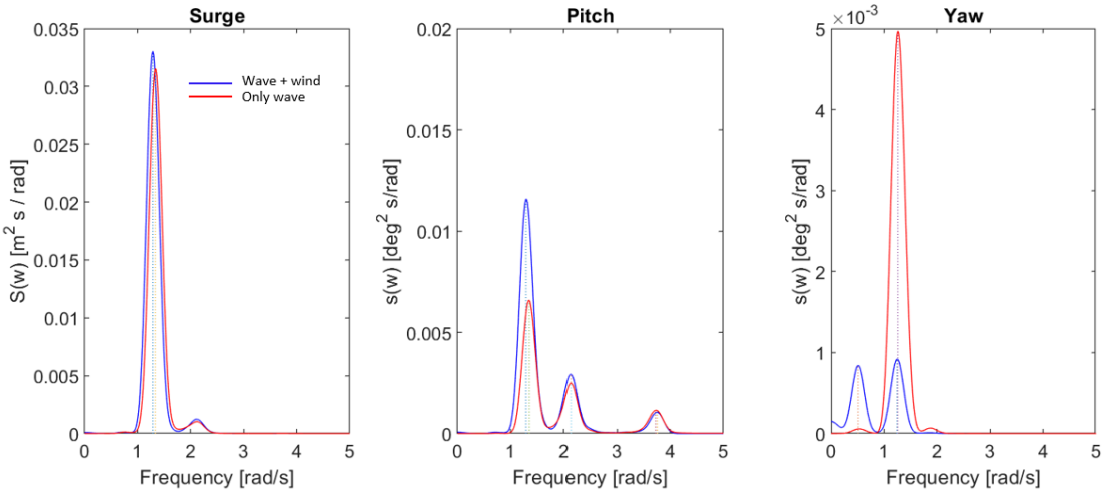

Figure 7.42: Power spectra of the blade motion; Hs = 1 m, Tp = 7.3 s, beam sea $\theta_{wv} = 0$ deg, $\theta_{wd} = 0$ deg.

7.5.2 Response Statistics

Case 1

In Figure 7.43 the standard deviations of the blade motion in six DOFs for increasing spectral peak periods in head sea are presented. The system response is greatest for Tp = 5 s. This coincide with the results from both the regular and the irregular analysis without wind, as the natural period for the jack-up legs is close to this period. Further, when comparing the different DOFs it is seen that the motion response for the case wind+waves generally induce larger response motions. The biggest difference is for the yaw motion, where the case with wind is about twice the size compared to the response due to only waves. The wind and wave direction is working normal to each other, hence large yaw rotations are expected.

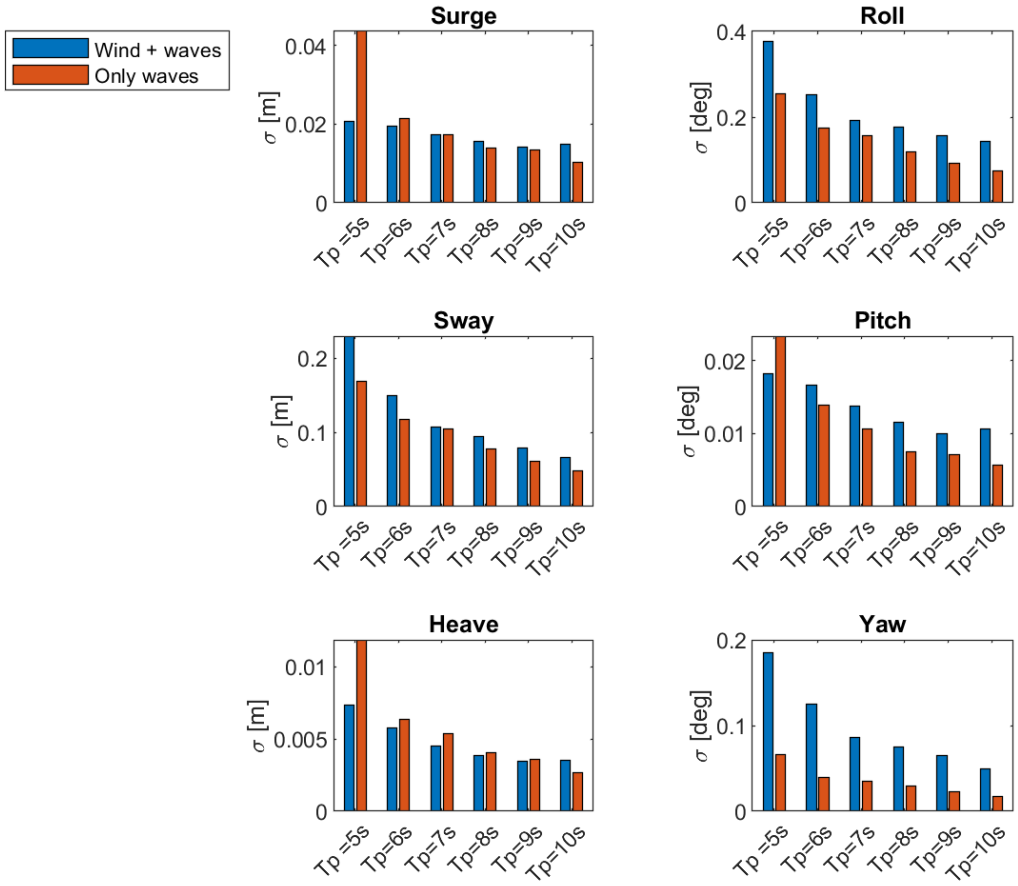

Figure 7.43: Standard deviation of the jack-up blade for varying Tp for only waves and wind+waves; Hs = 1 m, head sea $\theta_{wv} = 270$ deg, $\theta_{wd} = 0$ deg, $u_{wd} = 7$ m/s.

Case 2

Figure 7.44 illustrates the time series of the crane tip and blade motion in global y-direction. In figure (a) the full time series are plotted and figure (b) show the last 50 seconds of the time series. It is seen that the response of the crane and blade follow each other, but that the blade over all has a larger amplitude. As found in Section 7.5.1, the response motion correlates with the wave direction. Hence, crane tip motion is plotted in x_v and y_v for head sea and beam sea respectively.

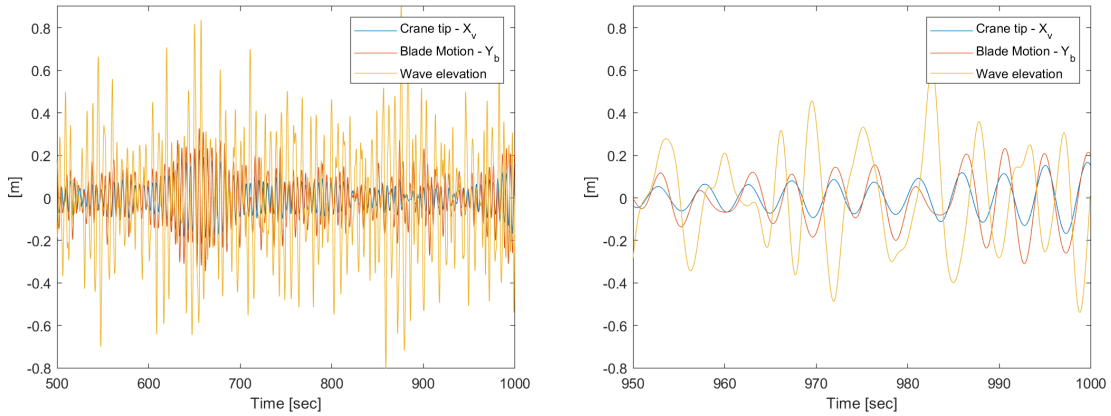

(a) 500 sec (b) 50 sec

Figure 7.44: Time series of the jack-up blade sway motion, the crane tip motion and the wave elevation; Hs = 1 m, Tp = 7.3 sec, head sea $\theta_{wv} = 270$ deg, $\theta_{wd} = 0$ deg.

In Figure 7.45 the time series of the crane tip and blade motion are presented. In figure (a) the full time series are shown and in Figure (b) only the last 50 seconds are plotted. When the wind and wave direction coincide the crane tip motions are larger relative to the blade motion. The over all amplitude magnitude is larger than for the time series with wave and wind direction normal to each other. This is expected when the external loads are working in the same direction.

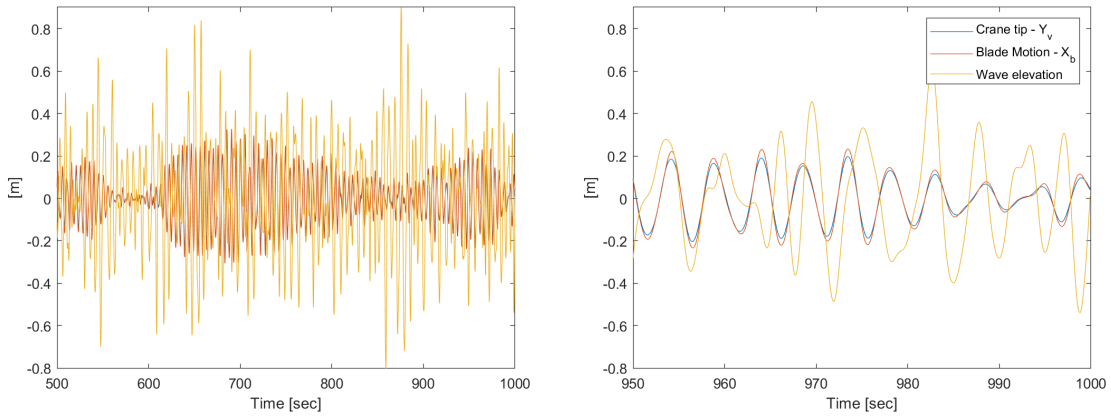

(a) 500 sec (b) 50 sec

Figure 7.45: Time series of the jack-up blade surge motion, the crane tip motion and the wave elevation; Hs = 1 m, Tp = 7.3 sec, beam sea $\theta_{wv} = 0$ deg, $\theta_{wd} = 0$ deg.

In Figure 7.46 the standard deviation for the six DOFs are compared for four different combinations of wind and wave directions. The set definitions are listed in Table 7.4. The surge, sway, roll and yaw motions are the motions with the highest magnitude of response. In general, for set 1, 2, 3, the response when exposed to both wind and wave loads induce the larger response motion than compared to the case of only waves. The exception is set 4, where both the wave and wind heading is 315 deg. In this case the system gets a larger response when only exposed to wave loads. Further, set 1 and set 2 induce the larges response motions when exposed to wind+waves.

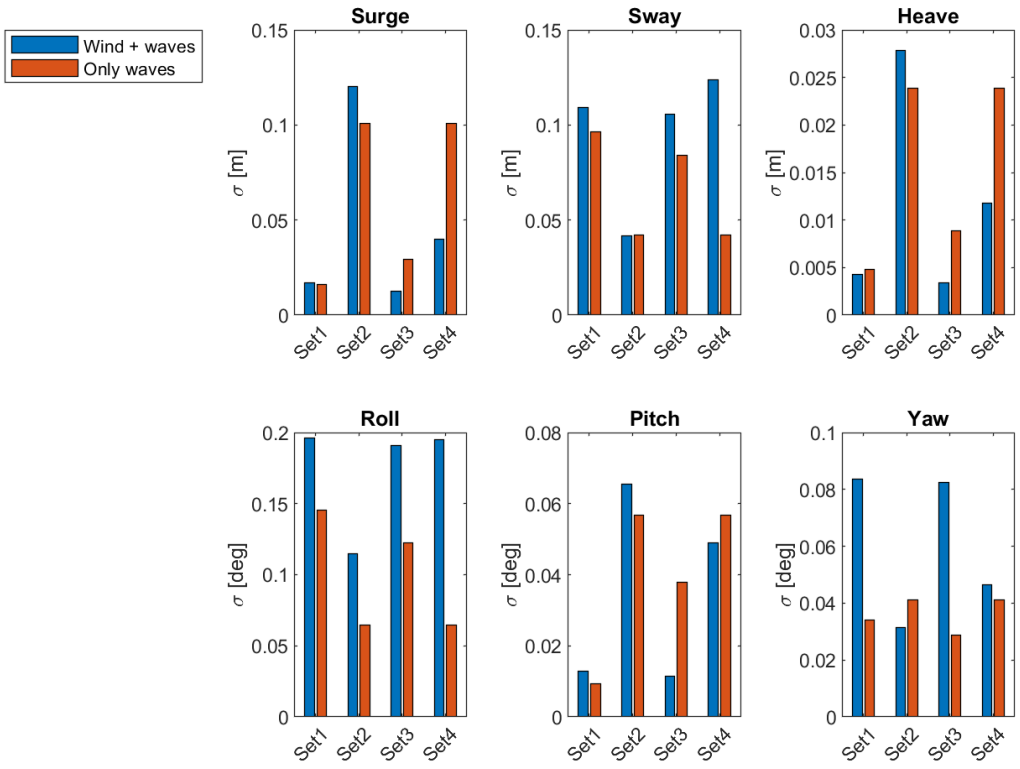

Figure 7.46: Standard deviation of the jack-up blade motion in the six DOFs with for varying wind and wave directions; Hs = 1 m, Tp = 7.3 sec

Table 7.4: Set definitions for Figure 7.46.

	θ_{wv} [deg]	θ_{wd} [deg]
Set 1	270	0
Set 2	0	0
Set 3	270	270
Set 4	315	315

7.5.3 Tension in lift wire and tugger lines

In figure 7.47 the standard deviation of the tension in the lift wire is compared for the following environmental conditions; only wave, only wind and wave+wind. These load conditions are compared for head sea, beam sea and quartering sea.

When comparing the effect of the loads, it is clear that the wave loads have a greater impact on the tension in the lift wire than the wind force. The case of wind+wave loads gives the highest tension for all wave headings. The lift wire is sensitive to motion in the vertical plane. From the previous sections it was found that both the crane tip motion and the blade heave motion were largest of magnitude in beam sea compared to head sea. Hence, the largest tension in the lift wire is in beam sea.

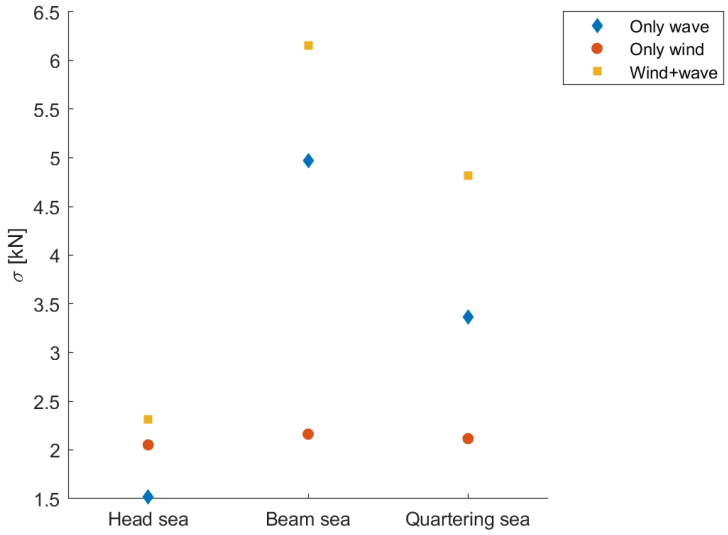

Figure 7.47: Standard deviation of the tension in the lift wire; head sea $\theta_{wv} = 270$ deg, beam sea $\theta_{wv} = 0$ deg, quartering sea $\theta_{wv} = 315$ deg, Hs = 1 m, Tp = 7.3 s.

The tugger lines are connected from the boom to the yoke in order to reduce the blade motions, mainly in the horizontal plane. Tugger line 1 is connected close to the blade COG while tugger line 2 is connected near the blade root. In Figure 7.48 is the standard deviation of the tension in both of the tugger lines for the following environmental loads; only waves, only wind and wind + waves. Further, these load conditions are compared in head sea, beam sea and quartering sea.

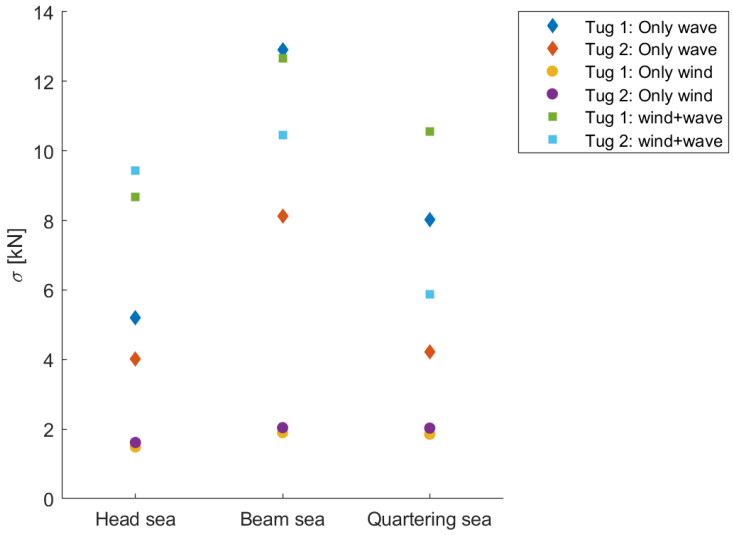

Figure 7.48: Standard deviation of the tension in the tugger lines; head sea $\theta_{wv} = 270$ deg, beam sea $\theta_{wv} = 0$ deg,quartering sea $\theta_{wv} = 315$ deg, Hs = 1 m, Tp = 7.3 s.

The tension in the tugger lines are highly effected by the wave loads. It is seen that the case of only wind load induce about the same tension in the tugger lines for all three wave headings. Over all, the case of wind and wave loads combined induce the highest tension in the tugger lines. As for the tension in the lift wire, the tension in the tugger lines is the highest for beam sea. This corresponds with the results from the previous sections, where beam sea condition in general induce the highest

vessel motions. Hence, high tension in the tugger lines are expected.

Figure 7.49 illustrate the tension in the tugger lines and lift wire for increasing Tp. It is seen that the tension is highly dependent of Tp. As the bending mode of the leg i around 5 seconds, it follows that there is higher tension in both the lift wire and the tugger lines.

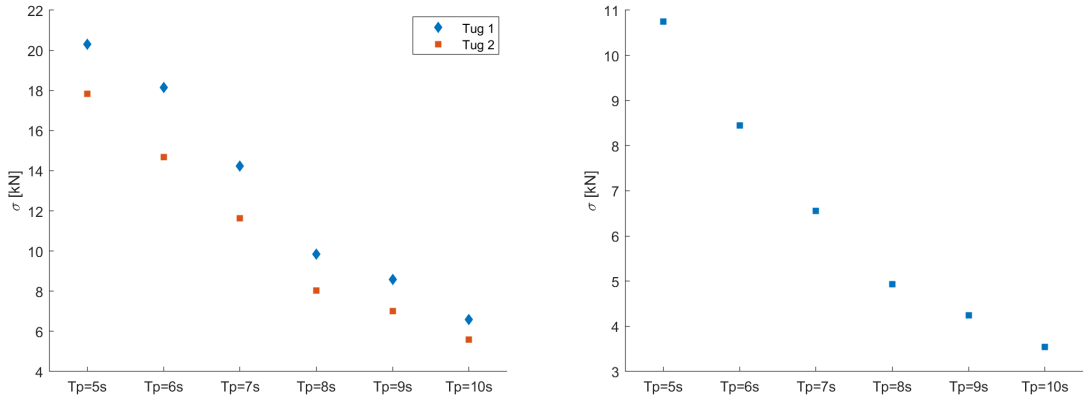

(a) Tugger lines

(b) Liftwire

Figure 7.49: The standard deviation of the tension in tugger lines and lift wire for varying Tp; Hs = 1 m, $\theta_{wv} = 0$ deg, $\theta_{wd} = 0$ deg, $U_w = 7$ m/s.

7.6 The Semi-submersible: Irregular Wave Analysis with Wind Loads

This section will present the results from the irregular wave analysis when accounting for wind loads acting on the SSCVs blade. The response parameter evaluated in this analysis is the blades COG motion and the crane tip motion. For the SSCV, the aerodynamic loads acting directly on the hull have negligible contribution to the responses because the wave-induced loads are to significant.

This analysis is conducted with two different environmental conditions which are presented in Table 7.5. The system properties will be described by power spectra of the blade motion, then the statistical properties for the three cases will be described.

Table 7.5: Parameters for the three main cases considered for the wave+wind analysis of the SSCV.

	Hs [m]	θ_{wd} [deg]	Fixed variables	Running variables
Case 1	1.0	0	θ_{wv}, U_w	Tp
Case 2	1.0	0	Tp, U_w	θ_{wv}

Figure 7.50 (a) present the time series of the wind velocity. As the time series show, the wind velocity is a varying parameter. Figure 7.50 (b) show how the wind load contributes to the blade roll motion.

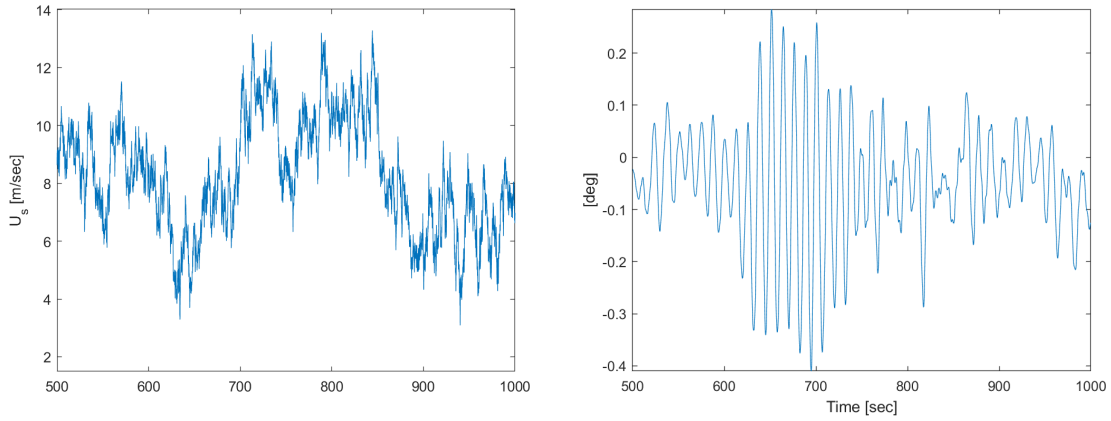

(a) Wind velocity (b) Blade roll response

Figure 7.50: Time series of the wind speed and the blade roll motion; θ_{wd} =0deg, U_w = 7.0m/s, Hs=0m.

Figure 7.51 present the standard deviations of the blade motion in all six DOFs when the blade only are exposed to wind loads. The only motion response of any significance is the roll motion. This is expected as the double pendulum motion is seen as roll motion for the blade. This analysis gives a clearer picture on how the wind is contributing when the wave loads are included in the analysis.

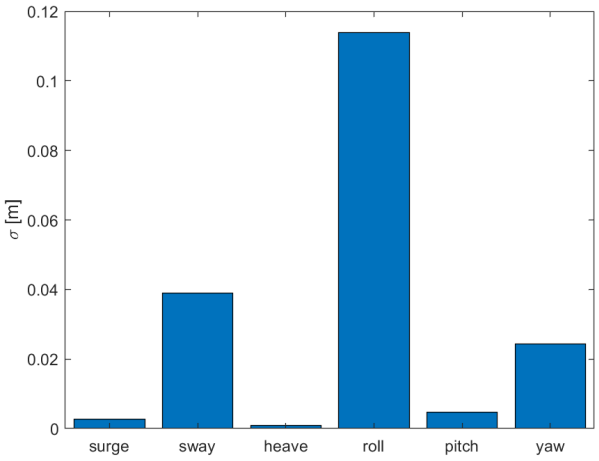

Figure 7.51: Standard deviation of the SSCVs blade motion; θ_{wd} = 0 deg, U_w = 7.0m/s, Hs=0m.

7.6.1 System Properties

Figure 7.52 show that the system in sway, roll and yaw excites at a frequency around 0.5 rad/s which is the double pendulum resonance in roll for the blade identified in the irregular wave analysis. In sway and roll motion the wave and wind case almost coincide with the only wave case, but the system holds more energy when wind loads are included. For the yaw response, the system when wind is included has larger excitation at a frequency approximately equal to 1.2 rad/s, compared to the only wave condition.

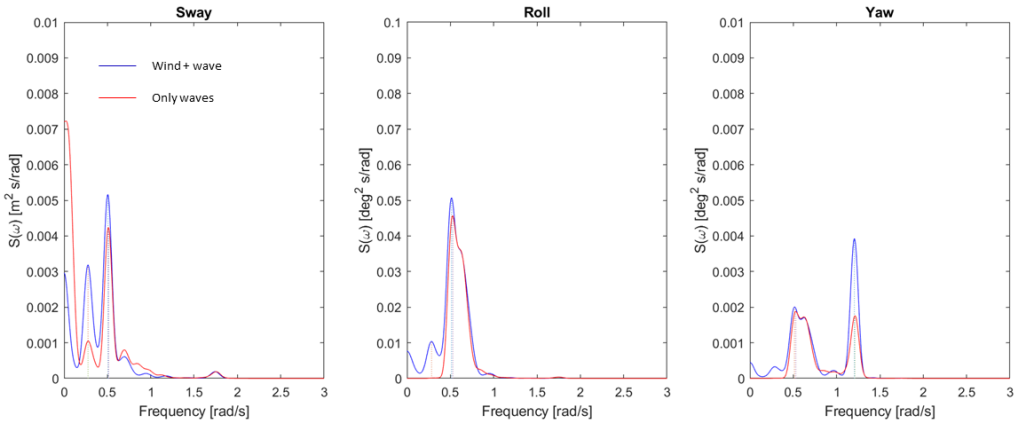

Figure 7.52: Power Spectra of the SSCVs blade motion; head sea $\theta_{wv} = 270$ deg; Hs=1 m; Tp= 7.3 s; $U_w = 7$ m/s; $\theta_{wd} = 0$ deg.

Figure 7.53 show that the system for the wind and wave analysis has less energy in the system than for the case with only waves in surge motion. This is due to the aerodynamic damping effect that reduces the pendulum motion of the blade when the wind and wave direction are aligned. For roll and pitch motion, the systems have significantly more energy when wind loads are acting on the blade compared with only wave loads. These three degrees of freedom analysed in this section are the assumed motion with response of any significance. This figure also show that at the pendulum resonance motion at frequency at $\omega = 0.5$ rad/s is significantly reduced in surge and pitch. This is due to the acting tugger lines. By comparing the motions in head and beam sea one can see that the pendulum resonance motion only occur for head sea because the wave acts across the effect from the tugger lines.

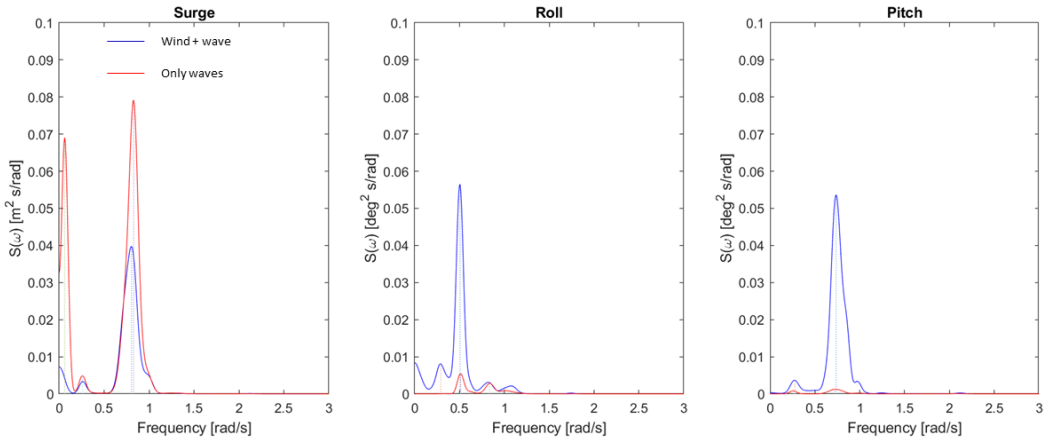

Figure 7.53: Power Spectra of the SSCVs blade motion; beam sea θ_{wv} = 0 deg; Hs=1m; Tp=7.3sec; U_w = 7.0 m/s; θ_{wd} = 0 deg.

7.6.2 Response Statistics

Case 1

Figure 7.54 presents the standard deviation of the blade motion in all six DOFs for different spectral peak periods. This analysis is conducted with waves propagating in head sea with Hs=1 m and with a wind velocity of 7 m/s. The figure show that for Tp= 10 s, the responses when there is no wind are significantly larger in all DOFs, which means that for high Tp, the largest contribution to the blade response is mainly from the incident wave loads acting on the vessel. The wind loads also introduces an aerodynamic damping effect on the blade which reduces the wave induced pendulum motion when Tp approaches T = 12 s. For Tp between 5 - 9 seconds, the responses are larger for all DOFs except for heave when wind loads are included. The sway, roll and yaw motion has generally larger responses compared to surge, heave and pitch, which correlates with the expected dominated response motion for the given wave direction. For head sea, the expected dominating DOFs for the blade is sway, roll and yaw, according to the coordinate system in Figure 7.2.

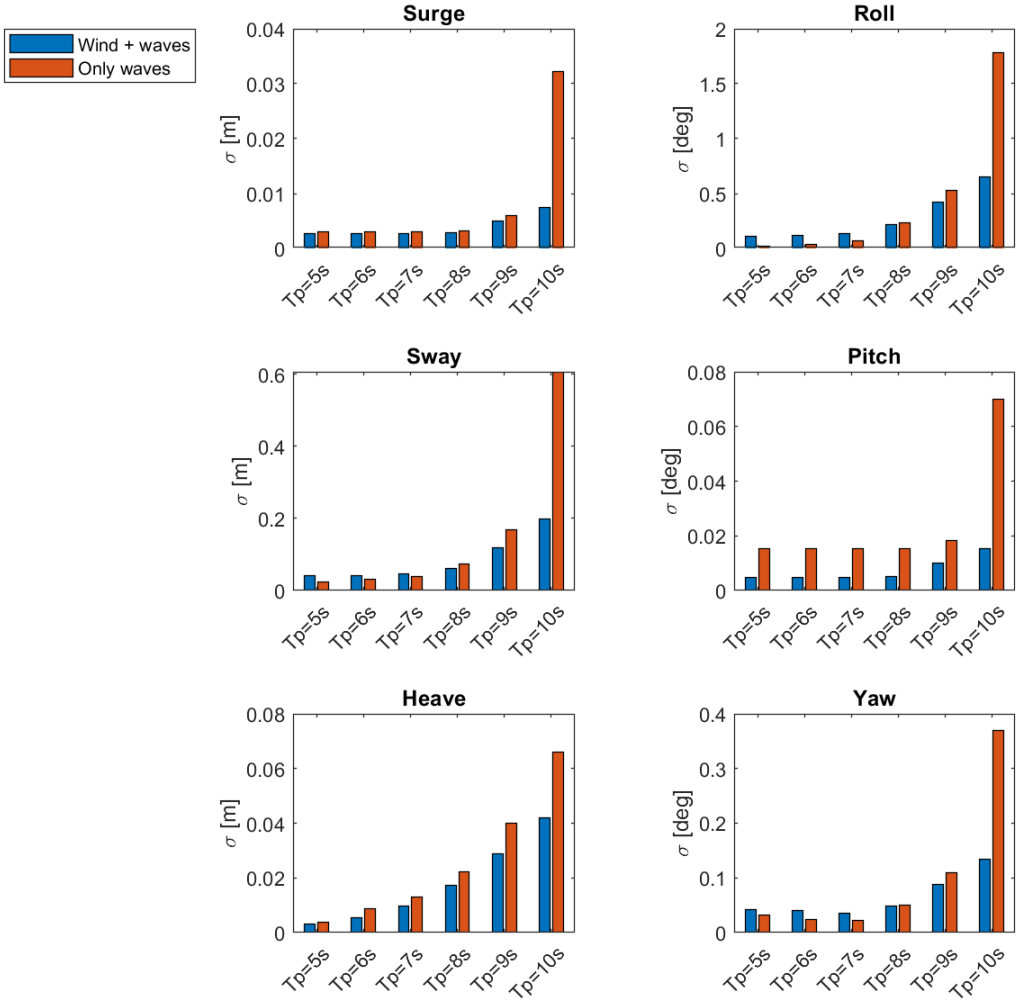

Figure 7.54: Standard deviations of the SSCVs blade motion for varying Tp; head sea θ_{wv} =270deg; Hs=1 m; U_w =7.0m/s; θ_{wd} =0 deg.

Case 2

In this case, the blade motion response is found for different combinations of wave and wind headings. The significant wave height and spectral peak period are fixed at 1 meter and 7.3 seconds with a wind velocity of 7 m/s. Figure 7.55 present the blade response for all six degrees of freedom for four different combinations of the wave and wind directions, which is described in detail in Table 7.6.

The standard deviations in Figure 7.55 shows that the blade surge motion is dependent of the wave direction. It shows that for beam sea the surge motion is significant compared to set 2 and 3, where the the waves propagate in head direction. From set 1 the roll motion of the blade will also be of significance when wind loads are included. However, this figure show that the roll motion is increased when wind and wave loads are acting on the system compared with only waves independent of the wave and wind directions.

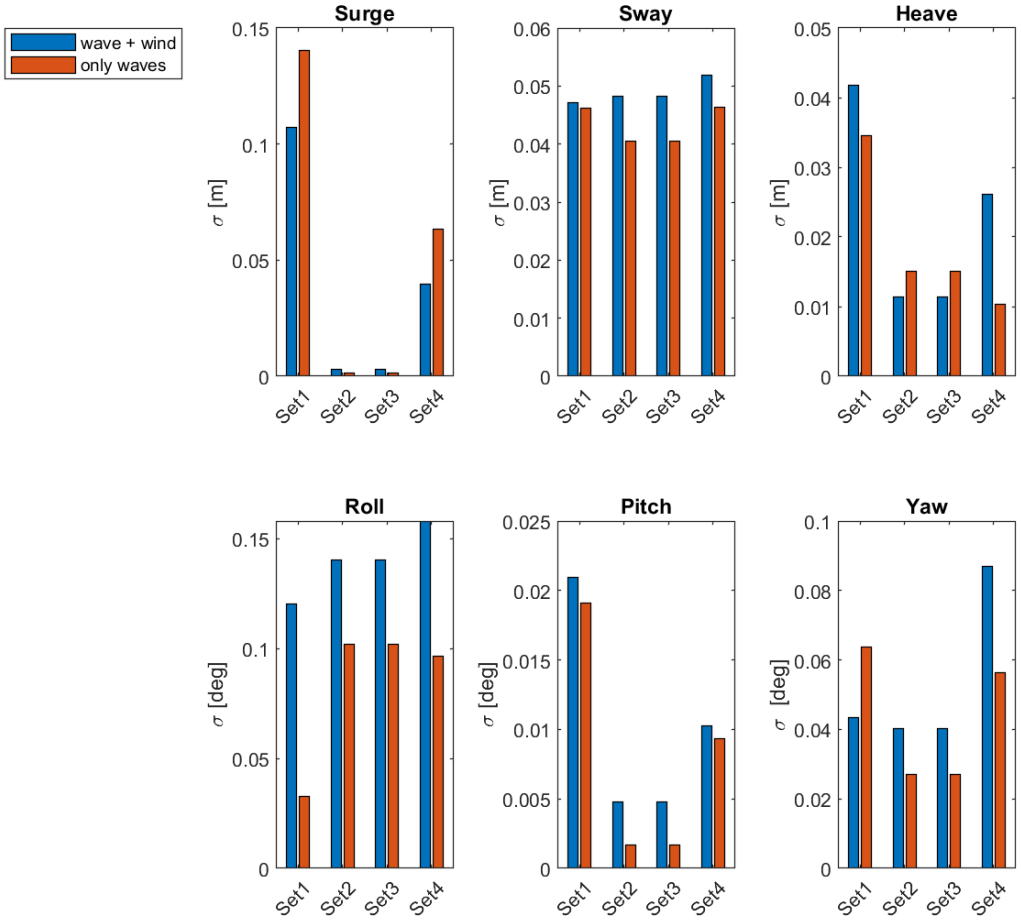

Figure 7.55: Standard deviations of the SSCVs blade motion for varying wave and wind directions; Hs=1 m, Tp = 7.3 s, U_w =7.0 m/s.

Table 7.6: Set definitions for Figure 7.55.

	θ_{wv} [deg]	θ_{wd} [deg]
Set 1	0	0
Set 2	270	0
Set 3	270	270
Set 4	315	315

Figure 7.56 show the blade motion, the crane tip motion and wave elevation over a period of time when wave and wind are acting in the same global x-direction. The crane tip and the blade response coincide, and the blade follow the crane tip response because the tugger lines work in global x-direction.

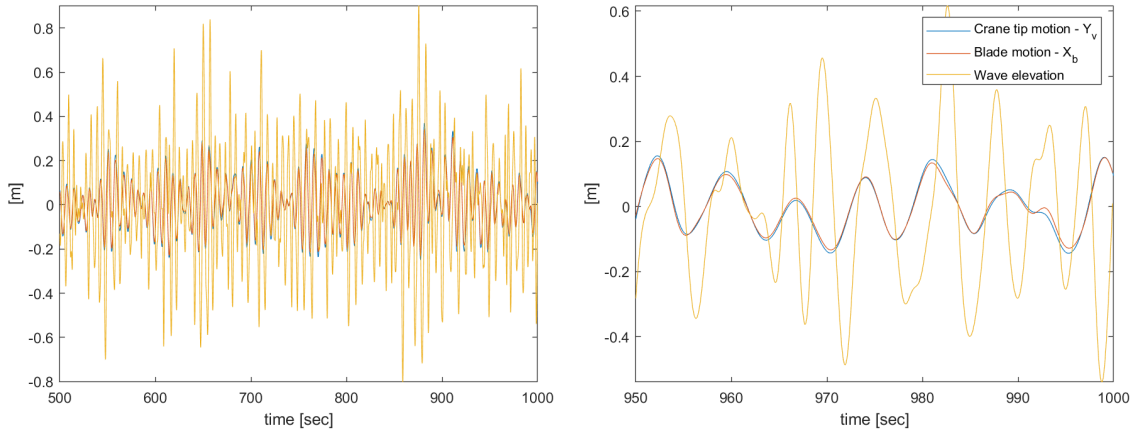

(a) 500 sec (b) 50 sec

Figure 7.56: Time series of the SSCVs crane tip motion, blade motion and wave elevation; beam sea θ_{wv} =0 deg; Hs= 1 m; Tp=7.3 s; U_w =7 m/s; θ_{wd} =0 deg.

Figure 7.57 show a time series of the blade motion, crane tip motion and the wave elevation when the waves propagate in head sea. The responses are in global y-direction, and the crane tip and blade motion does not coincide with the same precision as the responses in Figure 7.56. However, Figure 7.57 (b) shows the 50 last seconds of the simulation, and provide a more detailed plot of the time series. From this it shows that the tendency of the blade motion is the same as the crane tip, but with some irregularities. This is explained by the fact that the waves work across the effect of the tugger lines.

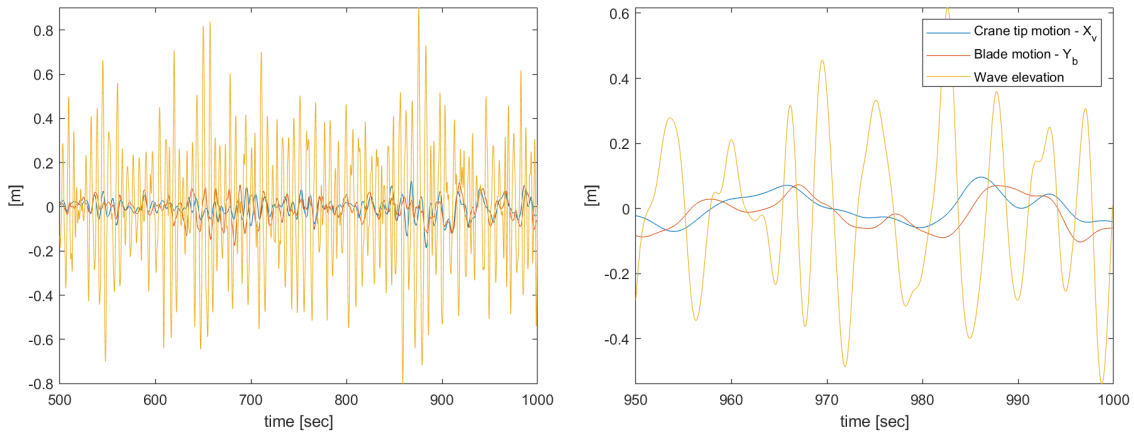

(a) 500 sec (b) 50 sec

Figure 7.57: Time series of the SSCVs crane tip motion, blade motion and wave elevation; head sea θ_{wv} =270 deg; Hs=1m; Tp=7.3sec; U_w =7m/s; θ_{wd} =0 deg.

7.6.3 Tension in lift wire and tugger lines

This section will present the tensin in the tugger lines and the lift wire for the SSCV. Hs=1 m, U_w =7 m/s and θ_{wd} = 0 deg are the fixed parameters. For the case with only wind and no waves, the tension is compared for head, beam and quartering wind direction.

Figure 7.58 present the standard deviation of the tension in each tugger line. Tug 1 is the line closes to the blade tip, while tug 2 is closest to the blade root. The figure show that the tension fluctuations are increased when wind force is included, and it is largest in quartering sea. This

can be connected with the large yaw motion the blade experiences in quartering sea, see Figure 7.55. When only wave loads are included, the tugger line tension is largest in beam sea. This is due to the large response motion in surge of the blade motion presented in Figure 7.55. For a sea state with no waves and only wind load acting on the blade, Figure 7.58 show that the tension variations in the tugger lines is not affected of the wind heading. This states that the contribution for the responses is mainly dependent of the different wave headings compared to different wind headings.

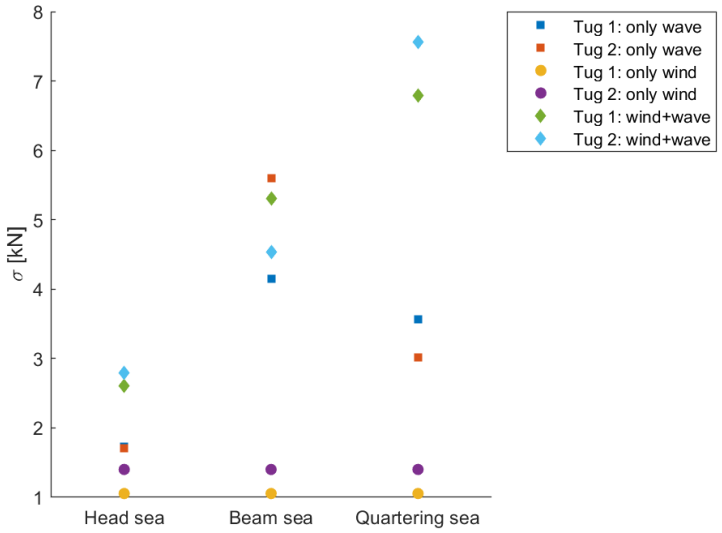

Figure 7.58: Standard deviation of the tension in the SSCVs tugger lines with varying wave directions; Hs = $1m$, Tp=7.3 sec; U_w =7.0m/s

Figure 7.59 show the lift wire tension for the blade. The lift wire is the connection between the crane tip and the yoke that holds the turbine blade. There is highest tension in the lift wire when waves and wind loads are included. Further, there is also larger tension when only wind loads are acting compared with only wave loads acting on the blade. The figure also show that the tension is largest in beam sea, which correlates with the heave response in beam sea for the blade presented in Figure 7.55.

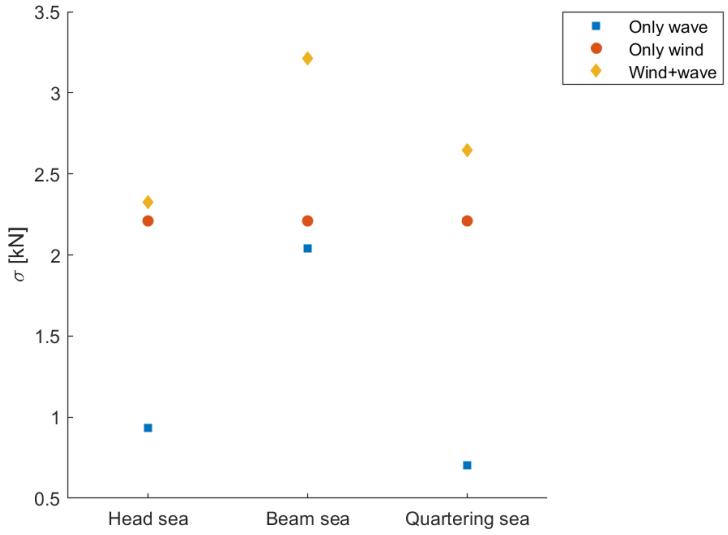

Figure 7.59: Standard deviation of the tension in the SSCVs lift wire with varying wave directions; Hs = $1m$, Tp=7.3 sec; U_w =7.0m/s

Figure 7.60 present the standard deviation of the tension in the tugger lines and the lift wire for varying spectral peak period. It is clear that the tension in both tugger lines and the lift wire are increasing for increasing Tp. This corresponds with the system properties of the SSCV and the larger motions that occur for large Tp.

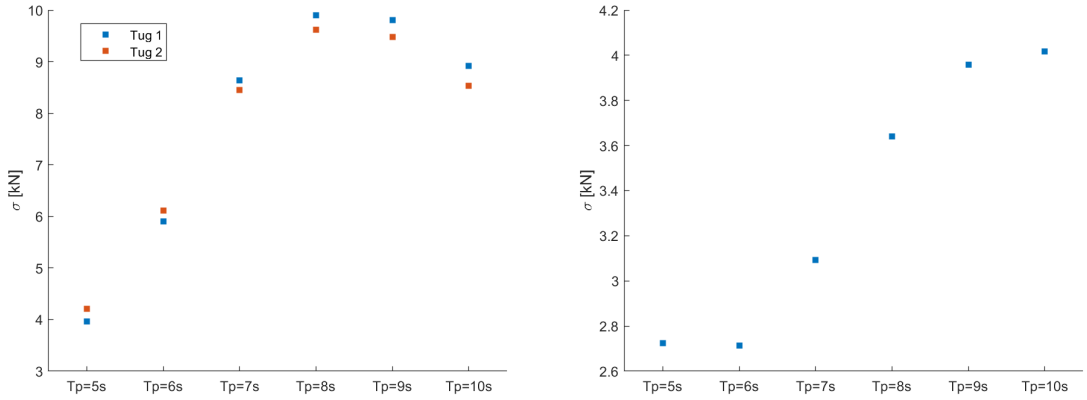

(a) Tugger lines

(b) Lift wire

Figure 7.60: Standard deviation of the tension in the SSCVs tugger lines and lift wire for varying Tp; Hs = 1 m, $\theta_{wv} = 0$ deg, $\theta_{wd} = 0$ deg, $U_w = 7$ m/s.

Chapter 8

Comparison and Discussion

8.1 Comparison

This section will present the comparison of the response statistics for the jack-up vessel and the SSCV. Firstly, the vessel response is compared. This is done both for varying spectral peak periods and for different wave headings. Secondly, the crane tip motion of the jack-up vessel and the SSCV is compared for beam sea, head sea and quartering sea. When comparing the vessel motion and the crane tip motion, the irregular analysis without wind is used. Further, the blade motion for the jack-up vessel and SSCV is compared for different combinations of Tp, wind direction and wave directions. Lastly, the lift wire tension and the tension in the tugger lines are compared for different the wave direction. When comparing the blade response, lift wire tension and tugger line tension, the irregular analysis with wind and wave loads are used.

8.1.1 System Properties

Natural periods, that were found in the regular analysis, for both installations systems are shown in Table 8.1 and 8.2.

Table 8.1: System properties of the jack-up structure.

	Leg - x_g 1st. mode	Leg - y_g 1st mode	Double Pendulum	Crane boom: 1st mode
ω_n [rad/s]	1.3	1.4	0.5	1.9
T_n [s]	4.83	4.49	12.0	3.31

Table 8.2: System properties of the SSCV.

	Surge	Sway	Heave	Roll	Pitch	Yaw	Double Pendulum
ω_n [rad/s]	0.0670	0.0635	0.2732	0.3491	0.3492	0.067	0.5
T_n [s]	93.8	98.9	23.0	18.0	18.0	93.8	12

8.1.2 Vessel Motion

In Figure 8.1 the standard deviations of the vessel motion is compared of the jack-up and the SSCV for increasing spectral peak periods. In Figure 8.1 the comparison is done for head sea and beam sea. In Figure 8.1 (a) the jack-up response is decreasing for increasing spectral peak periods. This is due to the natural period of the jack-up legs. For the SSCV the response is increasing for increasing spectral periods. The response for Tp = 7 s is about the same for the jack-up and the SSCV. Further, it is seen that the response for the SSCV only exceed the greatest motion for the jack-up for a Tp = 10 sec.

In beam sea there is overall larger response motions both for the jack-up vessel and the SSCV compared to head sea. Further, the SSCV response motion is at the same level for all Tp while the jack-up response follow the same pattern as for head sea; decreasing for increasing Tp. Even though the SSCV response motion in general are greater for all periods it does not exceed the magnitude of the greatest response for the jack up for any Tp.

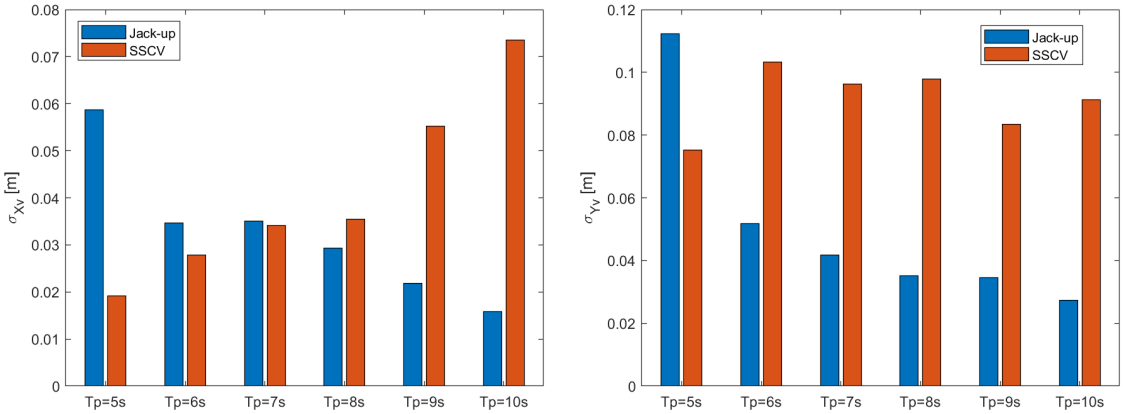

(a) Head sea, $\theta_{wv} = 270$ deg.

(b) Beam sea, $\theta_{wv} = 0$ deg.

Figure 8.1: Comparison of the standard deviation of the jack-up vessel and the SSCV with varying Tp; Hs= 1 m.

In Figure 8.2 the standard deviation for the two installation vessels in six DOFs is compared for head sea, beam sea and quartering sea. Overall, the SSCV response motions is larger than the jack-up vessel response motion. The exception is in head sea where the jack-up surge, sway, roll and yaw motion is greater for the jack-up than for the SSCV. It should be mentioned that it is both small differences and small motions in total. Further, it is seen that the greatest response motions is in beam sea for both of the installation vessels. Hence, the vessel sway and pitch motions is of highest magnitude.

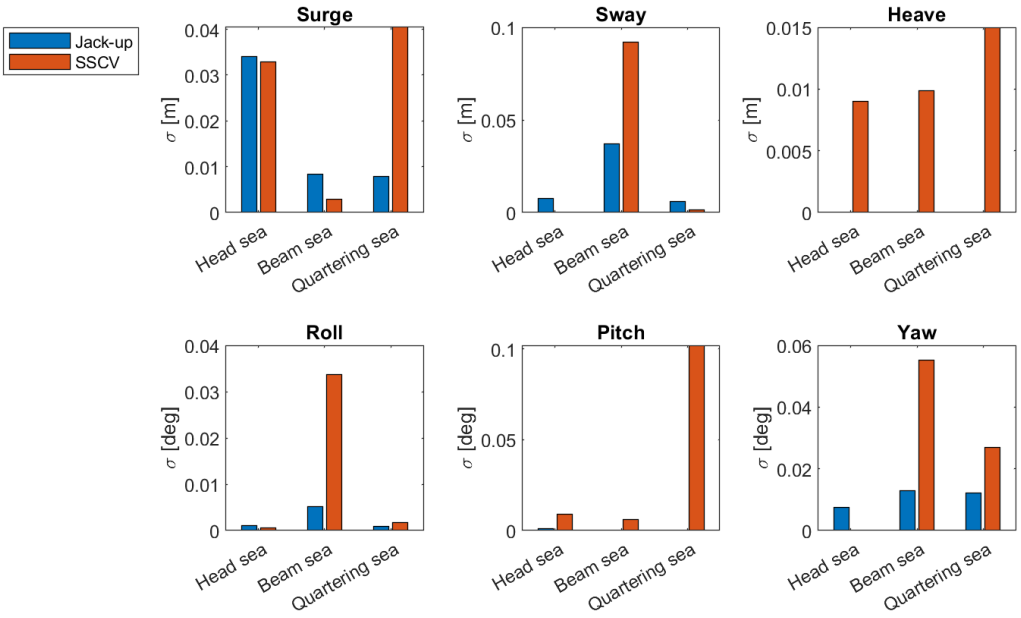

Figure 8.2: Comparison of standard deviation in six DOFs for the jack-up and SSCV for varying wave directions; Hs = 1 m, Tp = 7.3 s, beam sea $\theta_{wv} = 0$ deg, head sea $\theta_{wv} = 270$ deg and quartering sea $\theta_{wv} = 315$ deg.

8.1.3 Crane Tip Motion

In Figure 8.3 the crane tip motion is compared for the jack-up and the SSCV in head sea, beam sea and quartering sea. As for the vessel motion, the jack-up crane tip motion is larger than the SSCV in head sea for both translation in x_v and y_v. Beam sea induce the highest motions for the crane tip, of which the translation in y_v is the one of the highest magnitude. Compared to the vessel response, the crane tip response is higher. This is due to the height of the crane tip, the vessels rotational motion leads to large crane tip translation motion, as found in Chapter 7.

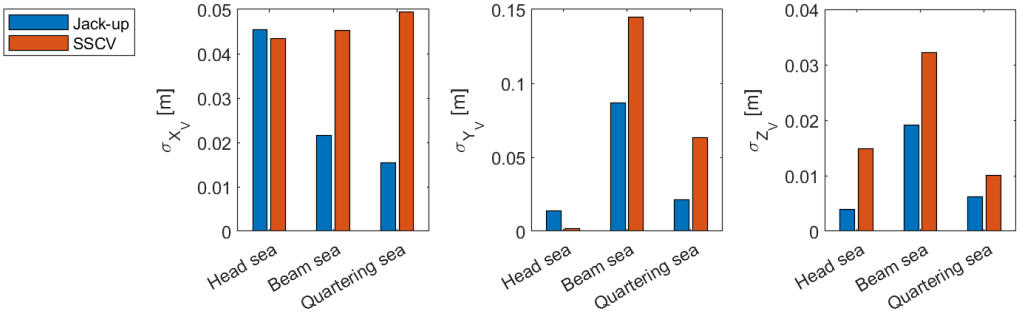

Figure 8.3: Comparison of standard deviation of the crane tip translations for varying wave directions for the jack-up and the SSCV; Hs = 1 m, Tp = 7.3 s; beam sea $\theta_{wv} = 0$ deg, head sea $\theta_{wv} = 270$ deg and quartering sea $\theta_{wv} = 315$ deg.

8.1.4 Blade Motion

This section presents the comparison of the blade motion. Figure 8.4 show the blade response in all six DOFs for varying Tp. As found in the regular analysis, the jack-up blade experiences most motion for low peak periods and the SSVC blade experience most motion for high peak periods.

This is seen for all DOFs in the figure. The jack-up blade have about no heave motion compared to the SSVC blade, as the the jack-up hull is elevated above the sea surface.

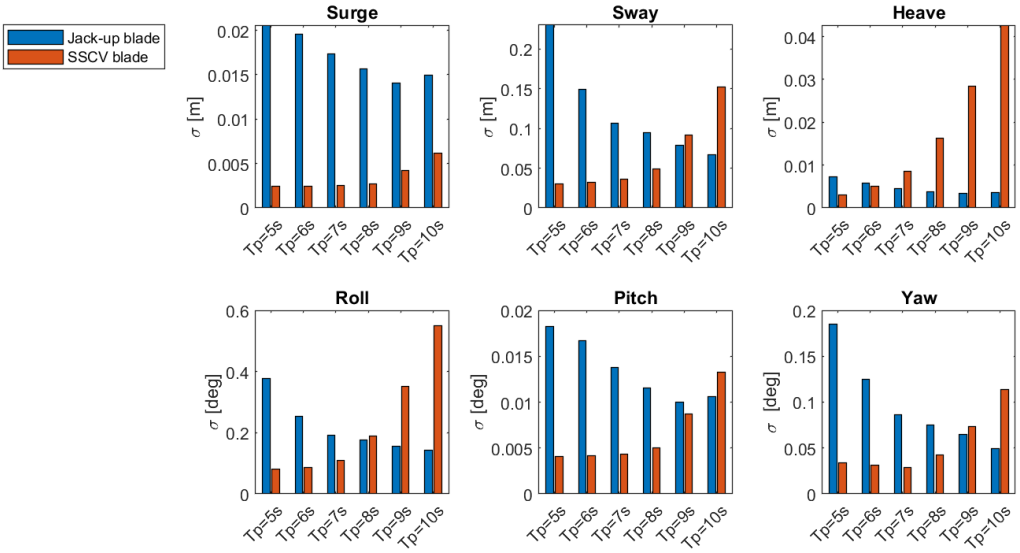

Figure 8.4: Comparison of the standard deviation of the blade motion with varying Tp for the jack-up and the SSCV; Hs=1m, head sea θ_{wv} = 270 deg, U_W = 7.0 m/s, θ_{wd} =0 deg.

Figure 8.5 compares the standard deviation of the blade motion with varying incident wave direction. When comparing the SSCV and the jack-up vessel, the SSCV generally have larger motion than the jack-up vessel. However, for the blade motion, the jack-up blade have the largest motions in most cases. The figure shows that the jack-up blade is sensitive to roll motion in all three directions compared to the SSCV blade. The roll motion is also the largest motion for both the jack-up blade and the SSCV blade. The heave motion is low for the jack-up blade. Overall, both the jack-up blade and the SSCV blade is sensitive to varying incident wave directions.

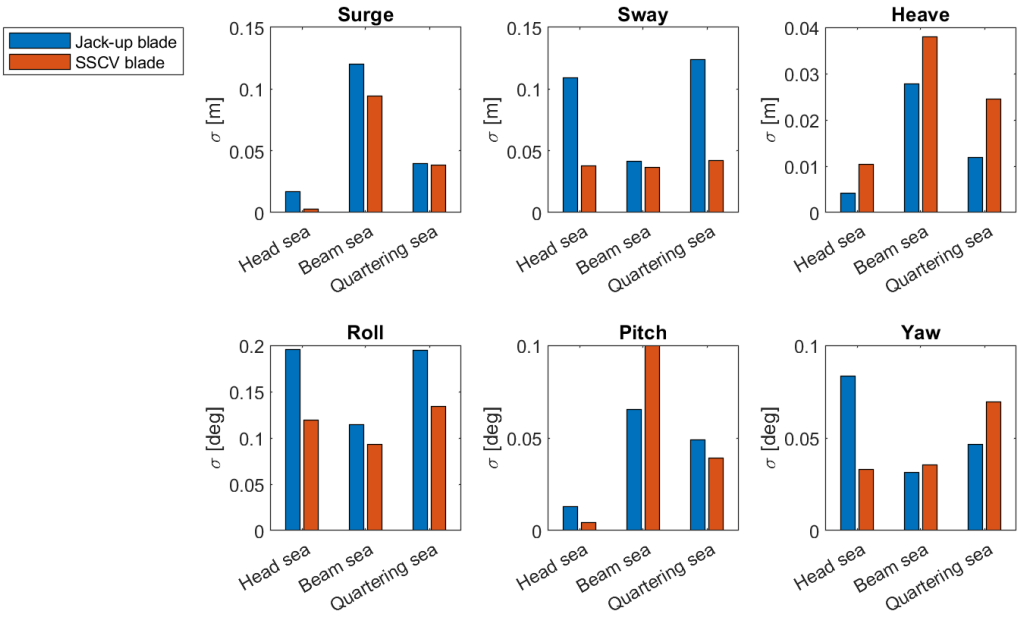

Figure 8.5: Comparison of the standard deviations of blade motion with varying wave directions for the jack-up and the SSCV; Tp= 7.3 sec, Hs= 1m, U_W = 7.0 m/s, θ_{wd} =0 deg.

Figure 8.6 and 8.7 compare the jack-up blade and the SSCV blade for only wave loads, only wind loads and wave + wind loads. This is to identify the contribution the incident wave loads and the aerodynamic have on the blade motion. Figure 8.6 present the responses in beam sea and Figure 8.7 present the responses in head sea. In both figures the blade response is larger for the jack-up when only wind loads are included in the analysis. This is as expected, since the jack-up hull is more exposed to wind than the SSCV hull. On the other hand, when only incident wave loads are included the SSCV blade have generally larger motion, due to the incident wave loads acting on the SSVC hull.

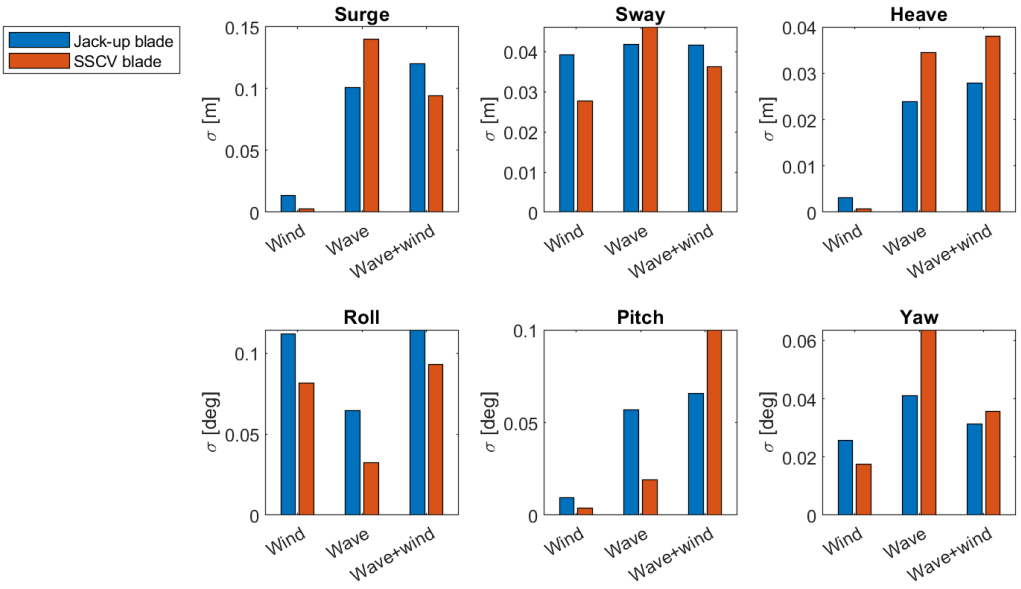

Figure 8.6: Standard deviations of blade motion in wind, waves and wave+wind for the jack-up and the SSCV; Tp= 7.3 sec, Hs= 1m, beam sea θ_{wv} =0 deg; U_W = 7.0 m/s, θ_{wd} =0 deg.

Figure 8.6 show that the blade surge and roll motion is sensitive to wave loads, and that the SSCV blade have larger motion than the jack-up blade. This is as expected in beam sea. For the SSCV blade, the pitch motion is sensitive to the combination of both wind and wave loads, where the pitch motion for the jack-up blade is only sensitive to the wave loads in beam sea. Overall, the blade motions are larger when the installation systems are exposed to the combination of aerodynamic loads and incident wave loads. In addition, surge, pitch and roll have significant contribution to the response motion compared to sway, heave and yaw in beam sea.

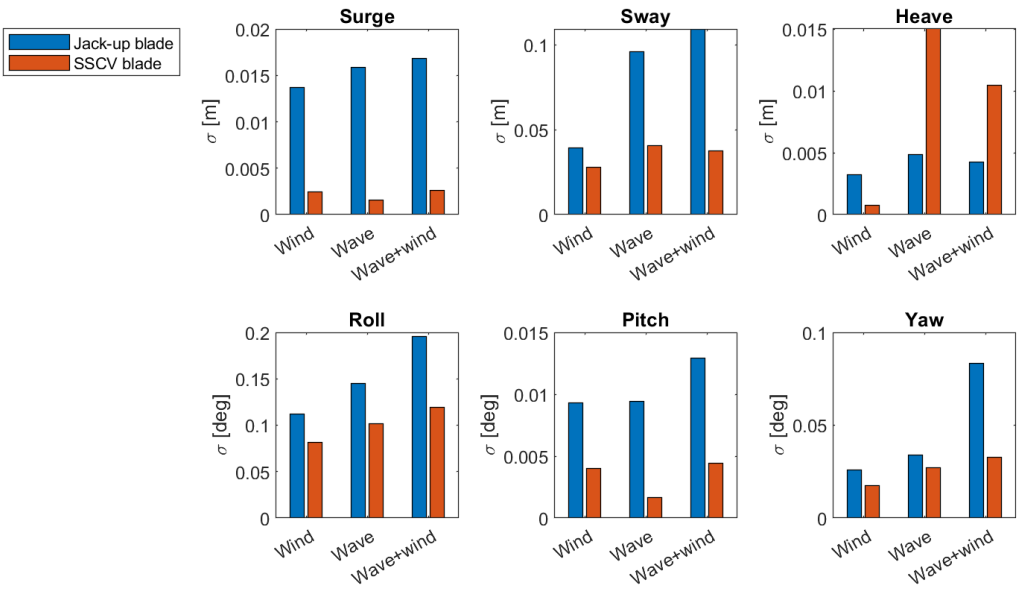

Figure 8.7: Standard deviations of blade motion in wind, waves ans wave+wind for the jack-up and the sscv; Tp= 7.3 sec, Hs= 1m, head sea θ_{wv} =270 deg; U_W = 7.0 m/s, θ_{wd} =0 deg.

Figure 8.7 show that in head sea the jack-up blade motions are larger than the SSCV blade motions in all DOFs. The exception is for heave motion when wave and wave+wind are included. The largest motion are in sway, roll and yaw, which are the significant DOFs in head sea for the blade. Looking at sway motion, the jack-up blade is more affected by the wave and wind loads compared to the SSCV blade. The sway motion is two times larger when aerodynamic forces and incident wave loads are included compared to only aerodynamic forces. The SSCV blade motion only have a small increase in motion when only wave loads are considered.

8.1.5 Tension

Figure 8.8 compare the lift wire tension for the jack-up vessel and the SSCV for head sea, beam sea and quartering sea. In head sea the lift wire tension for the jack-up and SSCV are at the same level. When the vessels are exposed to beam sea and quartering sea, the lift wire tension for the jack-up is significantly larger than for the SSCV. Both for the jack-up and the SSCV is is beam sea that induce the largest tension fluctuations.

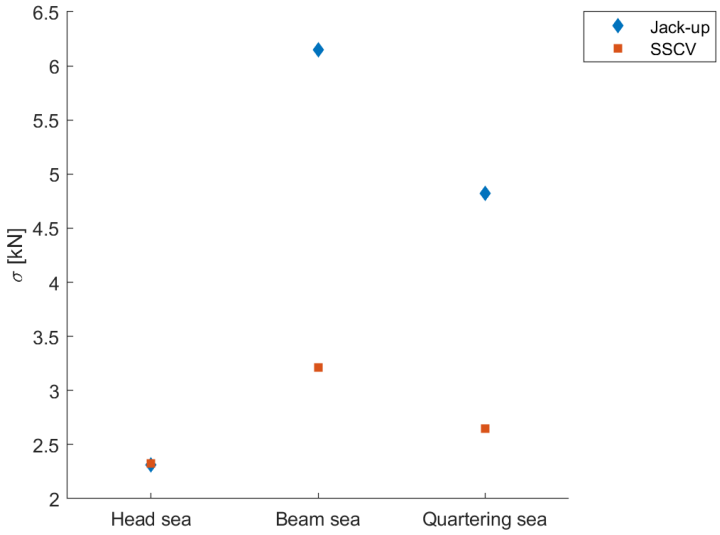

Figure 8.8: Standard deviation of lift wire tension with varying incident wave directions; U_w = 7 m/s, θ_{wd} =0 deg, Hs=1m, Tp= 7.3 s.

Figure 8.9 show the comparison between the variation in tugger line tension for the two installation vessels for varying incident wave directions. The figure show that the jack-up vessel have larger variation of tension in the tugger lines for all wave directions, and largest in beam sea. The SSCV have the largest tension fluctuations in quartering sea. For both vessel, head sea gives the smallest variations in tension in the tugger lines.

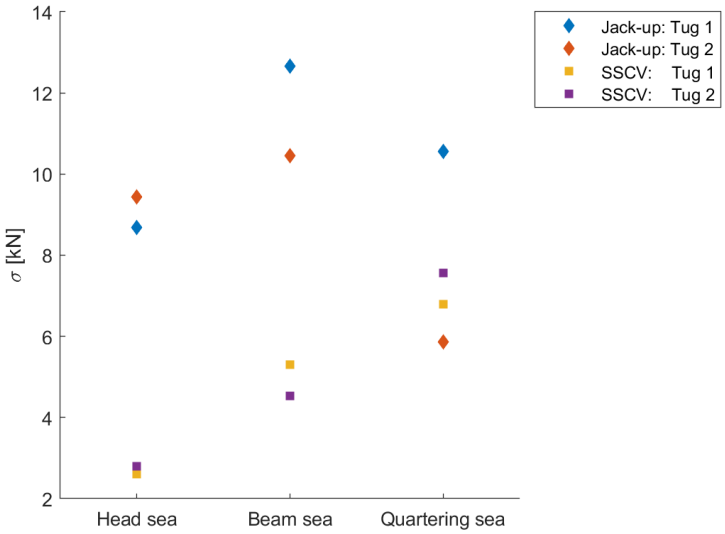

Figure 8.9: Standard deviation of tugger line tension with varying incident wave directions; U_w = 7 m/s, θ_{wd} =0 deg, Hs=1m, Tp = 7.3 s.

Figure 8.10 show the comparison of tension in the tugger lines for the jack-up and the SSCV for increasing Tp. The tension is higher for the jack-up for low Tp and higher for the SSCV for high Tp. This follows the system properties of the two installation systems.

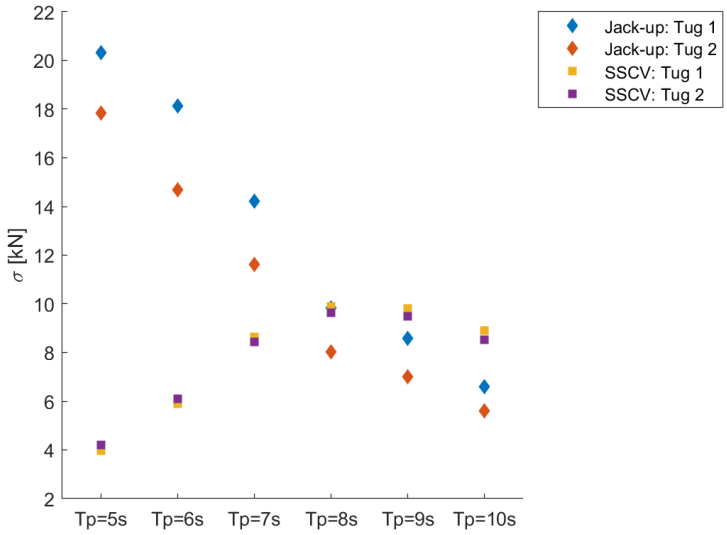

Figure 8.10: Standard deviation of tugger line tension with varying increasing Tp; θ_{wv} =0 deg, U_w = 7 m/s, θ_{wd} =0 deg, Hs=1m, Tp = 7.3 s.

8.2 Discussion

A comparative analysis between a jack-up crane vessel and a SSCV have been performed. The objective is to check if it is feasible for the two vessels to conduct a single blade installation to an offshore wind turbine blade at 60 meters water depth. The aim of this section is to interpret and evaluate the performed coupled dynamic response analysis, discuss the findings in Chapter 7 and the theory from the earlier chapters.

The single blade installation operation is sensitive to small changes in weather. It is therefore crucial to find a sufficient weather window for the installation operation, and the duration of the operation are an important factor. For the jack-up vessel, the duration of the operation have to include the lowering and the retrieval of the legs, which is a time consuming and sensitive phase of the operation. This demands a longer weather window than for the SSCV. The SSVC is also flexible and can relocate fast, which is a benefit as it is found in Chapter 7 that the vessel responses are sensitive for change of wave headings. The vessels may need to relocate and change headings if there is any change in the weather. This is a complicated process for the jack-up vessel. However, a SSCV have never been used for a single blade installation before. This is due to the wave induced motions, and because it is economical favorable to use a jack-up vessel.

Several assumptions were made in the analysis which have an influence on the obtained results. Firstly, the crane is modeled as fixed to the vessel for both the jack-up and the SSCV. Hence, the crane tip motion follows the vessel motion. This will lead to an underestimation of the response motion of the crane tip and the blade. The aerodynamic loads acting on the blade is modeled using the cross flow principle. The principle is based on the assumption that the blade element suits a 2D approximation and the inflow velocity normal to the blade is neglected. When all the contributions is summed up, the point of attack is in the blades center of gravity. The wind force will in principle not act as an evenly distributed load and hence the this assumption can lead to an underestimation of the response motions. Lastly, only a set of parameters are considered for the environmental conditions. Several combinations should be tested in order to ensure a safe operation. Further, it is assumed no current, which can lead to underestimation of the response motions.

The jack-up legs are modeled with a pinned foundation. As described in Section 4.3.3 the site specific soil interaction highly affect the system response motion. Pinned foundation model will

in general overestimate the response motion. In order to obtain more accurate results, the site specific soil properties have to be modeled. Further, leg interference are not taken into account for the legs. The spacing between the legs are relatively small and some wave interference are expected to occur. Unlike the jack-up vessel, it is assumed no wind loads acting on the SSCVs hull. This is because the contribution from the wind loads are marginal compared to the significant wave-induced loads acting directly on the hull.

The jack-up vessel and the SSCV has very different system properties. The jack-up vessel is sensitive to low wave periods, with a natural period of about 5 seconds. The SSCV are sensitive to high wave periods, with resonance frequencies above 20 seconds. The most common wave frequencies in areas where this kind of installation operations takes place are in the range between 5-10 seconds. This is the reason why the jack-up vessel have larger response motions than the SSCV for the low spectral peak periods, as shown in Figure 8.1 regardless of the incident wave-induced motion the SSCV experiences. The wave frequency response identified by the power spectra in Section 7.4.1 is due to the first order-wave loads, and as the plots show, not contributing to resonance motion of the SSCV. This is due to the mooring lines, they are designed to increase the natural period for the SSCV so the resonance period occur outside the range of the most common wave periods. However, the resonance motion shown in the same figures are due to the second order wave forces as the mean wave drift force and the slowly varying drift forces acting on the SSCV, which occur in waves with long periods.

As described in Chapter 3, operational limits for the installation operation have to be decided. Numerical analysis of the procedure is often employed in order to identifying the limiting parameters and establishing the limiting parameters. From the comparison it is found that both the jack-up and the SSCV response is more dependent of the significant wave height compared to the spectral peak period, assuming that the wave frequency is outside the range that induce resonance motions. Hence, the significant wave height and spectral peak period will be an limiting parameter for installation systems.

The jack-up vessel and SSCV properties are different, which makes one favorable over the other in different environmental conditions. It has been found that both of the vessels experience the highest response motion in beam sea. Further, the wind heading has a smaller contribution to the response. It was expected that the response was to increase with the alignment of the wind and wave direction and decrease with misalignment, as described in section 2.4. It is found that the response increase with alignment of the wind an wave heading in beam sea. The response motion is the same in head sea both for a wind direction in line and normal to the wave direction. The wave loads have a greater impact on the response motion than the wind loads, and is an important operational parameter that have to be taken into account when considering the operational limits. It was also found that the SSCV blade responses were reduced by an aerodynamic damping effect acting on the blade. Generally the responses when the SSCV only was exposed to incident wave loads were larger than when wind loads also were included in the analysis.

The tension in the lift wire and the tugger lines were also compared. The tugger lines are connected from the crane boom to the yoke, reducing motion in the global x-direction. In the system responses the double pendulum was only seen in global y-direction. This is a consequence of the fact that the tugger lines reduce the motion in global x-direction. Hence, the blade only experience roll motion. The tension in the tugger lines were highest for the jack-up for low Tp and highest for the SSCV for higher Tp. The tension in the tugger lines are induced by motion in the system. Hence, it is expected that the tension will follow the system properties of the system.

In general, the SSCV as a floating structure experience higher response motion due to the wave interaction. Beam sea induce the highest motions for both the jack-up vessel and the SSCV. Further, it was also found that in head sea the jack-up response motion in surge are larger than for the SSCV in Figure 8.2. Chapter 4.3.2 describe the P-Δ-influence that induce an translation in line with the wave direction. The area of the legs that interact with the waves are the same regardless of the wave direction. Hence, the contribution from the P-Δ-influence to the translation response remains. For the SSCV the geometry interacting with the water reduce the response motion in head sea. This can explain why the jack-up response is greater than the SSCV in head sea.

The critical parameter for the installation system will be the relative motion between the blade root and the nacelle hub. The nacelle hub will also experience wave induced motions. This means that both the natural periods of the installed foundation and the jack-up system have to be taken into consideration to avoid large motions and failure of the operation.

When performing an offshore crane operation, the stability of the vessel is reduced. Both the static and dynamic stability is decreased as described in Section 2.5. The roll motion of the vessel is a critical parameter in regards to the systems stability. In general the SSCV experience high roll motion due to wave loads in beam sea. This will decrease the vessels stability and have to be taken into consideration with regards to the operational limits.

Chapter 9

Conclusion and Further Work

9.1 Conclusion

A comparative analysis is preformed between a jack-up vessel and a SSCV. A numerical analysis of a single blade installation at a water depth of 60 meters is conducted. The main objective was to evaluate the motion response of the coupled dynamic analysis of the single blade installation and compare the blade motion. The main challenges was the increased water depth for the jack-up vessel and the wave-induced response motions for the SSCV.

Firstly, the difference of system properties for the installation vessel make them favorable in different environmental conditions. The jack-up legs will experience resonance at low wave period, where the bending mode of the legs are at 5 seconds. The SSCV will experience resonance at high wave periods, where in surge and sway motion the SSCV have natural period in the range of 90-100 seconds. This is found in the regular wave analysis.

In the irregular wave analysis it was found that outside the jack-up vessels resonance range, the SSCV experienced larger motions than the jack-up crane vessel. This is because the incident wave act directly on the SSCVs hull. Further, beam sea induced the highest motions and head sea induced the lowest motions for both installation vessels. The significant wave height was the significant parameter outside the resonance range for both installation systems. However, for wave periods within the resonance range the significant wave height became trivial.

It was found that the installation vessel response increased with alignment of wave and wind direction, towards 0 deg. The highest response motion is induced when the wind and wave direction is in line in global x-direction. It was in general seen that the response motion was more dependent of wave heading than wind heading. The response motion was significantly increased for the combination of wind and wave loads, compared to only wave loads. It was also found from the tension in the tugger lines that they are significant for the motion control of the blade. The tension followed the system properties of the installation systems. Hence, the jack-up crane vessel experienced high tension for low Tp and SSCV for high Tp.

In general, the wave loads are found to be a parameter of greater importance than the wind loads. Overall, the limiting parameters are found to be the significant wave height, spectral peak period and wave direction. The two installation vessels can be competitive, but further analysis have to be conducted.

9.2 Further Work

In order to conclude if it is feasible for the jack-up vessel and the SSCV to perform the single blade installation at 60 meters water depth in a safe and efficient matter, further analysis has to be performed. This section will list recommendations for further work.

- *Perform the analysis for more environmental conditions.*
  This analysis have only been performed for a limited number of sea states. It would therefor be of interest to perform the analysis for additional sea states, in order to see how the installation system behaves. This could include the contribution from the current, and examine if the current has any effect on the installation system. In addition, perform the analysis with a wider range of wind velocities and combinations of wind and wave direction.

- *Analyze the operational limits.*
  In this thesis the operational limits for the systems are unknown. Therefor, it would be interesting to analyze and identify the operational limits in order to make qualified decision for the allowable responses and for which sea states the installation can be performed in.

- *Calculate the blade root motion.*
  The responses parameters analyzed are the vessel, crane tip and the blade motion. Where the responses of the blade are found in the blades center of gravity. It would also be of interest to calculate the blade root position, and analyse the responses at the blade root.

- *Perform a fatigue analysis on the jack-up legs, and test for different sizes of the leg cross-section.*
  This thesis uses the same jack-up model as Y. Zhao developed in her PhD for 30 meter water depth. The only modification done was to change the length of the legs, so the jack-up vessel would be suitable for 60 meters water depth. However, the cross-section remained the same and it would be of interest to see how a change in size and geometry of the cross-section would influence the legs flexibility and further the system properties. This analyze does not consider if the used legs are feasible for 60 meter water depth.

- *Analyze the responses of the jack-up installation system with different foundations for the legs.*
  The jack-up legs in this thesis are modelled with a pinned foundation. As it is stated in this thesis, the soil-interaction effects the responses, and site specific modelling has to be done.

- *Find the hydrostatic coefficient for the SSCV for 60 meters water depth.*
  The only modification done for the SSCV model from Y. Zhaos PhD was to change the kinematic water depth and the distance between the sea surface and the sea floor in SIMA. The hydrostatic coefficients assumed the same as for the model at 30 meter water depth. It could be interesting to see if a new analyze of the hydrostatic coefficient in HydroD with 60 meter water depth will have any impact, regardless the assumed small differences.

- *Conduct the same simulation of this installation phase with another software.*
  The simulation have to be conducted with another software than SIMA in order to verify and validate the results from the analysis.

Bibliography

[1] Zhen Gao. Marine operations related to installation of offshore wind turbines. *Presentation: Summer School on Naval Architecture, Ocean Engineering and Mechanics Minhang Campus, Shanghai Jiao Tong Univeristy (SJTU)*, 2019.

[2] Simens. Simens gamesa crancks it up, 2020. URL `https://www.offshorewind.biz/2020/05/19/siemens-gamesa-cranks-it-up-to-15-mw-with-offshore-behemoth/`. Accessed on 05/06/2020.

[3] Det Norske Veritas. Dnv-os-h101: Marine operations, general, 2011.

[4] Zhen Gao Amrit Verma YUna Zhao Zhengru Ren, Zhiyu Jiang. A summary of the recent work at ntnu on marine operations related to installation of offshore wind turbines. *Department of Marine Technology, Faculty of Engineering and Technology, Norwegian University of Science and Technology*, 2018.

[5] Torgeir Moan Peter Christian Sandvik Yuna Zhao, Zhen Gao. Assessment of operational environmental limits for offshore single blade installation using response-based criteria. *Department of Marine Technology - NTNU*, 2019.

[6] Yuna Zhao. Numerical modeling and dynamic analysis of offshore wind turbine blade installation. *Department of Marine Technology, Faculty of Engineering and Technology, Norwegian University of Science and Technology*, 2019.

[7] WindEurope. Wind energy in europe in 2018. *Wind Europe*, 2019.

[8] GWEC. Global wind report 2018. 2019.

[9] Michael Muskulus Esther Dornhelm, Helene Seyr. Vindby - a serious offshore wind farm design game. *Research gate*, 2019.

[10] Geir Fuglerud Liv Randi Hultgreen Knut Minsaas MAgus Rasmussen Bjørn Sillerud Bjørn Sortland Harald Valland Jørgen Amdahl, Anders Endal. *TMR4100 - Marin Teknikk Intro*. Department of Marine Technology, Faculty of Engineering, Norwegian University of Science and Technology, 2011.

[11] Offshore wind energy, 2019. URL `https://webshop.flyingfocus.nl/en/shop/photobooks/21x30cm-en/offshore-wind-energy/`. Accessed on 27/10/2019.

[12] Xl monopiles, 2019. URL `http://www.esru.strath.ac.uk/EandE/Web_sites/14-15/XL_Monopiles/technical.html`. Accessed on 27/10/2019.

[13] Compact semi-submersible lift vessel 8655, 2019. URL `https://products.damen.com:443/en/ranges/decommissioningplugandabandonment/sslv8655`. Accessed on 27/10/2019.

[14] Sheer-leg crane vessel, 2019. URL `http://www.seaboats.net/floating-sheerleg-crane-xidp1308582.html`. Accessed on 27/10/2019.

[15] Mpi offshore, 2019. URL `https://www.linkedin.com/company/mpi-offshore/?originalSubdomain=no`. Accessed on 27/10/2019.

[16] Jumbo kinetic (heavy lift cargo), 2019. URL `https://www.linkedin.com/company/mpi-offshore/?originalSubdomain=no`. Accessed on 27/10/2019.

[17] Simens. Offshore wind power - how it all comes together, 2019. URL `https://www.youtube.com/watch?v=zUQifpcGTrg`. Accessed on 02/11/2019.

[18] Wind powrr Monthly. Fred olsen o&m providers, 2019. URL `https://www.windpowermonthly.com/article/1446965/fred-olsen-o-m-providers-merge`. Accessed on 05/12/2019.

[19] Tobias Pieffers. Fred olsen wins large offshore contract, 2019. URL `https://www.projectcargojournal.com/offshore/2019/05/01/fred-olsen-wins-large-offshore-wind-contract-from-mhi-vestas/`. Accessed on 05/12/2019.

[20] Zhengru Ren Zhen Gao Nils Petter Vedvik Amrit shankar Verma, Zhinyu Jiang. Response-based assessment of operational limits for mating blades on monopile-type offhore wind turbines. *Norwegian University of Science and Technology, at.*, 2019.

[21] Zhen Gao Peter Christian Sandvik Torgeir Moan Eric Van Buren Yuna Zhao, Zhengshun Cheng. Numerical modeling and analysis of the dynamic motion response of an offshore wind turbine blade during installation by a jack up vessel. *Department of Marine Technology, Faculty of Engineering and Technology, Norwegian University of Science and Technology*, 2018.

[22] Marilena Greco. *TMR 4215: Sea Loads - Lecture Notes*. Dept. of marine technology, NTNU, 2019.

[23] Ragnar Sigbjørnsson Ivar Langen. *Dynamic Analysis of Structures*. Department of Marine Technology, Faculty of Engineering, Norwegian University of Science and Technology.

[24] SINTEF OCEAN. *SIMO 4.10.3 User Guide*. 2017.

[25] UNFCCC. The paris agreement, 2019. URL `https://unfccc.int/process-and-meetings/the-paris-agreement/the-paris-agreement`. Accessed on 05/10/2019.

[26] WindEurope. Wind energy in europe in 2019. *Wind Europe*, 2020. URL `https://windeurope.org/wp-content/uploads/files/about-wind/statistics/WindEurope-Annual-Statistics-2019.pdf`.

[27] Lin Li Torgeir Moan Wilson Ivan Guachamin Acero, Zhen Gao. Methodology for assessment of the operational limits and operability of marine operations. *Science Direct*, 2016.

[28] Equinor. Equinor is the global leader in floating offshore wind solution, 2018. URL `https://www.equinor.com/no/what-we-do/hywind-where-the-wind-takes-us.html`. Accessed on 06/10/2019.

[29] windEurope. Market outlook 2023, 2019. URL `https://www.anev.org/wp-content/uploads/2019/10/Market-outlook-2019.pdf`. Accessed on 10/12/2019.

[30] Pål Preede Revheim. Hvor store kan vindturbiner egentlig bli?, 2017. URL `https://e24.no/naeringsliv/i/EWAvbj/hvor-store-kan-vindturbiner-egentlig-bli`. Accessed on 03.06.2020.

[31] Wind Europe. Floating offshore wind vision statement. *WindEurope*, 2017.

[32] Finn Gunnar Nielsen. *Lecture Notes in Marine Operations*. Department of Marine Hydrodynamics, Faculty of Marine Engineering, Norwegian University of Science and Technology, 2007.

[33] Wilson Ivan Guachamin Acero. Assessment of marine operations for offshore wind turbine installation with emphasis on response-based operational limits. *Department of Marine Technology, Faculty of Engineering Science and Technology, Norwegian University of Science and Technology*, 2016.

[34] Choo Yoo Sang. Design, construction and installation of offshore structures. *National University of Singapore, Department of Offshore Technology*, 2018.

[35] Kim Soo-young Kharoufi Hicham Kim Hyun-cheol Ahn Dang, Shin Sung-chul. Comparative evaluation of different offshore wind turbine installation vessels for korean west–south wind farm. *Science Direct*, 2017.

[36] Zhen Gao Amrit Verma Nils Petter Vedvik Zhengru Ren, Zhiyu Jiang. Impact assessment of a wind turbine blade root during an offshore mating process. *Faculty of Engineering and Technology, Norwegian University of Science and Technology*, 2019.

[37] Fred olsen windcarrier, 2019. URL `https://windcarrier.com/fleet`. Accessed on 04/11/2019.

[38] Zhen Gao Peter Christian Sandvik Yuna Zhao, Zhengshun Cheng. Numerical study on the feasibility of offshore single blade installation by floating crane vessel. *Department of Marine Technology, Faculty of Engineering and Technology, Norwegian University of Science and Technology*, 2019.

[39] Peter Christian Sandvik Zhen Gao Yuna Zhao, Zhengshun Cheng. An integrated dynamic analysis method for simulating installation of singe blades for wind turbines. *Department of Marine Technology, Faculty of Engineering and Technology, Norwegian University of Science and Technology*, 2018.

[40] SINTEF. A review of morisons equation for calcualting hydrodynamic loads on vertical-orientated cylinders, 2010. URL `https://www.sintef.no/globalassets/project/nowitech/wind_presentations/merz-k.o.-ntnu.pdf`. Accessed on 10/11/2019.

[41] Zhengshun Cheng Torgeir Moan Yuna Zhao, Zhen Gao. Effect of foundation modeling of a jack-up crane vessel on the dynamic motion response of an offshore wind turbine blade during installation. *Department of Marine Technology, Faculty of Engineering and Technology, Norwegian University of Science and Technology*, 2019.

[42] DNV. What is the difference between a frequency domain and time domain mooring analysis?, 2018. Accessed on 4/11/2019.

[43] Orcina. Orcaflex features and specification. URL `https://www.orcina.com/orcaflex/specification/`. Accessed on 04/11/2019.

[44] Offshore Engineering solutions. Industry software. URL `http://www.oesl.nl/inhouse-software`. Accessed on 04/11/2019.

[45] DNV Det Norske Veritas. Wadam software, 2018. URL `https://www.dnvgl.com/services/frequency-domain-hydrodynamic-analysis-of-stationary-vessels-wadam-2412?utm_campaign=structure_sesam&utm_source=google&utm_medium=cpc&gclid=Cj0KCQiAtf_tBRDtARIsAIbAKe35bpAJG7eEYlJpn3dGHLlv0UkvXHveVEUfWKNDQfHgkYWioao-xgwaAsvHEALw_wcB`. Accessed on 04/11/2019.

[46] WAMIT Inc. Wamit, 2018. URL `https://www.wamit.com/`. Accessed on 04/11/2019.

[47] SINTEF MARINTEK. Riflex - riser system analysis program. *DNV Software*, 2018.

[48] SINTEF MARINTEK. Simo - simulation of marine operations. *DNV Software*, 2018.

[49] International Organization of Standardization. Iso 29400:2015 ships and marine operations - offshore wind energy - port and marine operations, 2015. URL `https://www.standard.no/nettbutikk/produktkatalogen/produktpresentasjon/?ProductID=750490`. Accessed on 23/03/2020.

[50] Det Norske Veritas Germanischer Lloyd. Transport and installation of wind power plants, 2017. URL `https://rules.dnvgl.com/docs/pdf/DNVGL/ST/2017-06/DNVGL-ST-0054.pdf`. Accessed on 23/03/2020.

[51] Kjell Laarsen Nils Sødahl Harald Ormberg, Ivar J. Fylling. Coupled analysis of vessel motions and mooring and riser system dynamics. 1997.

[52] SIMO project Team. *SIMO - Theory Manual Version 4.0 rev.3*. MARINTEK - Norwegian Marine Technology Research Institute, 2013.